

Bayesian spatio-temporal methods for small-area estimation of HIV indicators

Imperial College London

Adam Howes

Department of Mathematics

Imperial College London

In partial fulfillment of the requirements for the degree of

Doctor of Philosophy

December 2023

Copyright

The copyright of this thesis rests with the author. Unless otherwise indicated, its contents are licensed under a Creative Commons Attribution-Non Commercial 4.0 International Licence (CC BY-NC). Under this licence, you may copy and redistribute the material in any medium or format. You may also create and distribute modified versions of the work. This is on the condition that: you credit the author and do not use it, or any derivative works, for a commercial purpose. When reusing or sharing this work, ensure you make the licence terms clear to others by naming the licence and linking to the licence text. Where a work has been adapted, you should indicate that the work has been changed and describe those changes. Please seek permission from the copyright holder for uses of this work that are not included in this licence or permitted under UK Copyright Law.

Statement of Originality

This thesis, and the work presented in it, is work that I conducted myself. In all cases where I describe others' work, I provide appropriate references.

For someone, or something.

Acknowledgements

Thank you to my supervisors Seth Flaxman and Jeff Eaton for their guidance and mentorship. I am grateful for the research environment provided by the Modern Statistics and Statistical Machine Learning Centre for Doctoral Training at Imperial and Oxford, the HIV Inference Group at Imperial, and the Machine Learning and Global Health Network across the UK, Denmark, Germany and Singapore. Thank you to Mike McLaren, Kevin Esveld, the Nucleic Acid Observatory team, and the Sculpting Evolution lab for hosting my visit to the MIT Media Lab. Thank you to Alex Stringer, and the Department of Statistics and Actuarial Science for hosting my visit to the University of Waterloo. My sense for what matters has been shaped (arguably improved) by the Effective Altruism community. This research was made possible by funding provided by the Bill & Melinda Gates Foundation and EPSRC.

Adam Howes
Imperial College London
December 2023

Abstract

Progress towards ending AIDS as a public health threat by 2030 is not being made fast enough. Effective public health response requires accurate, timely, high-resolution estimates of epidemic and demographic indicators. Limitations of available data make obtaining these estimates difficult. I developed and applied Bayesian spatio-temporal methods to meet this challenge. First, I examined models for area-level spatial structure. Second, I estimated district-level HIV risk group proportions, enabling behavioural prioritisation of prevention services, as put forward in the Global AIDS Strategy. Finally, I developed a novel deterministic Bayesian inference method, combining adaptive Gauss-Hermite quadrature with principal component analysis, motivated by the Naomi district-level model of HIV indicators. Together, the contributions in this thesis help to guide precision HIV policy in sub-Saharan Africa, as well as advancing Bayesian methods for spatio-temporal data.

Contents

List of Figures	ix
List of Tables	xiv
List of Abbreviations	xvi
List of Notations	xviii
1 Introduction	1
1.1 Chapter overview	2
2 The HIV/AIDS epidemic	4
2.1 Background	4
2.2 HIV surveillance	8
3 Bayesian spatio-temporal statistics	12
3.1 Bayesian statistics	12
3.2 Spatio-temporal statistics	17
3.3 Model structure	20
3.4 Model comparison	26
3.5 Survey methods	26
4 Models for spatial structure	30
4.1 Background	30
4.2 Models based on adjacency	30
4.3 Models using kernels	37
4.4 Simulation study	37
4.5 HIV prevalence study	37
4.6 Discussion	37

Contents

5 A model for risk group proportions	38
5.1 Background	38
5.2 Data	39
5.3 Model for risk group proportions	43
5.4 Prevalence and incidence by risk group	60
5.5 Discussion	64
6 Fast approximate Bayesian inference	70
6.1 Inference methods and software	71
6.2 A universal INLA implementation based on AD	85
6.3 The Naomi model	86
6.4 AGHQ in moderate dimensions	88
6.5 Malawi case-study	89
6.6 Discussion	91
7 Future work and conclusions	94
7.1 Strengths	94
7.2 Future work	95
7.3 Conclusions	95

Appendices

A Models for spatial structure	98
B A model for risk group proportions	99
B.1 The Global AIDS Strategy	99
B.2 Household survey data	100
B.3 Spatial analysis levels	102
B.4 Survey questions and risk group allocation	102
C Fast approximate Bayesian inference	104
C.1 Epilepsy example	104
C.2 Simplified Naomi model description	106
C.3 Model assessment	110
C.4 AGHQ and PCA-AGHQ details	110
C.5 Normalising constant estimation	110
C.6 Inference comparison	110
C.7 MCMC convergence and suitability	110

Contents

Works Cited

111

List of Figures

1.1 HIV/AIDS is the largest cause of annual DALYs among individuals aged >1 year in SSA (Global Burden of Disease Collaborative Network 2019). One DALY represents the loss of the equivalent of one year of full health, and is calculated by the sum of years of life lost and years lost due to disability. The disability weights vary between 0 (full health) and 1 (death) depending on severity of the condition.	2
2.1 Globally, yearly new HIV infections peaked in 1995, and have since decreased by 59% and yearly AIDS-related deaths peaked in 2004, and have since decreased by 68% (UNAIDS 2023a). Much of the disease burden is concentrated in eastern and southern Africa, as well as western and central Africa.	5
2.2 Adult (15-49) HIV prevalence varies substantially both within and between countries in SSA. These estimates from 2023 were generated by country teams using the Naomi small-area estimation model in a process supported by UNAIDS and are available from UNAIDS (2023a). White filled points are country-level estimates, and coloured points are district-level estimates. Results from Nigeria were not published. Data collection in the Cabo Delgado province of Mozambique was disrupted by conflict. Obtaining results for the Democratic Republic of the Congo required removing some districts from the model. Country names are given by three-letter codes as published by the International Organization for Standardization (ISO).	7

List of Figures

- 3.1 An example of Bayesian modelling and computation for a simple one parameter model. Here the likelihood is $y_i \sim \text{Poisson}(\phi)$ for $i = 1, 2, 3$ and prior distribution on the rate parameter is $\phi \sim \text{Gamma}(3, 1)$. I simulated observed data $\mathbf{y} = (1, 2, 3)$ from the distribution Poisson(2.5). As such, the true data generating process is within the space of models being considered (This situation is sometimes known (Bernardo and Smith 2001) as the \mathcal{M} -closed world, in contrast to the \mathcal{M} -open world where the model is said to be misspecified.) Furthermore, the posterior distribution is available in closed form as Gamma(9, 4). This is because the posterior distribution is in the same family of probability distributions as the prior distribution, and the model is described as being conjugate. Conjugate models are often used because of their convenience. Though other models may be more suitable, they will typically be more computationally demanding. In this situation, which is typical, the posterior distribution is more tightly peaked than the prior distribution. 14
- 3.2 NUTS can be used to sample from the posterior distribution in the example of Figure 3.1. Panel A shows a histogram of the NUTS samples as compared to the true posterior. Panel B shows a traceplot. Panel C shows the convergence of the empirical posterior mean to the true value. 16
- 3.3 The spatial location of Cape Town in South Africa could be considered a point. The ZF Mgcawu District Municipality on the other hand is an example of an area. World AIDS Day, designated on the 1st of December every year, could be considered a point in time. The second fiscal quarter, running through April, May and June, and denoted by Q2 represents a period of time. (In reality, both Cape Town and World AIDS Day are areas, rather than true point locations. Instances of infinitesimal point locations in everyday life are rare.) . 18
- 3.4 Simulation of a simple random sample $y_i \sim \text{Bin}(m, p_i)$ with varying sample size $m = 5, 25, 125$ in each of the $i = 1, \dots, 156$ constituencies of Zambia. Direct estimates were obtained by the ratio y_i/m . Modelled estimates were obtained using a logistic regression with linear predictor given by an intercept and a spatial random effect. HIV estimates for Zambia have previously been generated at the district-level, comprising 116 spatial units. Moving forward, there is interest in generating estimates at the higher-resolution constituency level, as program planning is devolved locally. This figure is adapted from a presentation I gave for the Zambia HIV Estimates Technical Working Group, available from <https://github.com/athowes/zambia-unaid>. 21

List of Figures

3.5	The setting of this figure matches that of Figure 3.4. Estimates from surveys with higher sample size have higher Pearson correlation coefficient R with the underlying truth. For a fixed sample size, correlation can be improved by using modelled estimates to borrow information across spatial units, rather than using the higher variance direct estimates. Points along the dashed diagonal line correspond to agreement between the estimate obtained from the survey and the underlying truth used to generate the data. For each sample size, using a spatial model increases the correlation between the estimates and underlying truth.	22
3.6	A simple example of group structure within data in which each individual $i = 1, \dots, n$ is associated to m_i observations y_{i1}, \dots, y_{im_i}	23
4.1	Figure caption.	35
4.2	Figure caption.	35
4.3	Figure caption.	36
5.1	Risk of acquiring HIV is depends on both individual-level risk behaviour and population-level HIV incidence. I assume that with no individual-level risk behaviour, there is no risk of acquiring HIV, independent of the population-level HIV incidence. The risk scale is intended to be illustrative, rather than interpreted quantitatively.	40
5.2	Surveys conducted 1999-2018 that were used in the analysis by year, survey type, sample size, and whether the survey included a specific question about transactional sex. Survey type included AIDS Indicator Surveys (AIS), Demographic and Health Surveys (DHS), the Botswana AIDS Impact Survey 2013 (BAIS), and Population-based HIV Impact Assessment (PHIA) surveys.	41
5.3	Flowchart giving classification of survey respondents to HIV risk groups.	43
5.4	For the multinomial logistic regression model, under the CPO criterion, including Besag spatial random effects rather than IID spatial random effects improved model performance. On the other hand, under the DIC and WAIC, where smaller values are preferred, the opposite was true. Though IID temporal random effects are preferred by all criteria AR1 temporal random effects performed very similarly, likely as there is a limited amount of temporal variation in the data to describe.	51

List of Figures

5.5	For the logistic regression model, the CPO, DIC, and WAIC each agreed that the model containing Besag spatial random effects and the <code>cfswrecent</code> covariates was best. Inclusion of Besag spatial random effects consistently improved each criterion, whereas improvements from inclusion of any covariates were marginal.	53
5.6	The disaggregation procedure I used produces an age distribution for FSW peaking in the 20-24 and 25-29 age groups, and declining for older age groups.	55
5.7	Probability integral transform (PIT) histograms (top row) and empirical cumulative distribution function (ECDF) difference plots (bottom row) for the final selected model.	56
5.8	The spatial distribution (posterior mean) of the AGYW risk group proportions in 2018. Estimates are stratified by risk group (columns) and five-year age group (rows). Countries in grey were not included in the analysis. A limitation of this figure is that using a common colour scale, desirable for other reasons, makes it challenging to see spatial variation in the FSW risk group.	57
5.9	National (in white) and subnational (in color) posterior means of the risk group proportions. Estimates are stratified by risk group (columns) and five-year age group (rows). Though the information presented is similar to that of Figure 5.8, this figure presents a clear view of within- and between-country variation in risk group proportions.	58
5.10	Figure caption.	59
5.11	Figure caption.	60
5.12	Percentage of new infections reached across all 13 countries, taking a variety of risk stratification approaches, against the percentage of at risk population required to be reached.	63
5.13	Figure caption.	66
6.1	Demonstration of the Laplace approximation for the simple Bayesian inference example of Figure 3.1. The unnormalised posterior is $p(\phi, \mathbf{y}) = \phi^8 \exp(-4\phi)$, and can be recognised as the unnormalised gamma distribution $\text{Gamma}(9, 4)$. The true log normalising constant is $\log p(\mathbf{y}) = \log \Gamma(9) - 9 \log(4) = -1.872046$, whereas the Laplace approximate log normalising constant is $\log \tilde{p}_{\text{LA}}(\mathbf{y}) = -1.882458$, resulting from the Gaussian approximation $p_{\mathcal{G}}(\phi \mathbf{y}) = \mathcal{N}(\phi \mu = 2, \tau = 2)$	74

List of Figures

6.2	The trapezoid rule with $k = 5, 25, 125$ equally-spaced ($\epsilon_i = \epsilon > 0$) quadrature nodes can be used to integrate the function $f(z) = z \sin(z)$ in the domain $[0, \pi]$. Here, the exact solution is $\pi \approx 3.1416$. As k increases and more nodes are used in the computation, the quadrature estimate becomes closer to the exact solution.	77
6.3	The Gauss-Hermite quadrature nodes $\mathbf{z} \in \mathcal{Q}(2, 3)$ for a two-dimensional integral with three nodes per dimension (A). Adaption occurs based on the mode (B) and covariance of the integrand via either the Cholesky (C) or spectral (D) decomposition of the inverse curvature at the mode. Here, the integrand is $f(z_1, z_2) = \text{sn}(0.5z_1, \alpha = 2) \cdot \text{sn}(0.8z_1 - 0.5z_2, \alpha = -2)$, where $\text{sn}(\cdot)$ is the standard skewnormal probability density function with shape parameter $\alpha \in \mathbb{R}$. For each quadrature rule, the estimate of the integral is given by.	80
6.4	See Figure 6.3.	90
6.5	Figure caption.	90
C.1	The potential scale reduction factor compares between- and within-estimates of univariate parameters. It is recommended only to use NUTS results if the value is less than 1.05, which it is for all parameters.	110

List of Tables

5.1	HIV risk groups and HIV incidence rate ratios relative to AGYW with one cohabiting sexual partner. The incidence rate ratio for women with non-regular or multiple sexual partner(s) was derived from analysis of longitudinal data by Slaymaker et al. (2020). Among FSW, the incidence rate ratio (25.0, 13.0, 9.0, 6.0, 3.0) depended on the level of HIV incidence among the general population (<0.1%, 0.1-0.3%, 0.3-1.0%, 1.0-3.0%, >3.0%), such that higher local HIV incidence in the general population corresponded to a lower incidence rate ratio for FSW. Estimates of HIV incidence rate ratios for FSW were derived by UNAIDS based on patterns of relative HIV prevalence among FSW compared to general population prevalence.	40
5.2	Four multinomial regression models were considered. Observation random effects θ_{ita} , included in all models, are omitted from this table.	46
5.3	Applying sum-to-zero constraints to interaction effects ensures that the main effect is not interfered with.	50
5.4	CPO, DIC, and WAIC values for the multinomial logistic regression model with corresponding standard errors.	51
5.5	Six logistic regression models were considered. The covariate <code>cfswever</code> denotes the proportion of men who have ever paid for sex and <code>cfswrecent</code> denotes the proportion of men who have paid for sex in the past 12 months.	52
5.6	CPO, DIC, and WAIC values for the logistic regression model with corresponding standard errors.	53
B.1	Prioritisation strata according to HIV incidence in the general population and behavioural risk.	99
B.2	Commitments to be met for each intervention in terms of proportion of the prioritisation strata reached. The symbol "-" represents no commitment.	99
B.3	All of the surveys that used in the analysis and their sample sizes, disaggregated by respondent age.	102

List of Tables

B.4 All of that surveys that were excluded from the analysis.	102
B.5 The numer of areas and analysis levels for each country that were used in the analysis.	102
B.6 The survey questions included in AIDS Indicator Survey (AIS) and Demographic and Health Surveys (DHS).	103
B.7 The survey questions included in Population-Based HIV Impact Assessment (PHIA) surveys.	103
C.1	106
C.2	107

List of Abbreviations

HIV	Human Immunodeficiency Virus.
AIDS	Acquired ImmunoDeficiency Syndrome.
PEPFAR	President’s Emergency Plan for AIDS Relief.
Global Fund	Global Fund to Fight AIDS, Tuberculosis, and Malaria.
HIV	Demographic and Health Surveys.
AIS	AIDS Indicator Survey.
PrEP	Pre-Exposure Prophylaxis.
PEP	Post-Exposure Prophylaxis.
FSW	Female Sex Worker(s).
MSM	Men who have Sex with Men.
PWID	People Who Inject Drugs.
ANC	Antenatal Clinic.
UNAIDS	United Nations Joint Programme on HIV/AIDS.
CDC	Centers for Disease Control and Prevention.
UAT	Unlinked Anonymous Testing.
PMTCT	Prevention of Mother-to-Child Transmission.
PLHIV	People Living with HIV.
MCMC	Markov Chain Monte Carlo.
VI	Variational Inference.
INLA	Integrated Nested Laplace Approximation.
GP	Gaussian Process.
CAR	Conditionally Auto-regressive.
ICAR	Intrinsic Conditionally Auto-regressive.
ART	Antiretroviral Therapy.
SAE	Small-Area Estimation.

List of Abbreviations

GMRF	Gaussian Markov Random Field.
HMC	Hamiltonian Monte Carlo.
GMRF	Gauss-Markov Random Field.
HMC	Hamiltonian Monte Carlo.
LGM	Latent Gaussian Model.
ELGM	Extended Latent Gaussian Model.
DIC	Deviance Information Criterion.
BIC	Bayesian Information Criterion.
WAIC	Watanabe-Akaike Information Criterion.
ESS	Effective Sample Size.
IID	Independent and Identically Distributed.
PPL	Probabilistic Programming Language.
CCD	Central Composite Design.
EB	Empirical Bayes.

List of Notations

\propto	Proportional to.
\mathbb{R}	The set of real numbers.
\mathbb{Z}	The set of integers.
\mathbb{Z}^+	The set of positive integers.
ρ	HIV prevalence.
λ	HIV incidence.
α	ART coverage.
\mathcal{S}	Spatial study region $\mathcal{S} \subseteq \mathbb{R}^2$.
$s \in \mathcal{S}$	Point location.
\mathcal{T}	Temporal study period $\mathcal{T} \subseteq \mathbb{R}$.
$t \in \mathcal{T}$	Time.
\mathbf{y}	Data, a n -vector (y_1, \dots, y_n) .
$\boldsymbol{\phi}$	Parameters, a d -vector (ϕ_1, \dots, ϕ_d) .
\mathbf{x}	Latent field, a N -vector (x_1, \dots, x_N) .
$\boldsymbol{\theta}$	Hyperparameters, a m -vector $(\theta_1, \dots, \theta_m)$.
$x \sim p(x)$	x has the probability distribution $p(x)$.
A_i	Areal unit.
$A_i \sim A_j$	Adjacency between areal units.
\mathbf{H}	Hessian matrix.
\mathbf{R}	Structure matrix.
\mathbf{Q}	Precision matrix.
$\boldsymbol{\Sigma}$	Covariance matrix.
\mathcal{N}	Gaussian distribution.
$k : \mathcal{X} \times \mathcal{X} \rightarrow \mathbb{R}$	Kernel function on the space \mathcal{X} .
$A_i \sim A_j$	Adjacency between areal units.

List of Notations

- \mathcal{Q} A set of quadrature nodes.
- $\omega : \mathcal{Q} \rightarrow \mathbb{R}$. . . A quadrature weighting function.
- $\mathcal{Q}(m, k)$. . . Gauss-Hermite quadrature points in m dimensions with k nodes per dimension, constructed according to a product rule.
- φ A standard (multivariate) Gaussian density.

1

Introduction

This thesis is about applied and methodological Bayesian statistics. It is applied and methodological in that I am concerned with real world questions and the means to answer them. The statistical approach is Bayesian because I used probability theory to arrive at conclusions based on models for observed data.

The real world questions are related to strategic information for planning the human immunodeficiency virus (HIV) epidemic response in sub-Saharan Africa (SSA). Over 40 years since the beginning of the epidemic, HIV is the largest annual cause of disability adjusted life years (DALYs) in SSA among non-infants [Global Burden of Disease Collaborative Network (2019); Figure 1.1]. Quantification of the epidemic using statistics is an important part of the public health response. Effective implementation of both HIV prevention and treatment requires strategic information. However, producing suitable estimates of relevant indicators is challenging.

The data I use were recorded from national household surveys or routinely collected from healthcare facilities providing HIV services. An important feature of these data are the location and time at which each observation was recorded. While diverse, spatio-temporal data have distinctive recurring commonalities across application settings. As a result, the work in this thesis both makes use of, and aspires to contribute to, modelling techniques from spatio-temporal statistics.

Introduction

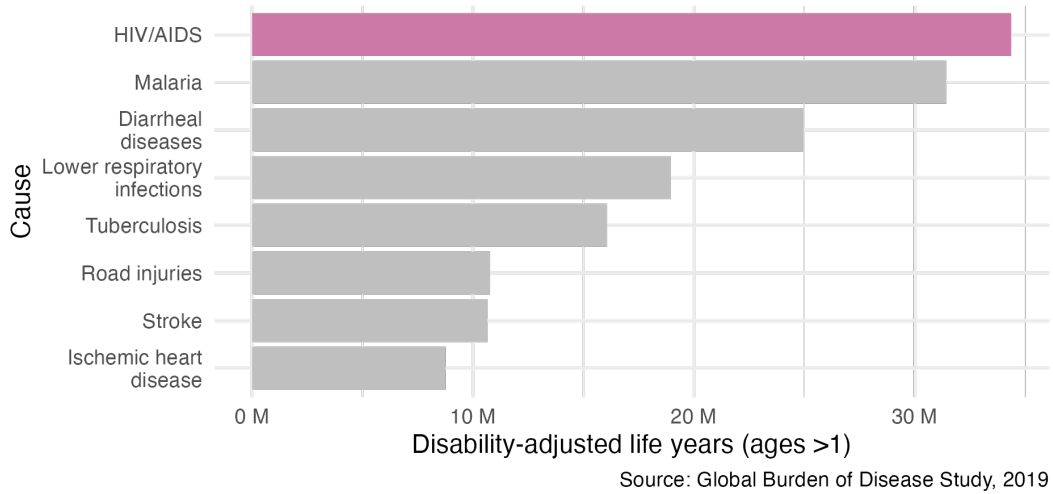


Figure 1.1: HIV/AIDS is the largest cause of annual DALYs among individuals aged >1 year in SSA (Global Burden of Disease Collaborative Network 2019). One DALY represents the loss of the equivalent of one year of full health, and is calculated by the sum of years of life lost and years lost due to disability. The disability weights vary between 0 (full health) and 1 (death) depending on severity of the condition.

Computation is an essential part of modern statistical practice. Each project in this thesis, and the thesis itself, is accompanied by R (R Core Team 2022) code, hosted on GitHub at <https://github.com/athowes>.

1.1 Chapter overview

This thesis is structured as follows:

- Chapter 2 provides an overview of the HIV/AIDS epidemic, and describing the challenges faced by disease surveillance efforts.
- Chapter 3 introduces the statistical concepts and notation used throughout the thesis, focusing on Bayesian modelling and computation, spatio-temporal statistics, and survey methods.
- Chapter 4: The prevailing model for spatial structure used in small-area estimation (Besag et al. 1991) was intended to analyse a grid of pixels. In disease mapping, we work using the districts of a country, which are typically not a grid. I evaluated the practical consequences of this concern (Howes, Eaton, et al. 2023+).

Introduction

- Chapter 5: Adolescent girls and young women are a demographic group at disproportionate risk of acquiring HIV infection. The Global AIDS Strategy recommends prioritising interventions on the basis of behaviour to prevent the most new infections using available resources. I estimated the size of behavioural risk groups across priority countries to enable implementation of this strategy, and assessed the potential benefits in terms of numbers of new infections prevented (Howes, Risher, et al. 2023). This work was included in the UNAIDS Global AIDS Update 2022 and 2023.
- Chapter 6: The Naomi small-area estimation model (Eaton et al. 2021) is used by countries to estimate district-level HIV indicators. With this model in mind, I developed an approximate Bayesian inference method combining adaptive Gauss-Hermite quadrature with principal components analysis (Howes, Stringer, et al. 2023+). I applied the method to data from Malawi, and analysed the consequences of inference method choice for policy relevant outcomes. Further, I open the door to a new class of fast, flexible, and accurate Bayesian inference algorithms.
- Chapter 7: Finally, I discuss avenues for future work, and my conclusions regarding the research, as well as its strengths and weaknesses.

Though chronological order is recommended, Chapters 4, 5 and 6 may be read in any order.

2

The HIV/AIDS epidemic

2.1 Background

HIV is a retrovirus which infects humans. If untreated, HIV can develop into a more advanced stage known as acquired immunodeficiency syndrome (AIDS). HIV primarily attacks a type of white blood cell vital for the function of the immune system. As a result, AIDS is characterised by increased risk of developing opportunistic infections such as tuberculosis or *Pneumocystis* pneumonias, which can result in death.

The first AIDS cases were reported in Los Angeles in the early 1980s (Gottlieb et al. 1981; Barré-Sinoussi et al. 1983). Since then, HIV has spread globally. Transmission occurs by exposure to specific bodily fluids of an infected person. The most common mode of transmission is via unprotected anal or vaginal sex, though transmission can also occur from a mother to her baby, or when drug injection equipment is shared. Approximately 86 million people have become infected with HIV, and of those 40 million have died of AIDS-related causes.

An ongoing global and multifaceted effort has been made to respond to the epidemic. The response has been shaped by local communities, civil society organisations, national governments, research institutions, pharmaceutical companies, international agencies like the Joint United Nations Programme on HIV/AIDS

The HIV/AIDS epidemic

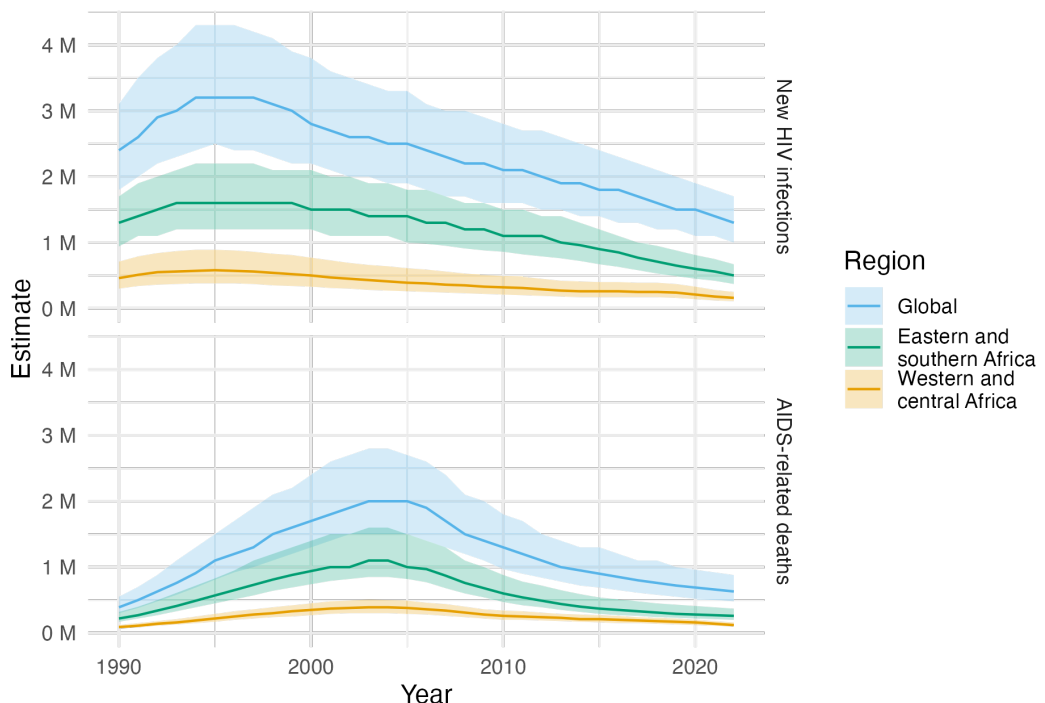


Figure 2.1: Globally, yearly new HIV infections peaked in 1995, and have since decreased by 59% and yearly AIDS-related deaths peaked in 2004, and have since decreased by 68% (UNAIDS 2023a). Much of the disease burden is concentrated in eastern and southern Africa, as well as western and central Africa.

(UNAIDS), and global health initiatives such like the President's Emergency Plan for AIDS Relief (PEPFAR) and the Global Fund to Fight AIDS, Tuberculosis, and Malaria (the Global Fund). To give an indication as to the scale of the response, the investment of \$100 billion by PEPFAR constitutes the “largest commitment by a single nation to address a single disease in history” (U.S. Department of State 2022).

Implementation of HIV prevention and treatment has significantly reduced the number of new HIV infections and AIDS-related deaths per year since their peak (Figure 2.1). The most significant evidence-based interventions, in chronological order, are described below:

- Condoms are an inexpensive and effective method for prevention of HIV and other sexually transmitted infections (STIs) such as *Chlamydia trachomatis*, *Neisseria gonorrhoeae*, syphilis, and *Trichomonas vaginalis*. Condom usage has increased significantly since 1990, which is estimated to have averted 117

The HIV/AIDS epidemic

million new HIV infections (Stover and Teng 2021). That said, there remain significant and difficult to close gaps in condom usage.

- Antiretroviral therapy (ART) is a combination of drugs which stop the virus from replicating in the body. A person living with HIV who takes ART daily can live a full and healthy life, transforming what was once a terminal illness to a treatable chronic condition. Of the 39 million people living with HIV (PLHIV) in 2022, around 76% were accessing ART. A staggering 21 million AIDS-related deaths are estimated to have been averted by ART (UNAIDS 2023b). ART reduces the amount of virus in the blood and genital secretions. If the virus is undetectable then there is significant evidence that it cannot be transmitted sexually (Cohen et al. 2011; Broyles et al. 2023). For this reason, in addition to providing life saving treatment, ART also operates as prevention. Particular efforts have been made to provide pregnant women with ART to reduce the chance of mother-to-child transmission (MTCT) (Siegfried et al. 2011).
- Voluntary medical male circumcision (VMMC) partially protects against female-to-male HIV acquisition. Three landmark randomised control trials (Auvert et al. 2005; Gray et al. 2007; Bailey et al. 2007) found complete surgical removal of the foreskin to result a reduction of HIV acquisition in men by 50-60%. Based on this evidence, VMMC has been recommended since 2007 by the World Health Organization (WHO) and UNAIDS as a key HIV intervention in high-prevalence settings. Scale up of VMMC across 15 priority countries between 2008 and 2019 is estimated to have already averted 340 thousand new HIV infections, though the future number of new HIV infections averted is likely to be much higher.
- Pre-exposure prophylaxis (PrEP) and post-exposure prophylaxis (PEP) are antiretroviral drugs which can be taken before and after exposure to prevent transmission. PrEP and PEP are more costly than some other prevention options, so primarily useful in high risk settings.

The HIV/AIDS epidemic

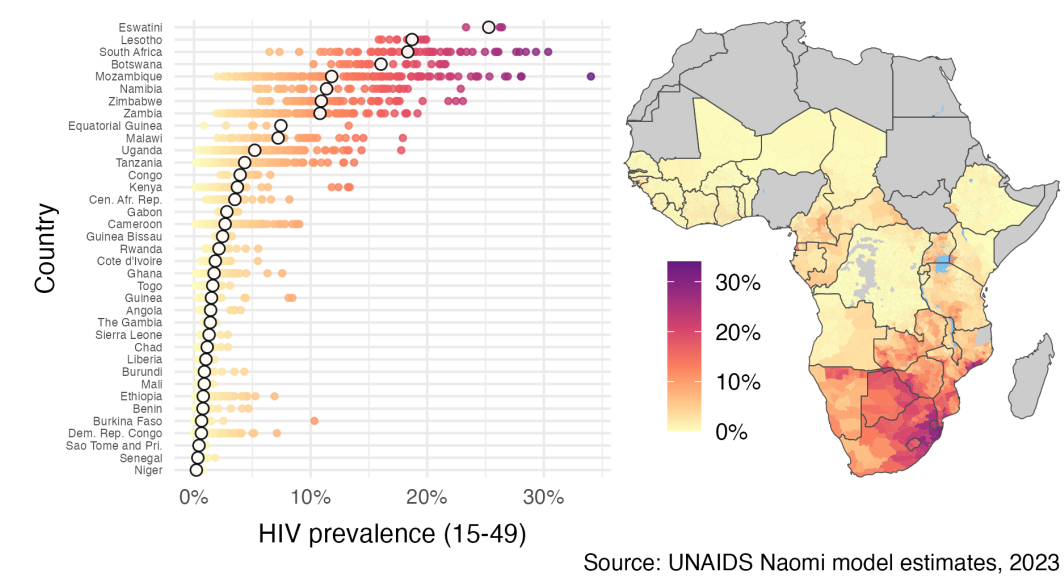


Figure 2.2: Adult (15-49) HIV prevalence varies substantially both within and between countries in SSA. These estimates from 2023 were generated by country teams using the Naomi small-area estimation model in a process supported by UNAIDS and are available from UNAIDS (2023a). White filled points are country-level estimates, and coloured points are district-level estimates. Results from Nigeria were not published. Data collection in the Cabo Delgado province of Mozambique was disrupted by conflict. Obtaining results for the Democratic Republic of the Congo required removing some districts from the model. Country names are given by three-letter codes as published by the International Organization for Standardization (ISO).

Though important progress had been made, there remains much more to do. In 2022, 1.3 million people were newly infected with HIV and there were 630 thousand AIDS-related deaths, more than one every minute (UNAIDS 2022). Bold fast-track targets have been set to accelerate the end of AIDS as global public health threat by 2030. Renewed commitments are required to meet these targets in the context of disruption to HIV services caused by the COVID-19 pandemic and a potential shortfall in HIV funding (Economist Impact 2023).

For available resources to have the greatest impact, it is important that the right HIV interventions are prioritised to the right populations, in the right place, and at the right time. This paradigm has been described as precision public health (Khoury

The HIV/AIDS epidemic

et al. 2016) at a population-level, by analogy to precision medicine at the individual-level. Differences in cost-effectiveness can be vast, with some interventions orders of magnitude more impactful than others (Ord 2013).

Disease burden varies substantially across multiple spatial scales. In some countries, the epidemic is concentrated in small populations, and national HIV prevalence is low. In others, the epidemic is sustained by heterosexual transmission, and national HIV prevalence is higher (typically >1%) These two epidemic settings are described as concentrated and generalised respectively (Tanser et al. 2014). Most of the countries severely affected by HIV are in sub-Saharan Africa (SSA). It is estimated that 66% of the 39 million PLHIV worldwide live in SSA. Adult HIV prevalence (ages 15-49) is higher than 10% (Figure 2.2) in some countries in southern Africa. Just as there is variation between countries, there is variation within countries. For example, adult HIV prevalence at the district municipality level in South Africa ranges from 6% in Namakwa to 30% in uMkhanyakude.

In all countries and contexts, some groups of people are at much higher risk than others. Groups of people at increased risk of HIV infection are known as key populations (KPs). Examples include men who have sex with men (MSM), female sex workers (FSW), people who inject drugs (PWID), and transgender people (TGP) (Stevens, Sabin, Garcia, et al. 2022). KPs are often marginalised, and face legal and social barriers. In concentrated settings, the majority of new HIV infections occur in KPs and their sexual partners. In generalised settings like SSA, risk is more diffuse across the population. For example, in SSA adolescent girls and young women (AGYW) are a large demographic group at increased risk of HIV infection (Risher et al. 2021; Monod et al. 2023) but not typically considered a KP.

2.2 HIV surveillance

HIV surveillance refers to the collection, analysis, interpretation and dissemination of data relating to HIV/AIDS. Surveillance can used to track epidemic indicators,

The HIV/AIDS epidemic

identify at-risk populations, find drivers of transmission, and evaluate the impact of prevention and treatment programs. Important indicators include:

- **HIV prevalence** is the proportion $\rho \in [0, 1]$ of the population who have HIV, typically written as a percentage. Both new infections and more PLHIV remaining alive by taking treatment increase HIV prevalence. As such, HIV prevalence should not be interpreted in isolation, and is primarily used indirectly to calculate other indicators. That said, in some circumstances when other indicators are difficult to estimate, HIV prevalence can be a useful proxy. The number of PLHIV is given by $N\rho$, where N is the population size.
- **HIV incidence** is the rate $\lambda \in \mathbb{R}$ of new HIV infections, typically written as number of new infections per 1000 person years. HIV incidence can be specified in terms of the change in HIV prevalence over some time period $\lambda = \Delta\rho/\Delta t$. Planning, delivery, and evaluation of prevention programming relies on estimates of HIV incidence. The number of new HIV infections is given by $N(1 - \rho)\lambda$.
- **ART coverage** is the proportion $\alpha \in [0, 1]$ of PLHIV who are on ART, typically written as a percentage. Estimates of ART coverage play a direct role in the provision of treatment services. The number of people taking ART is given by $N\rho\alpha$.

2.2.1 Data

What are the current data? What are the current approaches to using the data?

2.2.2 Challenges

Obtaining reliable, timely estimates at an appropriate spatial resolution is challenging. The most significant difficulties faced are:

1. **Data sparsity:** Collection of data is costly and time consuming. As a result, limited direct data might be available for the particular time, location, and

The HIV/AIDS epidemic

sub-population of interest. For example, in many countries the last conducted household survey is several years out of date.

2. **Missing data:** The sampling frame of a survey may not correspond to the target population. For example, many KPs are difficult to reach, and may be omitted from sampling frames. Individuals included on the sampling frame may choose not to respond. All surveys are subject to sampling error, as only a subset of the target population are sampled. Each of these issues can be characterised as being problems of missing data. I characterise missing data as referring to the shortfalls of any given study, and data sparsity as referring to limited availability of studies.
3. **Response and measurement biases:** Individuals may be hesitant to disclose their HIV status, or report higher risk behaviours, due to social desirability bias or a fear of discrimination or stigma. When available, biomarker data can be used to overcome under-reporting, but still may be subject to measurement errors.
4. **Denominators and demography:** Many indicators are rates or proportions, which rely on estimates of the population at risk in the denominator. Accurately estimating population denominators is itself a challenging task (Tatem 2017). Taking a ratio of uncertain quantities amplifies uncertainty, but is rarely properly accounted for.
5. **Inconsistent data collection and reporting:** The types of data that are collected might vary across space and time. Reporting protocols or definitions can also change.
6. **Reliance on epidemiological parameters:** Indicators rely on estimates of epidemiological parameters such as rates of disease progression. These parameters are typically obtained from cohort studies and may not generalise to the setting of interest. Further, they are typically applied coarsely, and without proper accounting for uncertainty.

2.2.3 Statistical approaches

The challenges above make direct interpretation of the data often misleading or impossible. Careful statistical modelling is required to overcome these limitations as best as possible.

1. **Borrowing information:** When little direct data are available, data judged to be indirectly related can be used to help improve estimation. For example, if limited data are available for individuals of a certain age in a particular country, it is likely reasonable to make use of data for individuals of a similar age in that country. As well as over age groups, information can be borrowed between and within countries, and across times.
2. **Evidence synthesis:** Multiple sources of evidence can be combined to overcome the limitations of any one data source. For example, infrequently run household surveys can be complemented by up to date programmatic data.
3. **Expert guidance:** Expert epidemiological, demographic, and local stakeholder guidance can be used to improve estimates. Ensuring the quality of any data used in the estimation process is essential.
4. **Uncertainty quantification:**

2.2.4 Future directions

Aims for HIV response going forward, and the surveillance capabilities needed to meet them:

1. **Greater reliance on routine health system data:** It is not recommended to include HIV testing in nationally representative household surveys in low (<2%) HIV prevalence settings (World Health Organization 2005). Patient-level HIV data systems (World Health Organization 2017) and case-based surveillance (CBS). Integration of HIV services with other health programs and strengthening of health systems.

3

Bayesian spatio-temporal statistics

3.1 Bayesian statistics

Bayesian statistics is a mathematical paradigm for learning information from data. It is especially well suited to facing the challenges posed by Section 2.2 because it allows for principled and flexible integration of prior domain knowledge. Additionally, uncertainty over all unknown quantities is handled as an integral part of the Bayesian paradigm. This section provides a brief and opinionated overview. For a more complete introduction, I recommend Gelman, Carlin, et al. (2013), McElreath (2020) or Gelman, Vehtari, et al. (2020).

3.1.1 Bayesian modelling

The Bayesian approach to data analysis is based on construction of a probability model for the observed data $\mathbf{y} = (y_1, \dots, y_n)$ together with parameters $\boldsymbol{\phi} = (\phi_1, \dots, \phi_d)$. Choice of the particular parameters used depends upon the requirements of the analysis. All quantities are assumed to be random variables, and the model is written as $p(\mathbf{y}, \boldsymbol{\phi})$, where $p(\cdot)$ denotes a probability distribution. Subsequent calculations are based on manipulation of this model using probability theory.

Models can be most naturally constructed from two parts, known respectively as the likelihood $p(\mathbf{y} | \boldsymbol{\phi})$ and the prior distribution $p(\boldsymbol{\phi})$. The joint distribution

is obtained by the product $p(\mathbf{y}, \boldsymbol{\phi}) = p(\mathbf{y} | \boldsymbol{\phi})p(\boldsymbol{\phi})$. The likelihood, as a function of $\boldsymbol{\phi}$ with \mathbf{y} fixed, reflects the probability of observing the data when the value of the parameters is $\boldsymbol{\phi}$. The prior distribution encapsulates beliefs about the parameters $\boldsymbol{\phi}$ before the data are observed.

Recommendations for specifying prior distributions vary. The extent to which subjective information should be incorporated into the prior distribution, and in doing so influence the posterior distribution, is a central topic of discussion. Proponents of the objective Bayesian paradigm (Berger 2006) put forward that the prior distribution should be non-informative, so as not to introduce subjectivity into the analysis. That said, we shall see in Section 3.3 that the distinction between likelihood and prior distribution can be unclear. As such, it may be argued that issues of subjectivity are not unique to the prior distribution, and ultimately the challenge of specifying the data generating process is better thought of more holistically.

The probability model can be simulated from to obtain samples $(\mathbf{y}, \boldsymbol{\phi}) \sim p(\mathbf{y}, \boldsymbol{\phi})$. If the samples of \mathbf{y} differ too greatly from what the analyst would expect, then the model does not capture their prior scientific understanding of the data. Models which do not produce plausible samples can be refined. Checks of this kind [Gelman, Carlin, et al. (2013); Chapter 6] can be used to help iteratively build models, adding complexity gradually as required.

3.1.2 Bayesian computation

The primary goal in a Bayesian analysis is to obtain the posterior distribution $p(\boldsymbol{\phi} | \mathbf{y})$. This distribution encapsulates probabilistic beliefs about the parameters given the observed data, and has a central role in use of the analysis for decision making. Using the eponymous Bayes' theorem, the posterior distribution is obtained by

$$p(\boldsymbol{\phi} | \mathbf{y}) = \frac{p(\mathbf{y}, \boldsymbol{\phi})}{p(\mathbf{y})} = \frac{p(\mathbf{y} | \boldsymbol{\phi})p(\boldsymbol{\phi})}{p(\mathbf{y})}. \quad (3.1)$$

Unfortunately, most of the time it is intractable to calculate the posterior distribution analytically. This is because of the potentially high-dimensional integral

$$p(\mathbf{y}) = \int p(\mathbf{y}, \boldsymbol{\phi}) d\boldsymbol{\phi} \quad (3.2)$$

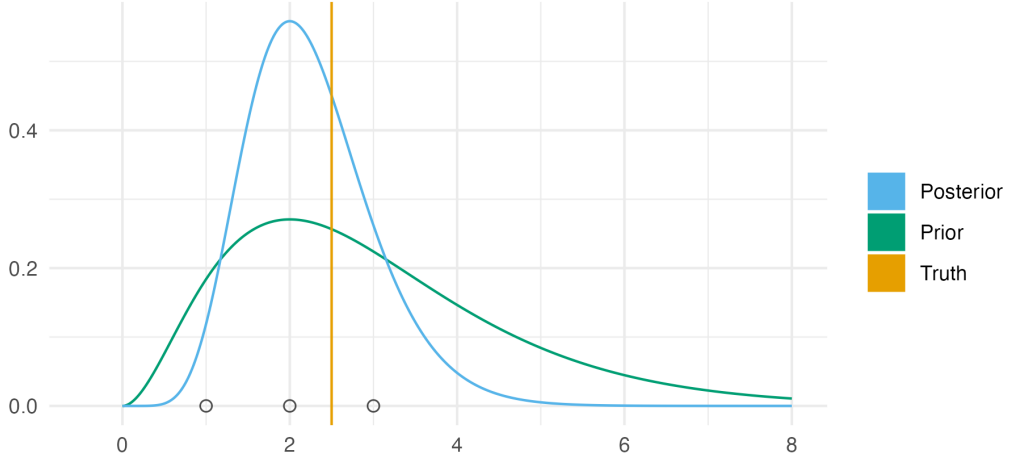


Figure 3.1: An example of Bayesian modelling and computation for a simple one parameter model. Here the likelihood is $y_i \sim \text{Poisson}(\phi)$ for $i = 1, 2, 3$ and prior distribution on the rate parameter is $\phi \sim \text{Gamma}(3, 1)$. I simulated observed data $\mathbf{y} = (1, 2, 3)$ from the distribution $\text{Poisson}(2.5)$. As such, the true data generating process is within the space of models being considered (This situation is sometimes known (Bernardo and Smith 2001) as the \mathcal{M} -closed world, in contrast to the \mathcal{M} -open world where the model is said to be misspecified.) Furthermore, the posterior distribution is available in closed form as $\text{Gamma}(9, 4)$. This is because the posterior distribution is in the same family of probability distributions as the prior distribution, and the model is described as being conjugate. Conjugate models are often used because of their convenience. Though other models may be more suitable, they will typically be more computationally demanding. In this situation, which is typical, the posterior distribution is more tightly peaked than the prior distribution.

in the denominator of Equation (3.1). The evidence $p(\mathbf{y})$ quantifies the probability of obtaining the data under the model, and... TODO. As such, although it is easy to evaluate a quantity proportional to the posterior distribution

$$p(\phi | \mathbf{y}) \propto p(\mathbf{y} | \phi)p(\phi), \quad (3.3)$$

it is typically difficult to evaluate the posterior distribution itself.

The difficulty in performing Bayesian inference in general may be thought of as analogous to the difficulty in calculating integrals. As with integration, in some cases closed form analytic solutions are available. Figure 3.1 illustrates one such case, where the prior distribution and posterior distribution are in the same family of probability distributions. For the more general case where no analytic solution is available, computational methods have been developed to approximate the posterior

distribution (Martin et al. 2023). These methods may broadly be divided into Monte Carlo algorithms, and deterministic approximations.

Monte Carlo algorithms

Monte Carlo algorithms (Robert and Casella 2005) aim to generate samples from the posterior distribution

$$\boldsymbol{\phi}_i \sim p(\boldsymbol{\phi} | \mathbf{y}), \quad i \in 1, \dots M. \quad (3.4)$$

These samples may be used in any future computations involving functions of the posterior distribution. For example, if $G = G(\boldsymbol{\phi})$ then the expectation of G with respect to the posterior distribution can be approximated by

$$\mathbb{E}(G | \mathbf{y}) = \int G(\boldsymbol{\phi}) p(\boldsymbol{\phi} | \mathbf{y}) d\boldsymbol{\phi} \approx \frac{1}{M} \sum_{i=1}^M G(\boldsymbol{\phi}_i). \quad (3.5)$$

Most quantities of interest can be cast as posterior expectations.

Markov chain Monte Carlo (MCMC) methods (Roberts and Rosenthal 2004) are the most popular class of sampling algorithms. Using MCMC, samples are generated from by simulating from an ergodic Markov chain with the posterior distribution as its stationary distribution. The Metropolis-Hastings [MH; Metropolis et al. (1953); Hastings (1970)] algorithm uses a proposal distribution $q(\boldsymbol{\phi}_{i+1} | \boldsymbol{\phi}_i)$ to generate candidate parameters for the next step in the Markov chain. Many MCMC algorithms, including the Gibbs sampler, are special cases of MH.

Other notable classes of sampling algorithms include importance sampling (IS) methods, in which the samples are weighted, and sequential Monte Carlo [SMC; Chopin, Papaspiliopoulos, et al. (2020)] methods based on sampling from a sequence of distributions. Though these methods have found applications in specific domains, MCMC is more widely used because of its generality and theoretical reliability.

In this thesis, I use the No-U-Turn sampler [NUTS; Hoffman, Gelman, et al. (2014)], a Hamiltonian Monte Carlo [HMC; Duane et al. (1987); Neal et al. (2011)] algorithm, as implemented in the Stan (Carpenter et al. 2017) probabilistic programming language (PPL). HMC uses derivatives of the posterior distribution to

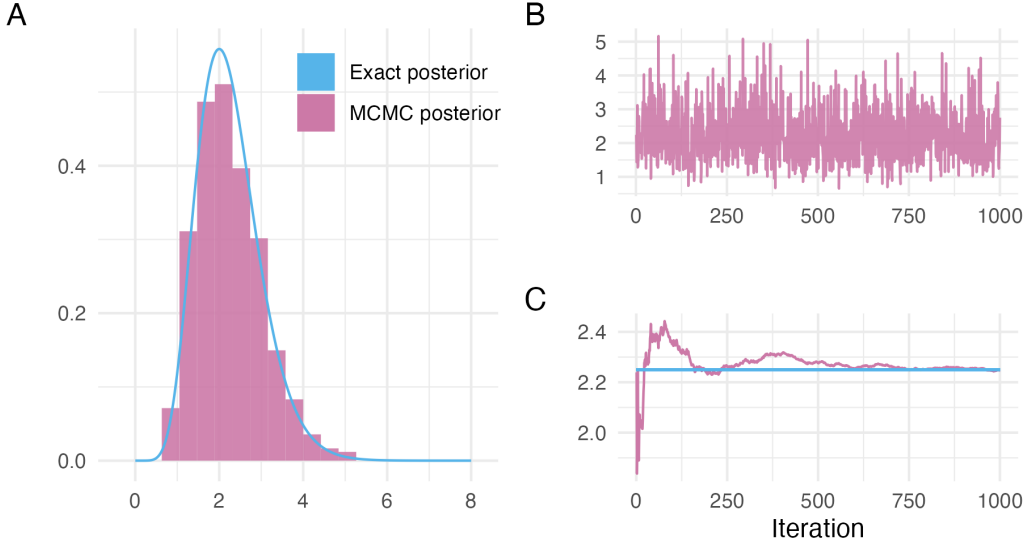


Figure 3.2: NUTS can be used to sample from the posterior distribution in the example of Figure 3.1. Panel A shows a histogram of the NUTS samples as compared to the true posterior. Panel B shows a traceplot. Panel C shows the convergence of the empirical posterior mean to the true value.

generate efficient Metropolis-Hastings proposal distributions based on Hamiltonian dynamics. NUTS automatically adapts the tuning parameters of HMC based local properties of the posterior distribution. Though not a one-size-fits-all solution, NUTS has been shown empirically to be a good choice for sampling from a range of posterior distributions.

After running an MCMC sampler, it is important to check diagnostics to assess accuracy and evaluate convergence. Panel B of Figure 3.2 shows a traceplot for a Markov chain which has converged.

Deterministic approximations

In variational inference [VI; Blei et al. (2017)] the approximate posterior distribution is assumed to belong to a particular family of functions. Optimisation algorithms are used to choose the best member of that family, typically by minimising the Kullback-Leibler divergence to the posterior distribution. VI is typically faster than Monte Carlo methods, especially for large datasets or models. However, it lacks theoretical guarantees and is known to often inaccurately estimate posterior variances

(Giordano et al. 2018). Developing diagnostics to evaluate the accuracy of VI is an important area of ongoing research (Yao et al. 2018). The expectation maximisation [EM; “Maximum likelihood from incomplete data via the EM algorithm” (1977)] and expectation propagation [EP; Minka (2001)] algorithms are closely related to VI.

Need to talk about: Laplace approximation. Quadrature. Integrated nested Laplace approximation. Unsure how much detail to go into here given that these approximations are the subject of Chapter 6.

3.1.3 Interplay between modelling and computation

Modern computational techniques and software like PPLs have succeeded in abstracting away calculation of the posterior distribution from the analyst for many models. However, computation remains intractable in the majority of cases. As such, the analyst need not only to be concerned with choosing a model suitable for the data, but also choosing a model for which the posterior distribution is tractable in reasonable time. As such, there is an important interplay between modelling and computation, wherein models are bound by the limits of computation. As computation improves, the space of models available to the analyst expands.

3.2 Spatio-temporal statistics

Spatio-temporal statistics (Cressie and Wikle 2015) concerns observations which are indexed by spatial or temporal location. In doing so, it unites the fields of spatial statistics (Bivand et al. 2008) and time series analysis (Shumway and Stoffer 2017).

3.2.1 Properties of spatio-temporal data

Spatio-temporal data have some important properties:

1. **Covariance structure:** According to Tobler’s first law of geography “everything is related to everything else, but near things are more related than distant things” (Tobler 1970). In “The Design of Experiments” Fisher (1936) observed that neighbouring crops were more likely to have similar yields than

Bayesian spatio-temporal statistics

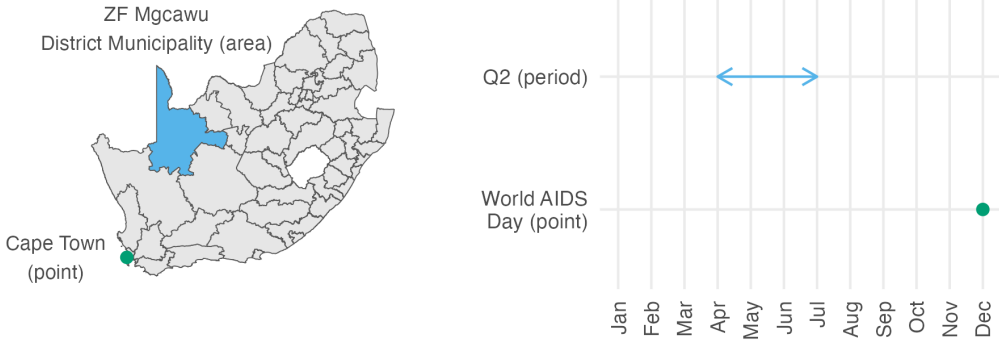


Figure 3.3: The spatial location of Cape Town in South Africa could be considered a point. The ZF Mgawu District Municipality on the other hand is an example of an area. World AIDS Day, designated on the 1st of December every year, could be considered a point in time. The second fiscal quarter, running through April, May and June, and denoted by Q2 represents a period of time. (In reality, both Cape Town and World AIDS Day are areas, rather than true point locations. Instances of infinitesimal point locations in everyday life are rare.)

those far apart. This law can be formalised using spatial covariance functions.

Spatial covariance functions are called isotropic when they apply equally in all directions, and stationary when they are invariant over space.

As well as space, an Tobler's first law applies to time. Observations made close together in time tend to be similar. Temporal covariance structures are often periodic.

The space-time covariance structure (Porcu et al. 2021) is said to be separable when it can be factorised as a product of individual spatial and temporal covariances, and nonseparable when it can't. A separable space-time covariance could have spatial and temporal components which are either independent and identically distributed (IID) or structured (Knorr-Held 2000).

Because of their covariance structure, spatio-temporal data are not IID. Only one observation of a spatio-temporal process is realised.

2. **Scales:** In this thesis I assume that the spatial study region $\mathcal{S} \subseteq \mathbb{R}^2$ has two dimensions, corresponding to latitude and longitude. Observations may be associated to a point $s \in \mathcal{S}$ or area $A \subseteq \mathcal{S}$ in the study region. The temporal

study period $\mathcal{T} \subseteq \mathbb{R}$ can more generally be assumed to be one dimensional. Together with time only moving forward, this feature is what distinguishes time from space. As with space, observations may be associated to a point $t \in \mathcal{T}$ or period of time $T \subseteq \mathcal{T}$. Figure 3.3 illustrates both types of observation for space and time.

As such, spatio-temporal observations can be made at various possible scales. Sometimes, we may want to model data at a scale it was not observed at. This is known as the change-of-support problem (Gelfand et al. 2001) and includes as special cases the problems of downscaling, upscaling, and dealing with so-called misaligned data. Closely related is the problem of wanting to jointly model data at different scales simultaneously.

3. **Size:** Data with both spatial and temporal dimensions are often large, making storage and operations on spatio-temporal data potentially difficult. Furthermore, models for spatio-temporal data typically require many parameters. Whereas large IID data can be modelled using a small number of parameters, each observation in a spatio-temporal dataset may need to be characterised by its own parameters. Large data combined with large models make Bayesian inference challenging.

3.2.2 Small-area estimation

Data always has a cost to collect. This cost can be significant, especially for data relating to people where collection is difficult to automate. As a result, given the large number of possible locations in space and time, often no or limited direct observations may be available for any given space-time location. Direct estimates of indicators of interest are either impossible or inaccurate in this setting.

Small-area estimation [SAE; Pfeffermann et al. (2013)] methods aim to overcome the limitations of small data by sharing information. In the spatio-temporal setting sharing of information occurs across space and time. The fact that observations in one spatio-temporal location are correlated with those at another can be used

to improve estimates. Figures 3.4 and 3.5 illustrate the unreliability of direct estimates from small sample sizes, and the way in which a spatial model may be used to overcome this limitation.

More generally, SAE methods are useful when data are limited for subpopulations of interest. These subpopulations could be generated by spatio-temporal variables, as well as by other variables such as demographics. Just as we expect there to be spatio-temporal correlation structure, we also can expect there to be demographic correlation structure. Those of the same sex are more likely to be similar, as are those of similar ages or socioeconomic strata.

3.3 Model structure

We have seen that in spatio-temporal statistics, observations are related to each other, and should not all be considered as IID. In this section, I will discuss ways in which these relationships can be encoded mathematically via the model structure.

3.3.1 Linear model

A linear model is given by

$$\begin{aligned} y_i &\sim \mathcal{N}(\mu_i, \sigma), \\ \mu_i &= \beta_0 + \sum_{l=1}^p \beta_l z_{li}, \\ \{\beta_j\} &\sim p(\{\beta_j\}), \\ \sigma &\sim p(\sigma). \end{aligned}$$

3.3.2 Generalised linear model

A generalised linear model (GLM) is given by. Things can then be removed from LGM, ELGM which are introduced here.

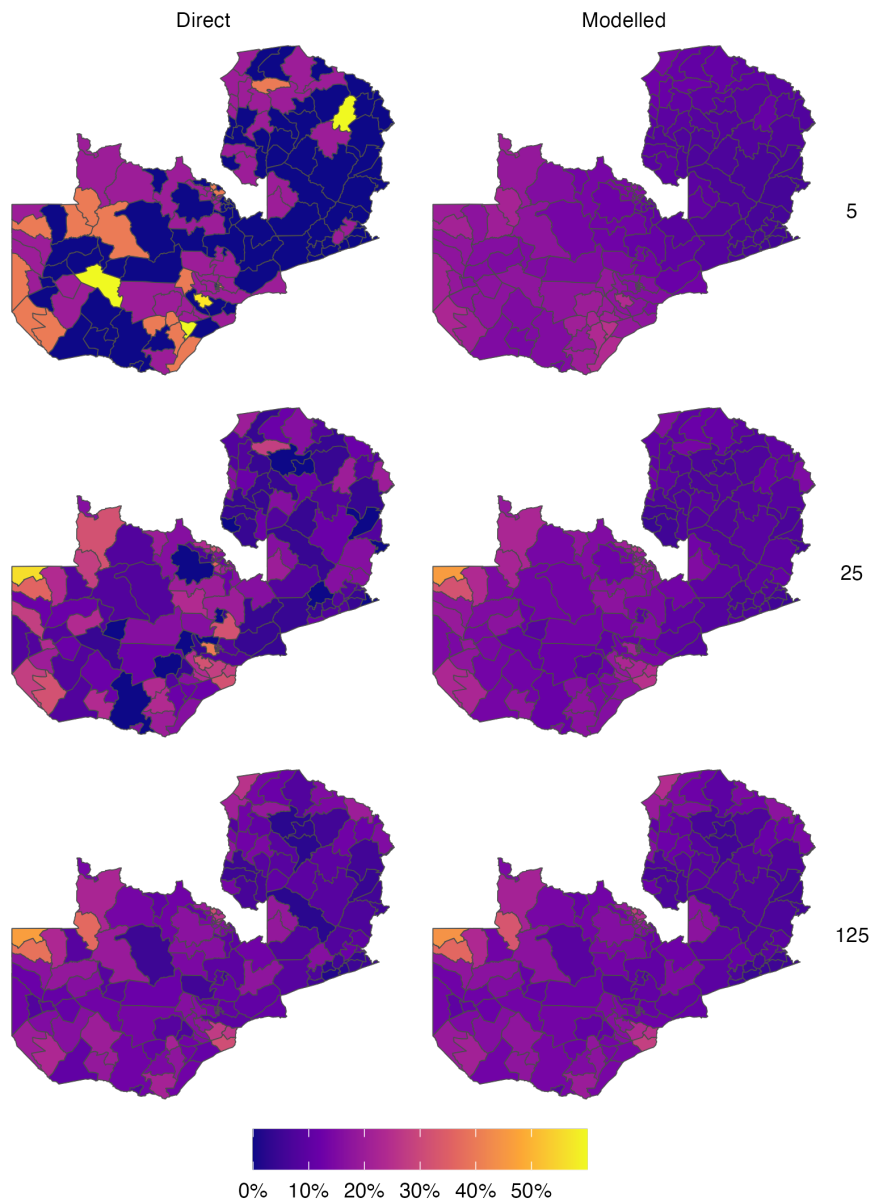


Figure 3.4: Simulation of a simple random sample $y_i \sim \text{Bin}(m, p_i)$ with varying sample size $m = 5, 25, 125$ in each of the $i = 1, \dots, 156$ constituencies of Zambia. Direct estimates were obtained by the ratio y_i/m . Modelled estimates were obtained using a logistic regression with linear predictor given by an intercept and a spatial random effect. HIV estimates for Zambia have previously been generated at the district-level, comprising 116 spatial units. Moving forward, there is interest in generating estimates at the higher-resolution constituency level, as program planning is devolved locally. This figure is adapted from a presentation I gave for the Zambia HIV Estimates Technical Working Group, available from <https://github.com/athowes/zambia-unaiads>.

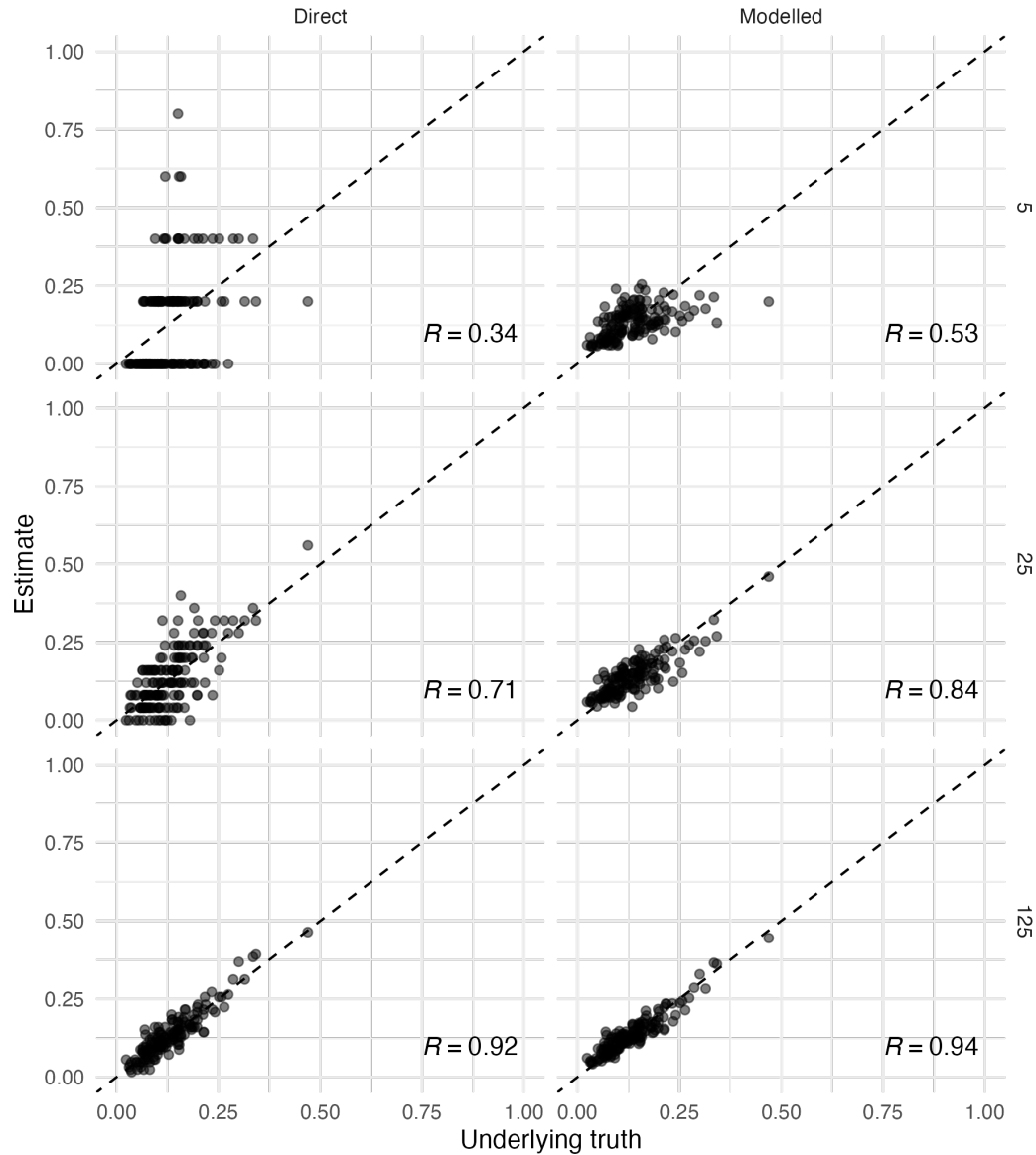


Figure 3.5: The setting of this figure matches that of Figure 3.4. Estimates from surveys with higher sample size have higher Pearson correlation coefficient R with the underlying truth. For a fixed sample size, correlation can be improved by using modelled estimates to borrow information across spatial units, rather than using the higher variance direct estimates. Points along the dashed diagonal line correspond to agreement between the estimate obtained from the survey and the underlying truth used to generate the data. For each sample size, using a spatial model increases the correlation between the estimates and underlying truth.

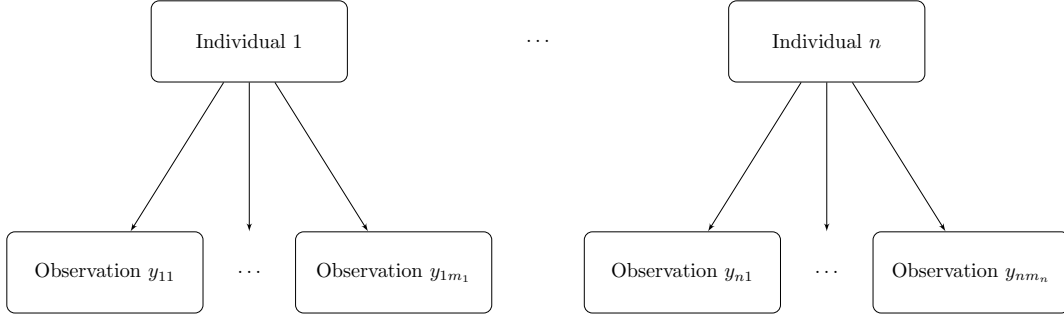


Figure 3.6: A simple example of group structure within data in which each individual $i = 1, \dots, n$ is associated to m_i observations y_{i1}, \dots, y_{im_i} .

3.3.3 Hierarchical models

Group structure is a simple, binary way in which observations are related. Figure 3.6 illustrates a case in which each individual in a study is observed some number of times, and observations of the same individual are grouped together. Observations from the same individual are more likely to be similar than observations of different individuals. Groups can also be nested within other groups, as well as crossed with each other.

Consider three models for this data, each of which with a Gaussian likelihood:

1. **Complete pooling:** In the complete pooling model, group structure is ignored and all observations are treated as IID

$$y_{ij} \sim \mathcal{N}(\mu, \sigma), \quad (3.6)$$

$$(\mu, \sigma) \sim p(\mu, \sigma). \quad (3.7)$$

2. **No pooling:** Alternatively, the groups can be modelled entirely separately with group specific mean μ_i and standard deviation σ_i parameters

$$y_{ij} \sim \mathcal{N}(\mu_i, \sigma_i), \quad (3.8)$$

$$(\mu_i, \sigma_i) \sim p(\mu_i, \sigma_i). \quad (3.9)$$

3. **Partial pooling:** In this model, some amount of information is shared

between the groups

$$y_{ij} \sim \mathcal{N}(\mu_i, \sigma), \quad (3.10)$$

$$\mu_i = \beta + u_i, \quad (3.11)$$

$$\beta \sim p(\beta), \quad (3.12)$$

$$\mathbf{u} \sim p(\mathbf{u}), \quad (3.13)$$

$$\sigma \sim p(\sigma), \quad (3.14)$$

where the vector $\mathbf{u} = (u_1, \dots, u_n)$. The parameter β applies to all groups, and each group is differentiated by a specific value of u_i . When inference is performed for the partial pooling model, the extent to which information is shared between groups is learnt rather than fixed at the outset, as with the complete or no pooling models.

Bayesian hierarchical or multilevel models allow control over whether and how information is shared across groups. In a three-stage hierarchical model, the parameters are partitioned such that $\phi = (\mathbf{x}, \boldsymbol{\theta})$. The model for data \mathbf{y} is then

$$\mathbf{y} \sim p(\mathbf{y} | \mathbf{x}, \boldsymbol{\theta}), \quad (3.15)$$

$$\mathbf{x} \sim p(\mathbf{x} | \boldsymbol{\theta}), \quad (3.16)$$

$$\boldsymbol{\theta} \sim p(\boldsymbol{\theta}), \quad (3.17)$$

with posterior distribution proportional to $p(\mathbf{x}, \boldsymbol{\theta} | \mathbf{y}) \propto p(\mathbf{y} | \mathbf{x}, \boldsymbol{\theta})p(\mathbf{x} | \boldsymbol{\theta})p(\boldsymbol{\theta})$. I refer to $\mathbf{x} = (x_1, \dots, x_n)$ as the latent field, and $\boldsymbol{\theta} = (\theta_1, \dots, \theta_m)$ as the hyperparameters.

3.3.4 Generalised linear mixed effects model

Fixed effects refer to those elements of the latent field which are constant across groups. Random effects refer to those elements of the latent field which vary across groups. These terms have notoriously many different, and incompatible, definitions which can cause confusion (Gelman 2005). I nonetheless find them useful to introduce here.

For concreteness, in the partial pooling model above, the latent field is $\mathbf{x} = (\beta, u_1, \dots, u_n)$. The scalar β is a fixed effect which applies to all n groups. The vector \mathbf{u} are random effects which alter the mean differently for each group. The only hyperparameter is the standard deviation $\theta = \sigma$.

Random effects can also be structured to share information between some groups more than others. In spatio-temporal statistics, structured spatial and temporal random effects are often used to impose smoothness. Spatial random effects are the subject of Chapter 4.

Give equation for a generalised linear mixed model (GLMM) here. Describe connection between generalised additive model [GAMs; Wood (2017); Hastie and Tibshirani (1987)] and GLMMs.

3.3.5 Latent Gaussian model

Latent Gaussian models [LGMs; Rue, Martino, and Chopin (2009)] are a class of three-stage Bayesian hierarchical models in which the middle layer is Gaussian. To be more precise, in an LGM, the likelihood is given by

$$\begin{aligned} y_i &\sim p(y_i | \eta_i, \boldsymbol{\theta}_1), \quad i = 1, \dots, n, \\ \mu_i &= \mathbb{E}(y_i | \eta_i) = g(\eta_i), \\ \eta_i &= \beta_0 + \sum_{l=1}^p \beta_j z_{ji} + \sum_{k=1}^r u_k(w_{ki}). \end{aligned}$$

Each response has conditional mean μ_i with inverse link function $g : \mathbb{R} \rightarrow \mathbb{R}$ such that $\mu_i = g(\eta_i)$. The likelihood has a product structure given by $p(\mathbf{y} | \boldsymbol{\eta}, \boldsymbol{\theta}_1) = \prod_{i=1}^n p(y_i | \eta_i, \boldsymbol{\theta}_1)$, where $\boldsymbol{\eta} = (\eta_1, \dots, \eta_n)$. The vector $\boldsymbol{\theta}_1 \in \mathbb{R}^{s_1}$, with s_1 assumed small, are additional parameters of the likelihood. The structured additive predictor η_i may include an intercept β_0 , fixed effects β_j of the covariates z_{ji} , and random effects $u_k(\cdot)$ of the covariates w_{ki} . The parameters β_0 , $\{\beta_j\}$, $\{u_k(\cdot)\}$ are each assigned Gaussian prior distributions, and can be collected into a vector $\mathbf{x} \in \mathbb{R}^N$ such that $\mathbf{x} \sim \mathcal{N}(\mathbf{0}, \mathbf{Q}(\boldsymbol{\theta}_2)^{-1})$ where $\boldsymbol{\theta}_2 \in \mathbb{R}^{s_2}$ are further hyperparameters, again with s_2 assumed small. Let $\boldsymbol{\theta} = (\boldsymbol{\theta}_1, \boldsymbol{\theta}_2) \in \mathbb{R}^m$ with $m = s_1 + s_2$ be all hyperparameters, with prior distribution $p(\boldsymbol{\theta})$.

3.3.6 Extended latent Gaussian model

Extended latent Gaussian models [ELGMs; Stringer et al. (2022)] facilitate modelling of data with greater non-linearities than an LGM. In an ELGM, the structured additive predictor is redefined as $\boldsymbol{\eta} = (\eta_1, \dots, \eta_{N_n})$, where $N_n \in \mathbb{N}$ is a function of n , and it is possible that $N_n \neq n$. Each mean response μ_i now depends on some subset $\mathcal{J}_i \subseteq [N_n]$ of indices of $\boldsymbol{\eta}$, with $\cup_{i=1}^n \mathcal{J}_i = [N_n]$ and $1 \leq |\mathcal{J}_i| \leq N_n$, where $[N_n] = \{1, \dots, N_n\}$. The inverse link function $g(\cdot)$ is redefined for each observation to be a possibly many-to-one mapping $g_i : \mathbb{R}^{|\mathcal{J}_i|} \rightarrow \mathbb{R}$, such that $\mu_i = g_i(\boldsymbol{\eta}_{\mathcal{J}_i})$. Put together, ELGMs are of the form

$$\begin{aligned} y_i &\sim p(y_i | \boldsymbol{\eta}_{\mathcal{J}_i}, \boldsymbol{\theta}_1), \quad i = 1, \dots, n, \\ \mu_i &= \mathbb{E}(y_i | \boldsymbol{\eta}_{\mathcal{J}_i}) = g_i(\boldsymbol{\eta}_{\mathcal{J}_i}), \\ \eta_j &= \beta_0 + \sum_{l=1}^p \beta_l z_{ji} + \sum_{k=1}^r u_k(w_{ki}), \quad j = 1, \dots, N_n, \end{aligned}$$

with latent field and hyperparameter prior distributions as in the LGM case.

The ELGM class is well suited to small-area estimation of HIV indicators, and so used throughout the thesis. While it can be transformed to an LGM using the Poisson-multinomial transformation (Baker 1994) the multinomial logistic regression model used in Chapter 5 is naturally written as an ELGM where each observation depends on the set of structured additive predictors corresponding to the set of multinomial observations. In Chapter 6, the Naomi small-area estimation model used to produce estimates of HIV indicators is shown to have the features of an ELGM.

3.4 Model comparison

Should this section be here? Talk about: BF, AIC, BIC, WAIC, LOO, LOO-CV, connections, things used later in the thesis.

3.5 Survey methods

Large national household surveys provide the highest quality population-level information about HIV indicators in SSA. Demographic and Health Surveys (DHS)

are funded by the United States Agency for International Development (USAID) and run every three to five years in most countries. Population-based HIV Impact Assessment (PHIA) surveys are funded by PEPFAR and run every four to five years in high HIV burden countries.

3.5.1 Survey notation and key terms

Consider a population of individuals $i = 1, \dots, N$ with outcomes of interest y_i . A census is a type of survey where all individuals are selected. Supposing responses from all individuals were recorded, then any population means can be calculated directly. For example, if $G_i = G(y_i)$ then the population mean of G is

$$\bar{G} = \frac{1}{N} \sum_{i=1}^N G(y_i). \quad (3.18)$$

In practice, it is usually too expensive to run a census. Instead, only a subset of the individuals are sampled. Furthermore, only a subset of those sampled have their outcome recorded, due to nonresponse or otherwise. Let S_i be an indicator for whether or not individual i is sampled, and R_i be an indicator for whether or not y_i is recorded. If $S_i = 0$ then $R_i = 0$. If $S_i = 1$ then individual i may not respond such that $R_i = 0$. The population mean may be estimated directly based on the recorded subset of the population by

$$\bar{G}_R = \frac{\sum_{i=1}^N R_i G(y_i)}{\sum_{i=1}^N R_i}, \quad (3.19)$$

where $m_R = \sum_{i=1}^N R_i$ is the recorded sample size.

A probability sample refers to the case when individuals are selected to be included in the survey at random. In a non-probability sample, inclusion or exclusion from the survey is deterministic. A simple random sample (SRS) is a probability sample where the sampling probability for each individual is equal, so that $P(S_i = 1) = 1/N$. The survey design is called complex when the sampling probabilities for each individual vary, such that $P(S_i = 1) = \pi_i$ with $\sum_{i=1}^N \pi_i = 1$ and $\pi_i > 0$.

Complex survey designs can offer both greater practicality and statistical efficiency than a SRS. However, particular care is required in analysing data

collected using complex survey designs. Under a complex design, not accounting for unequal sampling probabilities will result in bias. That said, even for a SRS, nonresponse can cause analogous bias.

3.5.2 Survey design

The DHS (DHS 2012) employs a two-stage sampling procedure. In the first stage, enumeration areas (EAs) from a recently conducted census are typically used as the primary sampling unit (PSU). The EAs are then stratified by region, as well as urban-rural. After appropriate sample sizes are determined, EAs sampled with probability proportional to size (PPS) measured In the second stage, the secondary sampling units (SSUs) are households. All households in the selected EAs are listed, before being sampled systematically. Finally, each selected household is visited, and all adults are interviewed.

The probability an individual is sampled is equal to the probability their household is sampled. The first-stage sampling probability of the j th cluster in stratum h given by

$$\pi_{1hj} = n_h \times \frac{N_{hj}}{\sum_j N_{hj}}, \quad (3.20)$$

where N_{hj} is the number of households and n_h be the number of clusters selected in stratum h . The second-stage sampling probability each household within the i th cluster in stratum h is

$$\pi_{1hj} = \frac{n_{hj}}{N_{hj}}, \quad (3.21)$$

where n_{hj} is the number of households selected in cluster j and stratum h . That is, each household in the cluster has equal selection probability. The overall selection probability of each household in cluster j of stratum h is $\pi_{hi} = \pi_{1hj} \times \pi_{2hj}$.

3.5.3 Survey analysis

Suppose a complex survey is run with sampling probabilities π_i . The standard method for taking into account that some individuals are more likely to be included

in the survey than others is to overweight the responses of those unlikely to be included, and underweight the responses of those likely to be included. This can be achieved using design weights $\delta_i = 1/\pi_i$, which can be thought of as the number of individuals in the population represented by the i th sampled individual. Let $P(R_i = 1 | S_i = 1) = v_i$ be the probability of response for sampled individual i . The problem of nonresponse can be treated in the same way using nonresponse weights $\gamma_i = 1/v_i$, which analogously can be thought of as the number of sampled individuals represented by the i th recorded individual. Multiplying the design and nonresponse weights gives survey weights $\omega_i = \delta_i \times \gamma_i$.

A weighted estimate (Hájek 1971) of the population mean using the survey weights ω_i is given by

$$\bar{G}_\omega = \frac{\sum_{i=1}^N \omega_i R_i G(y_i)}{\sum_{i=1}^N \omega_i R_i}. \quad (3.22)$$

Decomposing the additive error of this estimate provides useful intuition as to the potential benefits of survey weighting. Following Meng (2018) then under SRS

$$\bar{G}_\omega - \bar{G} = \frac{\mathbb{E}(\omega_i R_i G_i)}{\mathbb{E}(\omega_i R_i)} - \mathbb{E}(G_i) = \frac{\mathbb{C}(\omega_i R_i G_i)}{\mathbb{E}(\omega_i R_i)} \quad (3.23)$$

$$= \rho_{R_\omega, G} \times \sqrt{\frac{N - m_{R_\omega}}{m_{R_\omega}}} \times \sigma_G, \quad (3.24)$$

where $R_\omega = \omega R$. The data defect correlation (DDC) $\rho_{R_\omega, G}$ measures the correlation between the weighted recording mechanism and given function of the outcome of interest. To minimise the DDC then $G \perp\!\!\!\perp R_\omega$. The data scarcity $\sigma_{R_\omega} = \sqrt{(N - m_{R_\omega})/m_{R_\omega}}$ measures the effective proportion of the population who have been recorded. The problem difficulty σ_G measures the intrinsic difficulty of the estimation problem, and is independent of the sampling or analysis method.

For simplicity, let $G(y_i) = y_i$ and each $y_i \in \{0, 1\}$. We weight then model following Chen et al. (2014). While this approach acknowledges the survey design, it has some important limitations. We ignore clustering structure. All of this isn't great and that someone should figure this out (Gelman 2007).

4

Models for spatial structure

This chapter presents an investigation of spatial random effects specifications. My investigation was motivated by a fundamental question encountered during model construction. Namely, should the model be augmented to capture a conjectured feature of the data? The results are presented in Howes, Eaton, et al. (2023+). Code for the analysis in this chapter is available from <https://github.com/athowes/beyond-borders>.

4.1 Background

4.2 Models based on adjacency

4.2.1 The Besag model

Spatial structure can be encoded using a symmetric relation between areas. Let $i \sim j$ if the areas A_i and A_j are adjacent or neighbouring. Adjacency is often defined by a shared border, though other choices are possible (Paciorek et al. 2013). The Besag model (Besag et al. 1991) is an improper conditional auto-regressive (ICAR) model where the full conditional distribution of the i th spatial random effect is given by

$$u_i | \mathbf{u}_{-i} \sim \mathcal{N} \left(\frac{1}{n_{\delta i}} \sum_{j:j \sim i} u_j, \frac{1}{n_{\delta i} \tau_u} \right), \quad (4.1)$$

Models for spatial structure

where δi is the set of neighbours of A_i with cardinality $n_{\delta i} = |\delta i|$ and \mathbf{u}_{-i} is the vector of spatial random effects with the i th entry removed. The conditional mean of the random effect u_i is the average of its neighbours $\{u_j\}_{j \sim i}$ and the precision $n_{\delta i}\tau_u$ is proportional to the number of neighbours $n_{\delta i}$. By Brook's lemma (Rue and Held 2005) the set of full conditionals of the Besag model are equivalent to the Gaussian Markov random field (GMRF) given by

$$\mathbf{u} \sim \mathcal{N}(\mathbf{0}, \tau_u^{-1} \mathbf{R}^-), \quad (4.2)$$

where \mathbf{R}^- is the generalised inverse of the rank-deficient structure matrix \mathbf{R} , so-called because it defines the structure of the precision matrix, with entries

$$R_{ij} = \begin{cases} n_{\delta i}, & i = j \\ -1, & i \sim j \\ 0, & \text{otherwise.} \end{cases} \quad (4.3)$$

The Markov property arises due to the conditional independence structure $p(u_i | \mathbf{u}_{-i}) = p(u_i | \mathbf{u}_{\delta i})$ whereby each area only depends on its neighbours. This is reflected in the sparsity of \mathbf{R} such that $u_i \perp u_j | \mathbf{u}_{-ij}$ if and only if $R_{ij} = 0$. The structure matrix \mathbf{R} may also be expressed as the Laplacian of the adjacency graph $\mathcal{G} = (\mathcal{V}, \mathcal{E})$ with vertices $v \in \mathcal{V}$ corresponding to each area and edges $e \in \mathcal{E}$ between vertices i and j when $i \sim j$.

Rewriting Equation (4.2), the probability density function of \mathbf{u} is

$$p(\mathbf{u}) \propto \exp\left(-\frac{\tau_u}{2} \mathbf{u}^\top \mathbf{R} \mathbf{u}\right) \propto \exp\left(-\frac{\tau_u}{2} \sum_{i \sim j} (u_i - u_j)^2\right). \quad (4.4)$$

This density is a function of the pairwise differences $u_i - u_j$ and so is invariant to the addition of a constant c to each entry $p(\mathbf{u}) = p(\mathbf{u} + c\mathbf{1})$, leading to an improper uniform distribution on the average of the u_i . If \mathcal{G} is connected, in that by traversing the edges, any vertex can be reached from any other vertex, then there is only one impropriety in the model and $\text{rank}(\mathbf{R}) = n - 1$, while if \mathcal{G} is disconnected, and composed of $n_c \geq 2$ connected components with index sets I_1, \dots, I_{n_c} , then the corresponding structure matrix \mathbf{R} has rank $n - n_c$ and the density is invariant to the addition of a constant to each of the connected components $p(\mathbf{u}_I) = p(\mathbf{u}_I + c\mathbf{1})$ where $I = I_1, \dots, I_{n_c}$.

4.2.2 Best practises for the Besag model

Freni-Sterrantino et al. (2018) recommended three best practices:

1. The structure matrix \mathbf{R} should be rescaled to have generalised variance, defined by the geometric mean of the diagonal elements of its generalised inverse

$$\sigma_{\text{GV}}^2(\mathbf{R}) = \prod_{i=1}^n (\mathbf{R}_{ii}^-)^{1/n} = \exp\left(\frac{1}{n} \sum_{i=1}^n \log(\mathbf{R}_{ii}^-)\right), \quad (4.5)$$

equal to one, by replacing \mathbf{R} with $\mathbf{R}^* = \mathbf{R}/\sigma_{\text{GV}}^2(\mathbf{R})$. As the diagonal elements R_{ii}^- correspond to marginal variances, the generalised variance gives a measure of the average marginal variance. However, this measure, introduced by Sørbye and Rue (2014), ignores off-diagonal entries and more broadly any measure of typical variance could be used. Scaling mitigates the influence of the adjacency graph on the variance of \mathbf{u} . Allowing the variance to be controlled by τ_u alone is important as it allows for consistent, interpretable prior selection.

When the adjacency graph is disconnected it is not appropriate to scale the structure matrix \mathbf{R} uniformly since for a given precision τ_u , local smoothing operates on each connected component independently. As such, each connected component should be scaled independently to have generalised variance one giving $\mathbf{R}_I^* = \mathbf{R}_I/\sigma_{\text{GV}}^2(\mathbf{R}_I)$ where \mathbf{R}_I is the sub-matrix of the structure matrix corresponding to index set I .

2. When one of the connected components is a single area, known either as a singleton or an island, the probability density $\exp\left(-\frac{\tau_u}{2} \sum_{i \sim j} (u_i - u_j)^2\right)$ has no dependence on u_i . This is equivalent to using an improper prior $p(u_i) \propto 1$ and can be avoided by setting each singleton to have independent Gaussian noise $p(u_i) \sim \mathcal{N}(0, 1)$.
3. To avoid confounding of the spatial random effects with the intercept, it is recommended to place a sum-to-zero constraint on each non-singleton connected component. In other words, for each $|I| > 1$ that $\sum_{i \in I} u_i = 0$.

4.2.3 The reparameterised Besag-York-Mollié model

Often, as well as spatial structure, there exists IID over-dispersion in the residuals and it is inappropriate to use purely spatially structured random effects in the model. The Besag-York-Mollié (BYM) model of Besag et al. (1991) accounts for this in a natural way by decomposing the spatial random effect $\mathbf{u} = \mathbf{v} + \mathbf{w}$ into a sum of an unstructured IID component \mathbf{v} and a spatially structured Besag component \mathbf{w} , each of which with their own respective precision parameters τ_v and τ_w . The resulting distribution is

$$\mathbf{u} \sim \mathcal{N}(0, \tau_v^{-1}\mathbf{I} + \tau_w^{-1}\mathbf{R}^-). \quad (4.6)$$

Including both \mathbf{v} and \mathbf{w} is intended to enable the model to learn the relative extent of the unstructured and structured components via τ_v and τ_w . However, in this specification scaling of the Besag precision matrix \mathbf{Q} is not taken into account despite this issue being particularly pertinent when dealing with multiple sources of noise. In particular, placing a joint prior $(\tau_v, \tau_w) \sim p(\tau_v, \tau_w)$ which doesn't privilege either component is more easily accomplished if \mathbf{Q} and \mathbf{I} have the same scale. Additionally, supposing we have a prior belief that the over-dispersion is primarily IID and \mathbf{v} accounts for the majority of the dispersion, then it is not immediately obvious how to represent this belief using $p(\tau_v, \tau_w)$, without inadvertently altering the prior about the overall variation. This highlights identifiability issues of the parameters (τ_v, τ_w) resulting from them not being orthogonal. Building on the models of Leroux et al. (2000) and Dean et al. (2001) which tackle this identifiability problem, but do not scale the spatially structured noise, Simpson et al. (2017) propose a reparameterisation $(\tau_v, \tau_w) \mapsto (\tau_u, \phi)$ of the BYM model known as the BYM2 model and given by

$$\mathbf{u} = \frac{1}{\tau_u} \left(\sqrt{1 - \phi} \mathbf{v} + \sqrt{\phi} \mathbf{w}^* \right), \quad (4.7)$$

where τ_u is the marginal precision of \mathbf{u} , $\phi \in [0, 1]$ gives the proportion of the marginal variance explained by each component, and \mathbf{w}^* is a scaled version of \mathbf{w} with precision matrix given by the scaled structure matrix \mathbf{R}^* . When $\phi = 0$ the

Models for spatial structure

random effects are IID, and when $\phi = 1$ the random effects follow the Besag model. To borrow an analogy (Rue 2020) the parameterisation (τ_v, τ_w) is like having one hot water and one cold water tap, whereas the parameterisation (τ_u, ϕ) is like a mixer tap where the amount of water and its temperature can be adjusted separately.

4.2.4 Concerns about the Besag model's representation of space

The Besag model was originally proposed for use in image analysis, where areas correspond to pixels arranged in a regular lattice structure. Since then, it has seen wider use, including in situations, like small-area estimation of HIV, where the spatial structure is less regular. As such, I have a number of concerns about the model's applicability to this broader setting. This discussion is closely linked to the modifiable areal unit problem (Openshaw and Taylor 1979), whereby statistical conclusions change as a result of seemingly arbitrary changes in data aggregation, as well as the challenge of ecological inference and the ecological fallacy (Wakefield and Lyons 2010).

Adjacency compression

Summarising a geometry by an adjacency graph represents a loss of information. Many geometries share the same adjacency graph, and are as such isomorphic identical under the Besag model (Figure). This is not in itself a problem, but does prompt consideration as to whether the class of geometries with the same adjacency graph is sufficiently similar to merit identical models.¹ Intuitively, the more regular the spatial structure, the less information is lost in compression to an adjacency graph. In image analysis, very little spatial information is lost in compression of a lattice structure to an adjacency graph. On the other hand, the regions of a country, determined by political and geographic forces, tend to display

¹The regularity of realistic geometries may help to constrain each class to be more similar than it strictly has to be. In other words, although pathological geometries can be constructed, they are implausible in statistical practise and so not of great concern to us here.

Models for spatial structure

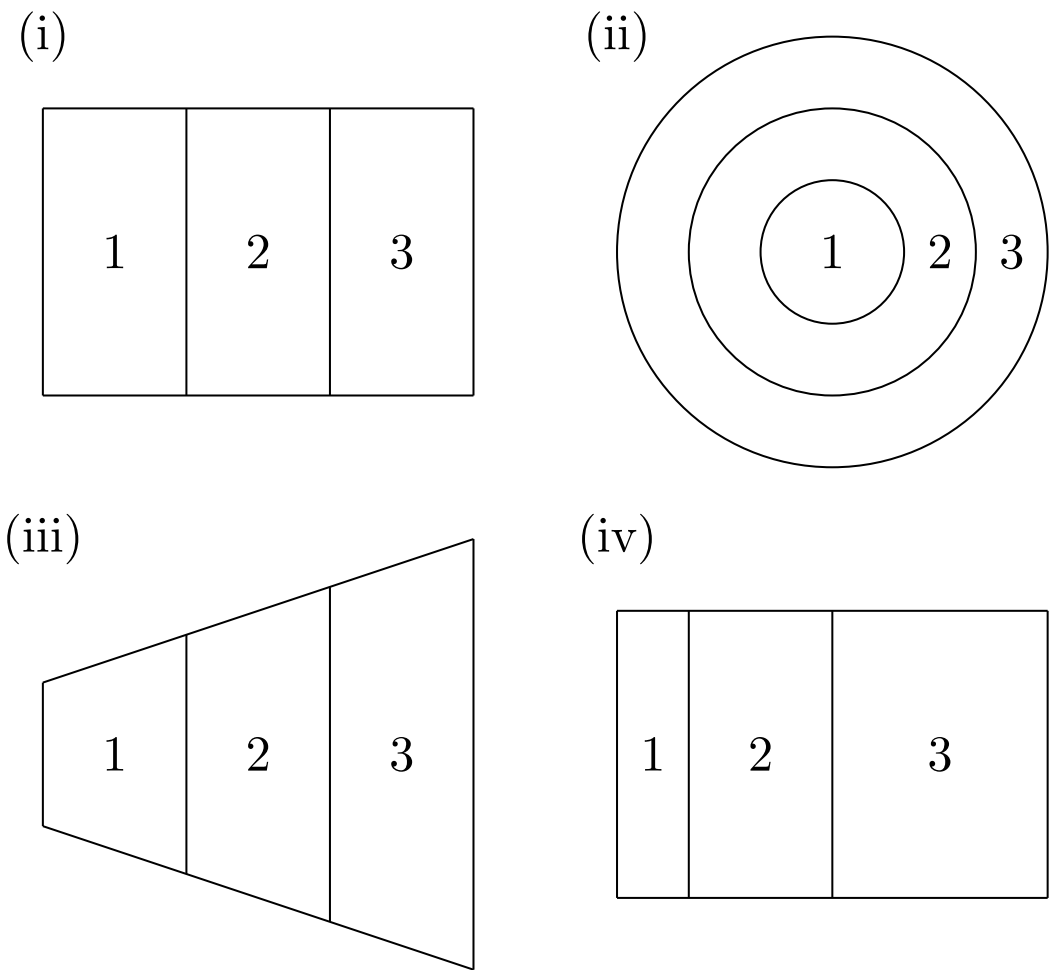


Figure 4.1: Figure caption.

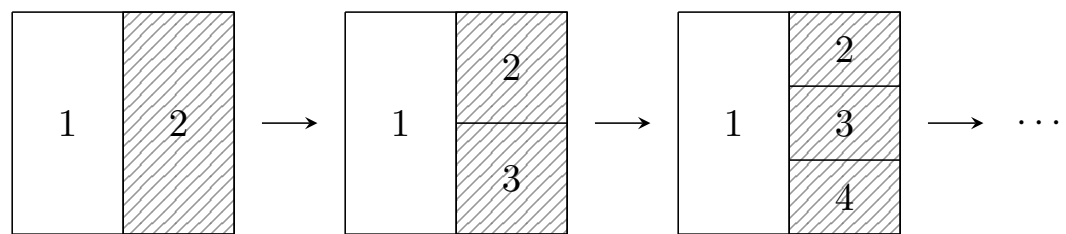


Figure 4.2: Figure caption.

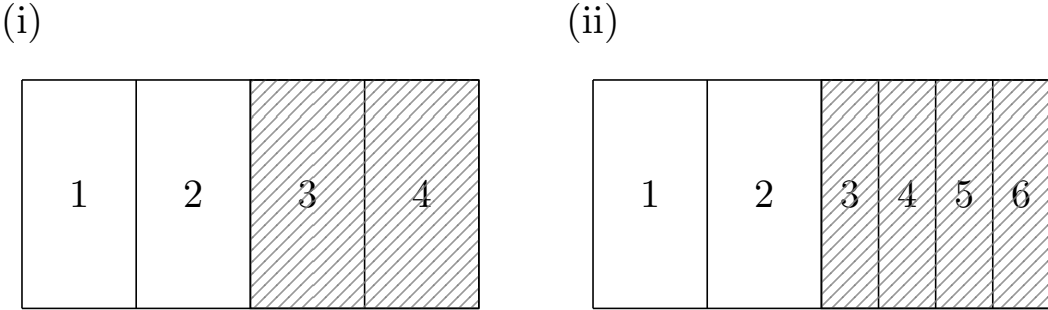


Figure 4.3: Figure caption.

greater irregularity. The appropriateness of adjacency compression therefore varies by the type of geometry common to the application setting.

Mean structure

In the Besag model all adjacent areas count equally. This assumption is unsatisfying: for most geometries, we expect different amounts of correlation between neighbours. Figure illustrates a number of heuristic features for neighbour importance, including length of shared border, and the proximity of centers of mass.

Variance structure

In Equation (4.1) the precision of u_i is proportional to its number of neighbours $n_{\delta i}$. It follows that as $n_{\delta i} \rightarrow \infty$ then $\text{Var}(u_i) \rightarrow 0$. This is illustrated by Figure where the area on the right is repeatedly divided such that its number of neighbours increases. This property is a consequence of averaging the conditional mean over a greater number of areas, which, in certain situations, can correspond to a greater amount of information. However, if the amount of information in the shaded area remains fixed, it is inappropriate that $\text{Var}(u_1)$ should tend to zero as a result of drawing additional, arbitrary, boundaries. In the image analysis setting this modelling assumption is reasonable: each pixel represents a fixed amount of information and a higher pixel density represents a greater amount of information. On the other hand, in public health and epidemiology, drawing boundaries to create additional areas is not expected to correspond to a greater amount of information.

Models for spatial structure

Suppose we fit a Besag model upon identical data using each of the two geometries in Figure. If the spatial variation is relatively smooth, dividing the shaded areas into two will result in a lower estimated variance σ_u^2 in geometry (ii) as compared with geometry (i) because there will appear to be less variation between neighbouring areas. This problem does not only apply locally: since the effect of σ_u^2 applies everywhere, the smoothing will change even in unaltered parts of the study region.

4.3 Models using kernels

4.4 Simulation study

4.5 HIV prevalence study

4.6 Discussion

Follstad and Rue (2003)

5

A model for risk group proportions

This chapter describes an application of Bayesian spatio-temporal statistics to small-area estimation of HIV risk group proportions. This work was conducted in collaboration with colleagues from the MRC Centre for Global Infectious Disease Analysis and UNAIDS. I developed the statistical model, building upon an earlier version of the analysis conducted by Dr. Kathryn Risher. The model and results for 13 countries are presented in Howes, Risher, et al. (2023), and implemented in a spreadsheet tool (<https://hivtools.unaids.org/pse/>) for use in national HIV response planning. The tool is being updated by inclusion of more countries to the analysis, and extension of the methodology, including to additional risk groups. Code for the analysis in this chapter is available from <https://github.com/athowes/multi-agyw>.

5.1 Background

In SSA, adolescent girls and young women (AGYW) aged 15-29 are at increased risk of HIV infection. Though AGYW are only 28% of the population, they comprise 44% of new infections (UNAIDS 2021a). HIV incidence for AGYW is 2.4 times higher than for similarly aged (15-29) males. The social and biological reasons for this disparity include structural vulnerabilities and power imbalances, age patterns

A model for risk group proportions

of sexual mixing, a younger age at first sex, and increased susceptibility to HIV infection. On this basis, AGYW have been identified as a priority population for HIV prevention services. Significant investments, such as the DREAMS partnership (Saul et al. 2018) and by the Global Fund (The Global Fund 2018), have been made to support prevention programming.

The Global AIDS Strategy 2021-2026 (UNAIDS 2021b) was adopted by the United Nations (UN) General Assembly in June 2021, and “outlines the strategic priorities and actions to be implemented by global, regional, country and community partners to get on-track to ending AIDS”. It proposed stratifying HIV prevention packages to AGYW based on two factors

1. local population-level HIV incidence, and
2. individual-level sexual risk behaviour.

Risk of acquiring HIV depends on both factors. As such, prioritisation of prevention services is more efficient if both factors are taken into account. I illustrate this stylistically in Figure 5.1. The strategy encourages programmes to define targets for the proportion of AGYW to be reached with a range of interventions. Implementation of the strategy by national HIV programmes and stakeholders requires data on the population size and HIV incidence in each risk group by location.

5.2 Data

5.2.1 Behavioural data from household surveys

A model for risk group proportions

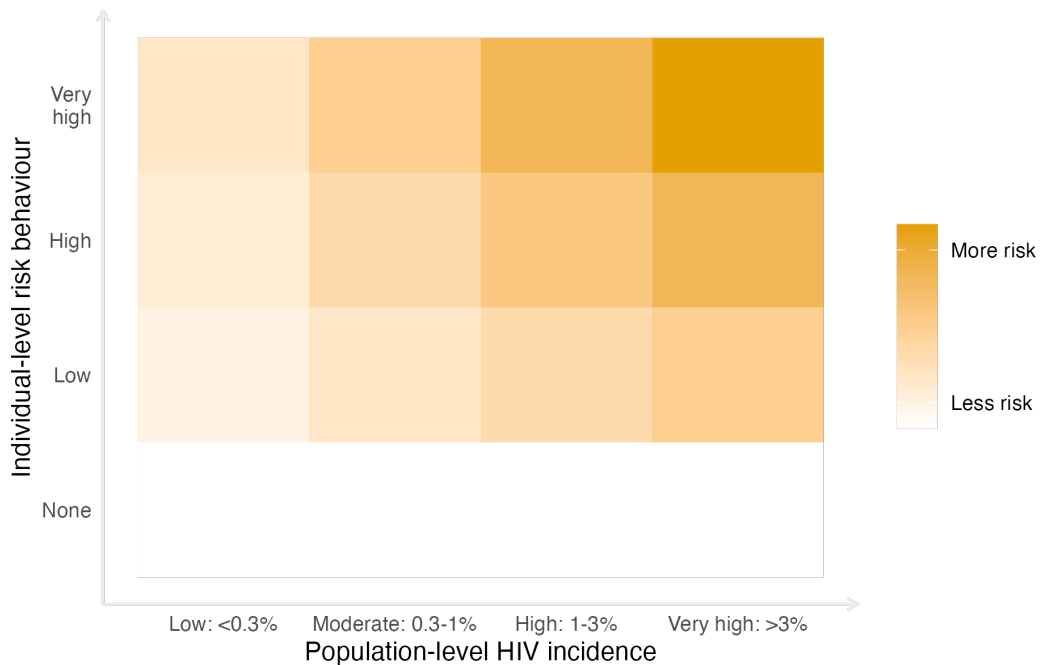


Figure 5.1: Risk of acquiring HIV depends on both individual-level risk behaviour and population-level HIV incidence. I assume that with no individual-level risk behaviour, there is no risk of acquiring HIV, independent of the population-level HIV incidence. The risk scale is intended to be illustrative, rather than interpreted quantitatively.

Table 5.1: HIV risk groups and HIV incidence rate ratios relative to AGYW with one cohabiting sexual partner. The incidence rate ratio for women with non-regular or multiple sexual partner(s) was derived from analysis of longitudinal data by Slaymaker et al. (2020). Among FSW, the incidence rate ratio (25.0, 13.0, 9.0, 6.0, 3.0) depended on the level of HIV incidence among the general population (<0.1%, 0.1-0.3%, 0.3-1.0%, 1.0-3.0%, >3.0%), such that higher local HIV incidence in the general population corresponded to a lower incidence rate ratio for FSW. Estimates of HIV incidence rate ratios for FSW were derived by UNAIDS based on patterns of relative HIV prevalence among FSW compared to general population prevalence.

Risk group	Description	Incidence rate ratio
None	Not sexually active	0.0
Low	One cohabiting sexual partner	1.0 (baseline)
High	Non-regular or multiple partner(s)	1.72
Very High	Reporting transactional sex (later adjusted to correspond to FSW)	3.0-25.0 (varied depending on local HIV incidence)

I used household survey data from 13 countries identified by the Global Fund

A model for risk group proportions

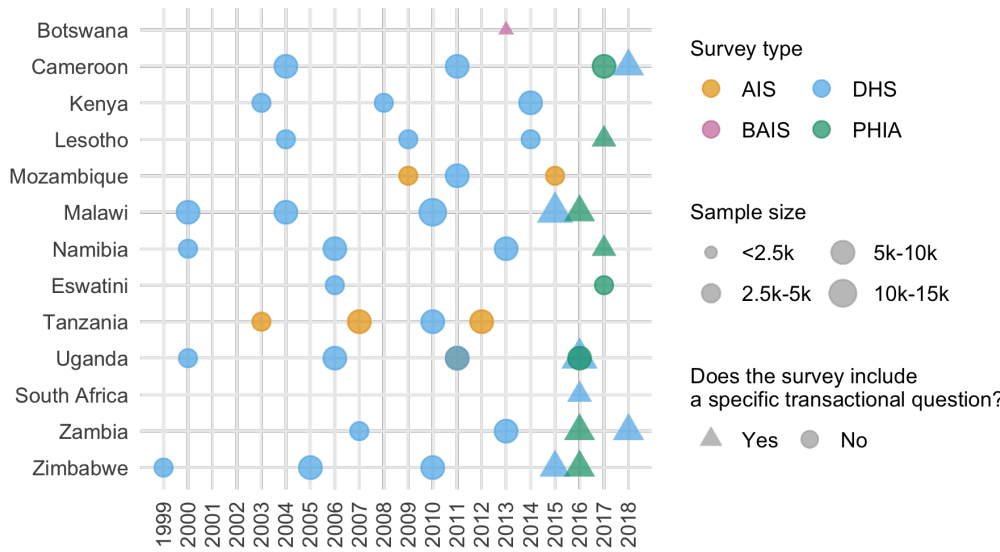


Figure 5.2: Surveys conducted 1999-2018 that were used in the analysis by year, survey type, sample size, and whether the survey included a specific question about transactional sex. Survey type included AIDS Indicator Surveys (AIS), Demographic and Health Surveys (DHS), the Botswana AIDS Impact Survey 2013 (BAIS), and Population-based HIV Impact Assessment (PHIA) surveys.

(The Global Fund 2018) as priority countries for implementation of AGYW HIV prevention. These countries were Botswana, Cameroon, Kenya, Lesotho, Malawi, Mozambique, Namibia, South Africa, Eswatini, Tanzania, Uganda, Zambia and Zimbabwe. Surveys conducted in these countries between 1999 and 2018 were included in which both women were interviewed about their sexual behaviour, and sufficient geographic information was available to locate survey clusters to health districts. There were 46 suitable surveys (Figure 5.2), with a total sample size of 274,970 women aged 15-29 years. Of the respondents, 103,063 were aged 15-19 years, 92,173 were aged 20-24 years, and 79,734 were aged 25-29 years. The median number of surveys per country was four, ranging from one in Botswana and South Africa to six in Uganda.

For each survey, I classified respondents into one of four behavioural risk groups $k = 1, 2, 3, 4$ according to reported sexual risk behaviour in the past 12 months (Figure 5.3). In increasing order of HIV acquisition risk, these risk groups were:

- $k = 1$: Not sexually active

A model for risk group proportions

- $k = 2$: One cohabiting sexual partner
- $k = 3$: Non-regular or multiple sexual partner(s), and
- $k = 4$: Reporting transactional sex.

The HIV incidence rate ratio RR_k was assumed to vary by risk group (Table 5.1), with the one cohabiting partner risk group as baseline.

Exact survey questions varied slightly across survey types and between survey phases. Questions captured information about whether the respondent had been sexually active in the past twelve months, and if so with how many partners. For their three most recent partners, respondents were also asked about the type of partnership. Possible partnership types included spouse, cohabiting partner, partner not cohabiting with respondent, friend, sex worker, sex work client, and other. Full survey questions used are in Appendix B.4. In the case of inconsistent responses, women were categorised according to the highest risk group they fell into, ensuring that the categories were mutually exclusive.

Some surveys included a specific question asking if the respondent had received or given money or gifts for sex in the past twelve months. In these surveys, 2.64% of women reported transactional sex. In surveys without such a question, women almost never (0.01%) answered that one of their three most recent partners was a sex work client. This incomparability made it inappropriate to include surveys without a specific transactional sex question when estimating the proportion of the population who engaged in transactional sex. Of the total 46 surveys included in the analysis, 12 had a specific transactional sex question, with a total sample size of 62,853 (28,753 aged 15-19 years, 26,324 aged 20-24 years, and 7,776 aged 25-29 years). The sample size for women aged 25-29 is smaller because there were 6 DHS surveys which excluded women 25-29 from the transactional sex survey question.

5.2.2 Other data

In addition to the household survey behavioural data, I used estimates of population, PLHIV and new HIV infections stratified by district and age group from HIV

A model for risk group proportions

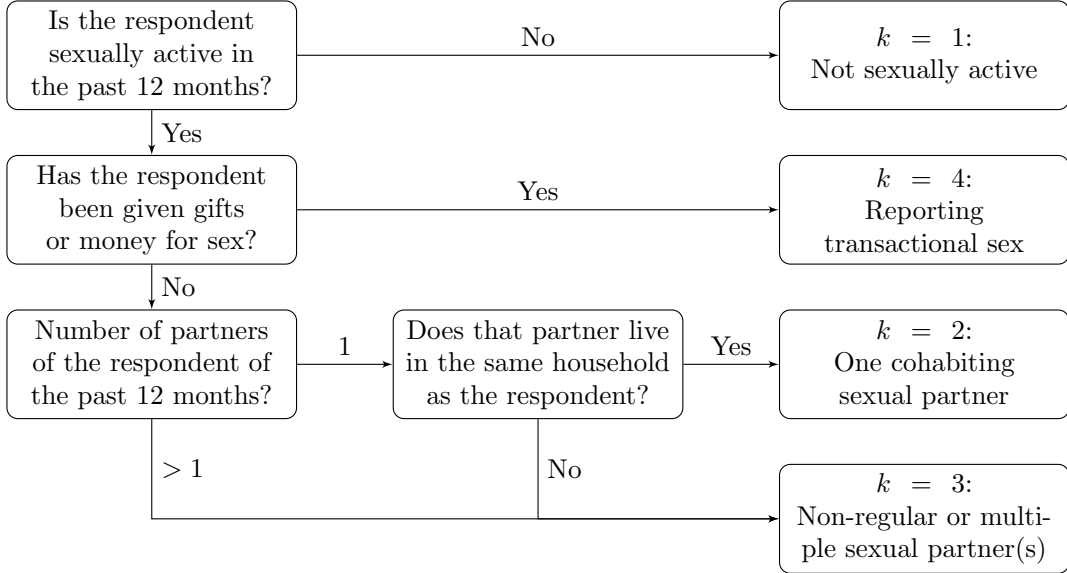


Figure 5.3: Flowchart giving classification of survey respondents to HIV risk groups.

estimates published by UNAIDS that were developed using the Naomi model (Eaton et al. 2021). I used the most recent 2022 estimates for all countries, apart from Mozambique where, due to data accuracy concerns, I used the 2021 estimates (in which the Cabo Delgado province is excluded due to disruption by conflict). I used administrative area hierarchy and geographic boundaries corresponding to those used for health service planning by countries. Exceptions were Cameroon and Kenya, where I conducted analyses one level higher at the department and county levels, respectively.

5.3 Model for risk group proportions

Owing to the incomparability in estimating the $k = 4$ risk group across surveys, I took a two-stage modelling approach to estimate the four risk group proportions. Denote being in either the third or fourth risk group as $k = 3^+$. First, using all the surveys, I used a spatio-temporal multinomial logistic regression model to estimate the proportion of AGYW in the risk groups $k \in \{1, 2, 3^+\}$. This model is described in Section 5.3.1. Then, using only those surveys with a specific transactional sex question, I fit a spatial logistic regression model to estimate the proportion of

A model for risk group proportions

those in the $k = 3^+$ risk group that were in the $k = 3$ and $k = 4$ risk groups respectively. This model is described in Section 5.3.2.

5.3.1 Spatio-temporal multinomial logistic regression

Let $i \in \{1, \dots, n\}$ denote districts partitioning the 13 studied AGYW priority countries $c[i] \in \{1, \dots, 13\}$. Consider the years 1999-2018 denoted as $t \in \{1, \dots, T\}$, and age groups $a \in \{15-19, 20-24, 25-29\}$. Let $p_{itak} > 0$ with $\sum_{k=1}^{3^+} p_{itak} = 1$, be the probabilities of membership of risk group k .

Multinomial logistic regression

A standard multinomial logistic regression model (e.g. Gelman, Carlin, et al. 2013) is specified by

$$\mathbf{y}_{ita} = (y_{ita1}, \dots, y_{ita3^+})^\top \sim \text{Multinomial}(m_{ita}; p_{ita1}, \dots, p_{ita3^+}), \quad (5.1)$$

$$\log \left(\frac{p_{itak}}{p_{ita1}} \right) = \eta_{itak}, \quad k = 2, 3^+, \quad (5.2)$$

where the number in risk group k is y_{itak} , the fixed sample size is $m_{ita} = \sum_{k=1}^{3^+} y_{itak}$, and $k = 1$ is chosen as the baseline category. This model is not an latent Gaussian model [LGM; Rue, Martino, and Chopin (2009)] because each observation y_{itak} for $k \in \{1, 2, 3^+\}$ depends non-linearly on multiple structured additive predictors $\{\eta_{itak}, k = 1, 2, 3^+\}$.

The model, defined over 940 districts, 20 years, 3 age groups, and 3 risk groups, is too large for MCMC to be tractable in reasonable time. To recast this model as an LGM, I used the multinomial-Poisson transformation (detailed in Section 5.3.1). This modification allowed inference to be performed using the INLA (Rue, Martino, and Chopin 2009) algorithm via the R-INLA package (Martins et al. 2013). Inferences from INLA in the LGM setting are accurate and substantially faster than MCMC.

The multinomial-Poisson transformation

The multinomial-Poisson transformation (Baker 1994) reframes a given multinomial logistic regression model, like that described in Equations (5.1) and (5.2), as an equivalent Poisson log-linear model. The equivalent model is of the form

$$y_{itak} \sim \text{Poisson}(\kappa_{itak}), \quad (5.3)$$

$$\log(\kappa_{itak}) = \eta_{itak}. \quad (5.4)$$

The basis of the transformation is that conditional on their sum Poisson counts are jointly multinomially distributed (McCullagh and Nelder 1989) as follows

$$\mathbf{y}_{ita} | m_{ita} \sim \text{Multinomial}\left(m_{ita}; \frac{\kappa_{ita1}}{\kappa_{ita}}, \dots, \frac{\kappa_{ita3^+}}{\kappa_{ita}}\right), \quad (5.5)$$

where $\kappa_{ita} = \sum_{k=1}^{3^+} \kappa_{itak}$. The probabilities p_{itak} may then be obtained using the softmax function

$$p_{itak} = \frac{\exp(\eta_{itak})}{\sum_{k=1}^{3^+} \exp(\eta_{itak})} = \frac{\kappa_{itak}}{\sum_{k=1}^{3^+} \kappa_{itak}} = \frac{\kappa_{itak}}{\kappa_{ita}}. \quad (5.6)$$

Under the equivalent model, in Equation (5.3) the sample sizes m_{ita} are treated as random rather than fixed such that

$$m_{ita} = \sum_k y_{itak} \sim \text{Poisson}\left(\sum_k \kappa_{itak}\right) = \text{Poisson}(\kappa_{ita}). \quad (5.7)$$

Using Equations (5.5) for $p(\mathbf{y}_{ita} | m_{ita})$ and Equation (5.7) for $p(m_{ita})$, the joint distribution is given by

$$p(\mathbf{y}_{ita}, m_{ita}) = \exp(-\kappa_{ita}) \frac{(\kappa_{ita})^{m_{ita}}}{m_{ita}!} \times \frac{m_{ita}!}{\prod_k y_{itak}!} \prod_k \left(\frac{\kappa_{itak}}{\kappa_{ita}}\right)^{y_{itak}} \quad (5.8)$$

$$= \prod_k \left(\frac{\exp(-\kappa_{itak}) (\kappa_{itak})^{y_{itak}}}{y_{itak}!} \right) \quad (5.9)$$

$$= \prod_k \text{Poisson}(y_{itak} | \kappa_{itak}). \quad (5.10)$$

As expected, Equation (5.10) corresponds to the product of independent Poisson likelihoods defined in Equation (5.3). This exercise demonstrates that the Poisson log-linear model contains within it a multinomial likelihood, with a Poisson prior on the sample size.

A model for risk group proportions

For this model to be equivalent to a multinomial logistic regression model, the normalisation constants m_{ita} must be recovered exactly. That is to say, their posterior distributions should be as close as possible to a Dirac delta distribution with value zero everywhere but the known value of the sample size. To ensure that this is the case, observation-specific random effects θ_{ita} can be included in the equation for the linear predictor. Multiplying each of $\{\kappa_{itak}\}_{k=1}^{3^+}$ by $\exp(\theta_{ita})$ has no effect on the category probabilities, but does provide the necessary flexibility for κ_{ita} to recover m_{ita} exactly. Although in theory an improper prior distribution $\theta_{ita} \propto 1$ should be used, I found that in practice, by keeping η_{ita} otherwise small using appropriate constraints, so that arbitrarily large values of θ_{ita} are not required, it is sufficient (and practically preferable for inference) to instead use a vague prior distribution.

Model specifications

Table 5.2: Four multinomial regression models were considered. Observation random effects θ_{ita} , included in all models, are omitted from this table.

Category β_k	Country ζ_{ck}	Age α_{ack}	Spatial ϕ_{ik}	Temporal γ_{tk}
M1 IID	IID	IID	IID	IID
M2 IID	IID	IID	Besag	IID
M3 IID	IID	IID	IID	AR1
M4 IID	IID	IID	Besag	AR1

I considered four models (Table 5.2) for η_{ita} in the equivalent Poisson log-linear model of the form

$$\eta_{ita} = \theta_{ita} + \beta_k + \zeta_{c[i]k} + \alpha_{ac[i]k} + u_{ik} + \gamma_{tk}. \quad (5.11)$$

Observation random effects $\theta_{ita} \sim \mathcal{N}(0, 1000^2)$ with a vague prior distribution were included in all models to ensure the multinomial-Poisson transformation was valid. To capture country-specific proportion estimates for each category, I included category random effects $\beta_k \sim \mathcal{N}(0, \tau_\beta^{-1})$ and country-category random effects $\zeta_{ck} \sim \mathcal{N}(0, \tau_\zeta^{-1})$. Heterogeneity in risk group proportions by age was allowed by including age-country-category random effects $\alpha_{ack} \sim \mathcal{N}(0, \tau_\alpha^{-1})$. I

A model for risk group proportions

considered several specifications for the space-category u_{ik} and time-category effects γ_{tk} , described in Sections 5.3.1 and 5.3.1.

Use of the multinomial-Poisson transformation required all random effects to include interaction with category k , because any random effects which did not include interaction with category would give no change in category probabilities. The only exception were the observation random effects, which were included as a device to ensure the transformation is valid, rather than to model the data.

Spatial random effects For the space-category random effects u_{ik} I considered two specifications:

1. Independent and identically distributed (IID) $u_{ik} \sim \mathcal{N}(0, \tau_u^{-1})$,
2. The Besag improper conditional autoregressive (ICAR) model (Besag et al. 1991) grouped by category

$$\mathbf{u} = (u_{11}, \dots, u_{n1}, \dots, u_{13+}, \dots, u_{n3+})^\top \sim \mathcal{N}(\mathbf{0}, (\tau_u \mathbf{R}_u^*)^-).$$

The scaled structure matrix $\mathbf{R}_u^* = \mathbf{R}_b^* \otimes \mathbf{I}$ is given by the Kronecker product of the scaled Besag structure matrix \mathbf{R}_b^* and the identity matrix \mathbf{I} , and $-$ denotes the generalised matrix inverse. I followed best practices for the Besag model as described in Chapter 4. To implement the Kronecker product I used the `group` option in R-INLA [Section 3.5.5; Gómez-Rubio (2020)] setting the random effect to be `f(area_idx, model = "besag", group = cat_idx, control.group = list(model = "iid"), ...)`. Though the Kronecker product is symmetric, performance is better in R-INLA when the more complicated effect is written as the first variable rather than the grouping variable.

In preliminary testing I used the BYM2 model (Simpson et al. 2017) in place of the Besag. I found that the proportion parameter posteriors tended to be highly peaked at the value one. For simplicity and to avoid numerical issues, by using Besag random effects I effectively decided to fix this proportion to one.

A model for risk group proportions

Temporal random effects For the time-category random effects γ_{tk} I considered two specifications:

1. IID $\gamma_{tk} \sim \mathcal{N}(0, \tau_\gamma^{-1})$,
2. First order autoregressive (AR1) grouped by category

$$\boldsymbol{\gamma} = (\gamma_{11}, \dots, \gamma_{13^+}, \dots, \gamma_{T1}, \dots, \gamma_{T3^+})^\top \sim \mathcal{N}(\mathbf{0}, (\tau_\gamma \mathbf{R}_\gamma^*)^-).$$

The scaled structure matrix $\mathbf{R}_\gamma^* = \mathbf{R}_r^* \otimes \mathbf{I}$ is given by the Kronecker product of a scaled AR1 structure matrix \mathbf{R}_r^* and the identity matrix \mathbf{I} . The AR1 structure matrix \mathbf{R}_r is obtained by precision matrix of the random effects $\mathbf{r} = (r_1, \dots, r_T)^\top$ specified by

$$r_1 \sim \left(0, \frac{1}{1 - \rho^2}\right), \quad (5.12)$$

$$r_t = \rho r_{t-1} + \epsilon_t, \quad t = 2, \dots, T, \quad (5.13)$$

where $\epsilon_t \sim \mathcal{N}(0, 1)$ and $|\rho| < 1$. As with the structured spatial random effects, I implemented this Kronecker product using the `group` option via `f(year_idx, model = "ar1", group = cat_idx, control.group = list(model = "iid"), ...)`. Again the more complicated variable was written first.

A note on spatio-temporal interaction random effects I also considered including separable space-time-category random effects δ_{itk} in the model, using the specification

$$\boldsymbol{\delta} = (\delta_{111}, \dots, \delta_{nT3^+})^\top \sim \mathcal{N}(\mathbf{0}, (\tau_\delta \mathbf{R}_\delta^*)^-), \quad (5.14)$$

where \mathbf{R}_δ^* is a Kronecker product of the relevant space, time and category structure matrices. These specifications were:

1. IID spatial and IID temporal (Type I) $\mathbf{R}_\delta^* = \mathbf{I} \otimes \mathbf{I} \otimes \mathbf{I}$,
2. Besag spatial and IID temporal (Type II) $\mathbf{R}_\delta^* = \mathbf{R}_b^* \otimes \mathbf{I} \otimes \mathbf{I}$,
3. IID spatial and AR1 temporal (Type III) $\mathbf{R}_\delta^* = \mathbf{I} \otimes \mathbf{R}_a^* \otimes \mathbf{I}$,
4. Besag spatial and AR1 (Type IV) $\mathbf{R}_\delta^* = \mathbf{R}_b^* \otimes \mathbf{R}_a^* \otimes \mathbf{I}$,

A model for risk group proportions

where the first, second and third elements of the Kronecker product represent space, time and category (always IID) structure matrices respectively. The interaction type in brackets (e.g. Type I) is given according to the Knorr-Held (2000) framework.

Though three-way Kronecker products are not directly supported in R-INLA, I implemented each specification using a combination of the `group` and `replicate` options [Section 6.5.2; Gómez-Rubio (2020)]. For example, for the Type IV effects the random effects were specified by `f(area_idx_copy, model = "besag", group = year_idx, replicate = cat_idx, control.group = list(model = "ar1"))`. I was able to run these models for single countries, keeping only years at which surveys occurred in those countries. However, when fitting all countries jointly I found inclusion of the space-time-category random effects to be intractable, and as such decided not to include them in the model.

Prior distributions All random effect precision parameters $\tau \in \{\tau_\beta, \tau_\zeta, \tau_\alpha, \tau_u, \tau_\gamma, \tau_\delta\}$ were given independent penalised complexity (PC) prior distributions (Simpson et al. 2017) with base model $\sigma = 0$ given by

$$p(\tau) = 0.5\nu\tau^{-3/2} \exp(-\nu\tau^{-1/2}) \quad (5.15)$$

where $\nu = -\ln(0.01)/2.5$ such that $\mathbb{P}(\sigma > 2.5) = 0.01$. For the lag-one correlation parameter ρ , I used the PC prior distribution, as derived by Sørbye and Rue (2017), with base model $\rho = 1$ and condition $\mathbb{P}(\rho > 0 = 0.75)$. I chose the base model $\rho = 1$ corresponding to no change in behaviour over time, rather than the alternative $\rho = 0$ corresponding to no correlation in behaviour over time, as I judged the former to be more plausible a priori.

Identifiability constraints

To facilitate interpretability of the posterior inferences, I applied sum-to-zero constraints (Table 5.3) such that none of the category interaction random effects altered overall category probabilities. In testing of the space-time-category random

A model for risk group proportions

effects, I applied analogous sum-to-zero constraints to maintain roles of the space-category and time-category random effects. In some cases it was not possible to implement all three sets of constraints for the three-way interactions in R-INLA.

Table 5.3: Applying sum-to-zero constraints to interaction effects ensures that the main effect is not interfered with.

Random effects	Constraints
Category	$\sum_k \beta_k = 0$
Country	$\sum_c \zeta_{ck} = 0, \forall k$
Age-country	$\sum_a \alpha_{ack} = 0, \forall c, k$
Spatial	$\sum_i u_{ik} = 0, \forall k$
Temporal	$\sum_t \gamma_{tk} = 0, \forall k$
Spatio-temporal	$\sum_i \delta_{itk} = 0, \forall t, k; \sum_t \delta_{itk} = 0, \forall i, k; \sum_k \delta_{itk} = 0, \forall i, t$

Survey weighted likelihood

I accounted for the survey design using a weighted pseudo-likelihood where the observed counts y are replaced by effective counts y^* , as described in Section 3.5. These counts may not be integers, and as such the Poisson likelihood given in Equation (5.3) is not appropriate. Instead, I used a generalised Poisson pseudo-likelihood $y^* \sim \text{xPoisson}(\kappa)$ given by

$$p(y^*) = \frac{\kappa^{y^*}}{\lfloor y^*! \rfloor} \exp(-\kappa), \quad (5.16)$$

to extend the Poisson distribution to non-integer weighted counts. This working likelihood is implemented by `family = "xPoisson"` in R-INLA.

Model selection

I selected the model including Besag spatial random effects and IID temporal random effects based on the conditional predictive ordinate (CPO) criterion (Pettit 1990). For comparison, I also computed the deviance information criterion (DIC) (Spiegelhalter, Best, et al. 2002) and widely applicable information criterion (WAIC) (Watanabe 2013). Each of these criterion can be calculated in R-INLA without requiring model refitting. The results are presented in Figure 5.4.

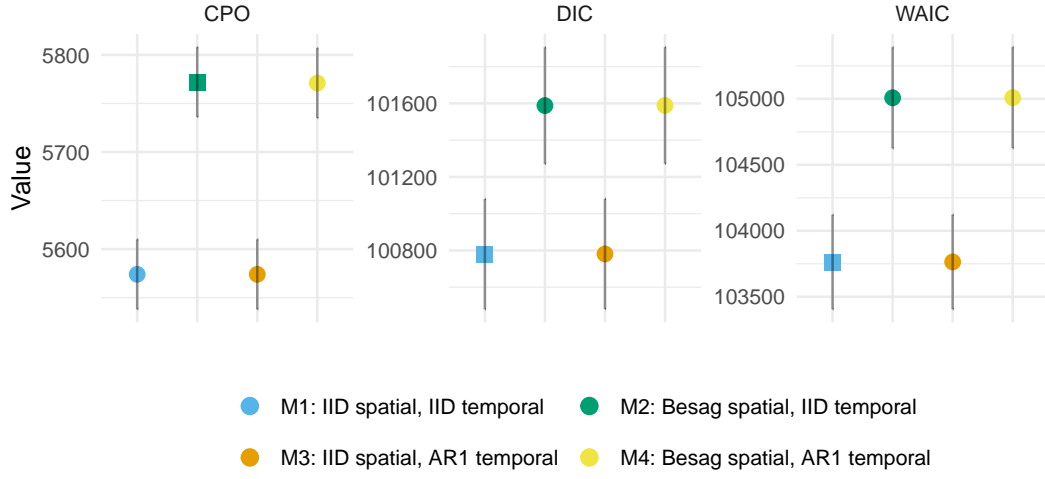


Figure 5.4: For the multinomial logistic regression model, under the CPO criterion, including Besag spatial random effects rather than IID spatial random effects improved model performance. On the other hand, under the DIC and WAIC, where smaller values are preferred, the opposite was true. Though IID temporal random effects are preferred by all criteria AR1 temporal random effects performed very similarly, likely as there is a limited amount of temporal variation in the data to describe.

Table 5.4: CPO, DIC, and WAIC values for the multinomial logistic regression model with corresponding standard errors.

	M1	M2	M3	M4
CPO	5573 (36)	5772 (36)	5574 (36)	5771 (36)
DIC	100780 (300)	101588 (317)	100781 (300)	101589 (317)
WAIC	103763 (358)	105008 (383)	103763 (358)	105009 (383)

5.3.2 Spatial logistic regression

To estimate the proportion of those in the $k = 3^+$ risk group that were in the $k = 3$ and $k = 4$ risk groups respectively, I fit logistic regression models of the form

$$y_{ia4} \sim \text{Binomial}(y_{ia3} + y_{ia4}, q_{ia}), \quad (5.17)$$

$$q_{ia} = \text{logit}^{-1}(\eta_{ia}), \quad (5.18)$$

where

$$q_{ia} = \frac{p_{ia4}}{p_{ia3} + p_{ia4}} = \frac{p_{ia4}}{p_{ia3^+}}. \quad (5.19)$$

This two-step approach allowed all surveys to be included in the multinomial regression model, but only those surveys with a specific transactional sex question

A model for risk group proportions

to be included in the logistic regression model. As all such surveys occurred in the years 2013-2018 (Figure 5.2), I assumed q_{ia} to be constant with respect to time.

Model specifications

Table 5.5: Six logistic regression models were considered. The covariate `cfswever` denotes the proportion of men who have ever paid for sex and `cfswrecent` denotes the proportion of men who have paid for sex in the past 12 months.

	Intercept β_0	Country ζ_c	Age α_{ac}	Spatial u_i	Covariates
L1	Constant	IID	IID	IID	None
L2	Constant	IID	IID	Besag	None
L3	Constant	IID	IID	IID	<code>cfswever</code>
L4	Constant	IID	IID	Besag	<code>cfswever</code>
L5	Constant	IID	IID	IID	<code>cfswrecent</code>
L6	Constant	IID	IID	Besag	<code>cfswrecent</code>

I considered six logistic regression models (Table 5.5). Each included a constant intercept $\beta_0 \sim \mathcal{N}(-2, 1^2)$, country random effects $\zeta_c \sim \mathcal{N}(0, \tau_\zeta^{-1})$, and age-country random effects $\alpha_{ac} \sim \mathcal{N}(0, \tau_\alpha^{-1})$. The Gaussian prior distribution on β_0 placed 95% prior probability on the range 2-50% for the percentage of those with non-regular or multiple partners who report transactional sex. I considered two specifications (IID, Besag) for the spatial random effects u_i . To aid estimation with sparse data, I also considered national-level covariates for the proportion of men who have paid for sex ever `cfswever` or in the last twelve months `cfswrecent` (Hodgins et al. 2022). For both random effect precision parameters $\tau \in \{\tau_\alpha, \tau_\zeta\}$ I used the PC prior distribution with base model $\sigma = 0$ and $\mathbb{P}(\sigma > 2.5 = 0.01)$. For both regression parameters $\beta \in \{\beta_{\text{cfswever}}, \beta_{\text{cfswrecent}}\}$ I used the prior distribution $\beta \sim \mathcal{N}(0, 2.5^2)$.

Survey weighted likelihood

As with the multinomial regression model, I used survey weighted counts y^* and sample sizes m^* . I used a generalised binomial pseudo-likelihood $y^* \sim \text{xBinomial}(m^*, q)$ given by

$$p(y^* | m^*, q) = \binom{\lfloor m^* \rfloor}{\lfloor y^* \rfloor} q^{y^*} (1 - q)^{m^* - y^*} \quad (5.20)$$

A model for risk group proportions

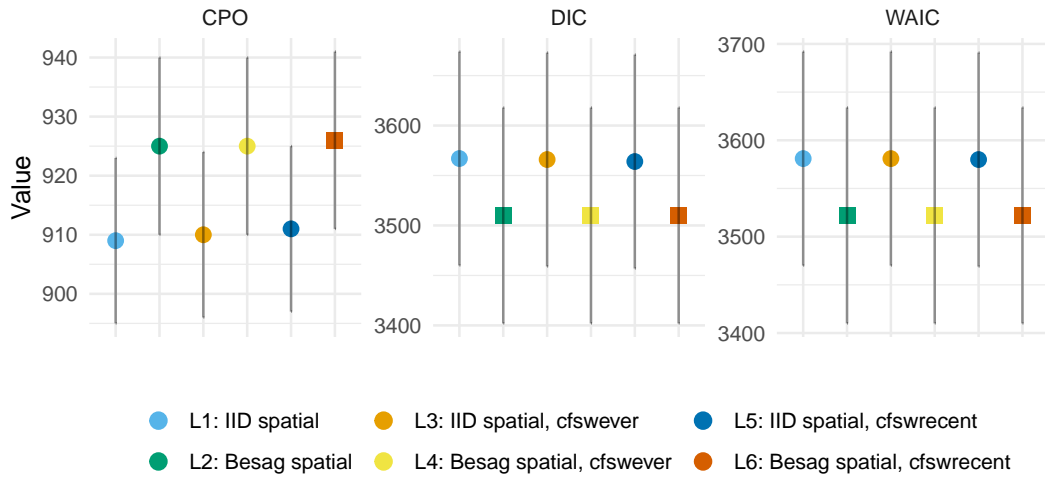


Figure 5.5: For the logistic regression model, the CPO, DIC, and WAIC each agreed that the model containing Besag spatial random effects and the `cfsrecent` covariates was best. Inclusion of Besag spatial random effects consistently improved each criterion, whereas improvements from inclusion of any covariates were marginal.

to extend the binomial distribution to non-integer weighted counts and sample sizes. This working likelihood is implemented by `family = "xBinomial"` in R-INLA.

Model selection

I selected the model including Besag spatial effects and `cfsrecent` covariates according to the CPO criterion. All results, including DIC and WAIC, are presented in Table and Figure 5.5. Inclusion of Besag spatial random effects, rather than IID, consistently improved performance. Benefits from inclusion of covariates were more marginal. As some countries had no suitable surveys, I nonetheless preferred to include covariate information so that estimates in these countries would be based on some country-specific data.

Table 5.6: CPO, DIC, and WAIC values for the logistic regression model with corresponding standard errors.

	L1	L2	L3	L4	L5	L6
DIC	4662 (110)	4605 (111)	4662 (110)	4605 (111)	4662 (110)	4605 (111)
WAIC	4692 (115)	4624 (115)	4692 (115)	4624 (115)	4692 (115)	4624 (115)
CPO	950 (15)	969 (15)	951 (15)	970 (15)	950 (15)	970 (15)

5.3.3 Model combination

How were the models combined? Using samples.

5.3.4 Female sex worker population size adjustment

Having had sex “in return for gifts, cash or anything else in the past 12 months” is not considered sufficient to constitute sex work. As such, I adjusted the estimates obtained based on the transactional sex survey question to match FSW population size estimates obtained using an alternative method, which I describe below. The estimates of the non-regular or multiple sexual partner(s) population size were changed to facilitate changing of the FSW population size. This approach retained subnational variation informed by the transactional sex survey question.

I used the estimates adult (15-49) FSW population size by country from a Bayesian meta-analysis of key population specific data sources (Stevens, Sabin, Arias Garcia, et al. 2022). To disaggregate these estimates by age, I took the following steps. First, I calculated the total sexually debited population in each age group, by country. To describe the distribution of age at first sex, I used skew logistic distributions (Nguyen and Eaton 2022) with cumulative distribution function given by

$$F(x) = (1 + \exp(\kappa_c(\mu_c - x)))^{-\gamma_c}, \quad (5.21)$$

where $\kappa_c, \mu_c, \gamma_c > 0$ are country-specific shape, shape and skewness parameters respectively. Next, I used the assumed $\text{Gamma}(\alpha = 10.4, \beta = 0.36)$ FSW age distribution in South Africa from the Thembisa model (Johnson and Dorrington 2020) to calculate the implied ratio between the number of FSW and the sexually debited population in each age group. I assumed the South African ratios were applicable to every country, allowing calculation of the number of FSW by age group in all 13 countries. The resulting age trends obtained (Figure 5.6) reflect country-level variation in demographics and age-at-first-sex.

A model for risk group proportions

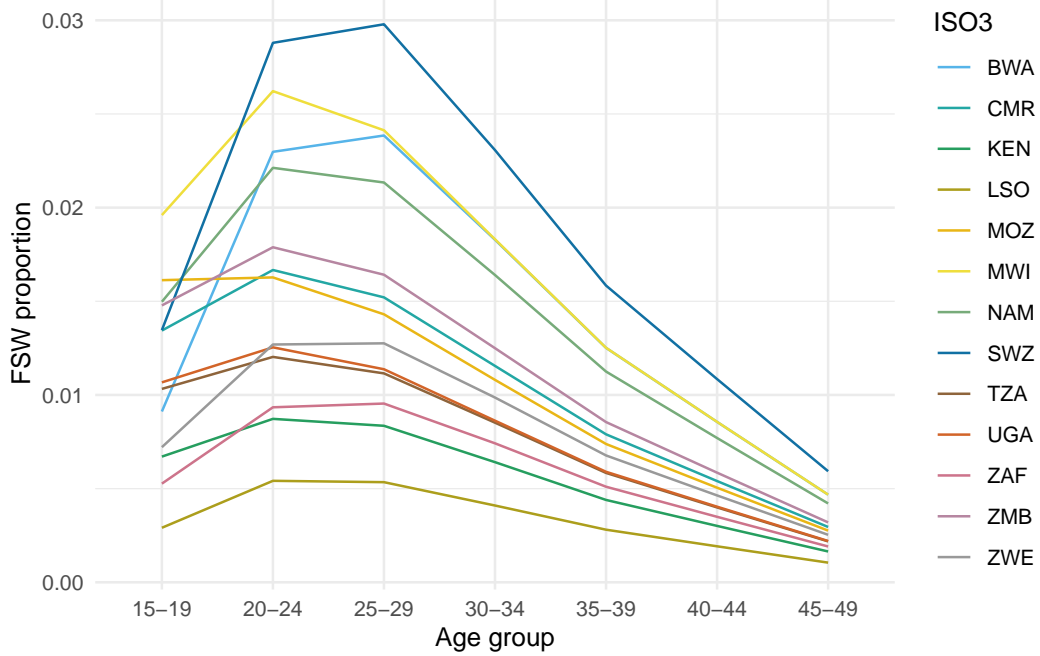


Figure 5.6: The disaggregation procedure I used produces an age distribution for FSW peaking in the 20-24 and 25-29 age groups, and declining for older age groups.

5.3.5 Results

Coverage assessment

To assess the calibration of the fitted model, I calculated the quantile q of each observation within the posterior predictive distribution. For calibrated models, these quantiles, known as probability integral transform (PIT) values (Dawid 1984; Bosse et al. 2022), should follow a uniform distribution $q \sim \mathcal{U}[0, 1]$. To generate samples from the posterior predictive distribution, I applied the multinomial likelihood to samples from the latent field, setting the sample size to be the floor of the Kish effective sample size. Using the PIT values, it is possible to calculate the empirical coverage of all $(1 - \alpha)100\%$ equal-tailed posterior predictive credible intervals. These empirical coverages can be compared to the nominal coverage $(1 - \alpha)$ for each value of $\alpha \in [0, 1]$ to give empirical cumulative distribution function (ECDF) difference values. This approach has the advantage of considering all possible confidence values at once. To test for uniformity, I used the binomial distribution based simultaneous confidence bands for ECDF difference values developed by Säilynoja et al. (2021). I found the only significant deviation from uniformity occurred in

A model for risk group proportions

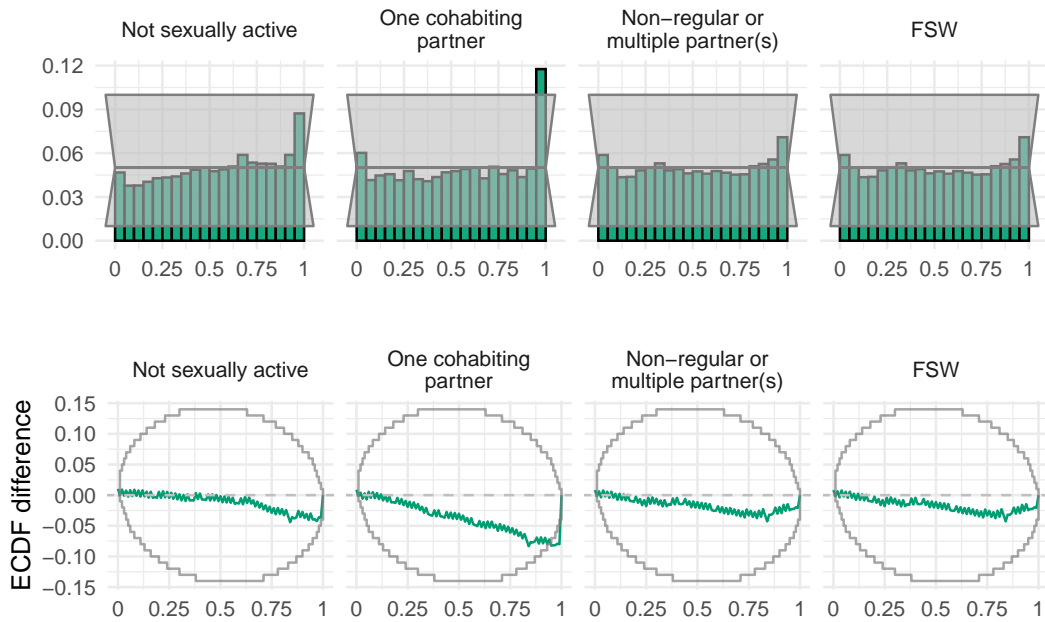


Figure 5.7: Probability integral transform (PIT) histograms (top row) and empirical cumulative distribution function (ECDF) difference plots (bottom row) for the final selected model.

the right-hand tail of the one cohabiting partner risk group. That is to say, the proportion of the PIT values which were greater than 0.95 was significantly more than would be expected under a calibrated model.

Estimates

Figure 5.11 and Figure 5.9 show posterior mean estimates for the proportion in each risk group for the final model in 2018, the most recent year included in our analysis. I focused on the most recent estimates because they are the most relevant to inform ongoing HIV policy. In subsequent results, all estimates refer to 2018, unless otherwise indicated.

The median national FSW proportion was 1.1% (95% CI 0.4–1.9) for the 15-19 age group, 1.6% (95% CI 0.6–2.8) for the 20-24 age group and 1.9% (95% CI 0.5–3.5) for the 25-29 age group, in line with the results displayed in Figure 5.6.

In the 20-24 and 25-29 year age groups, the majority of women were either cohabiting or had non-regular or multiple partner(s). Countries in eastern and

A model for risk group proportions

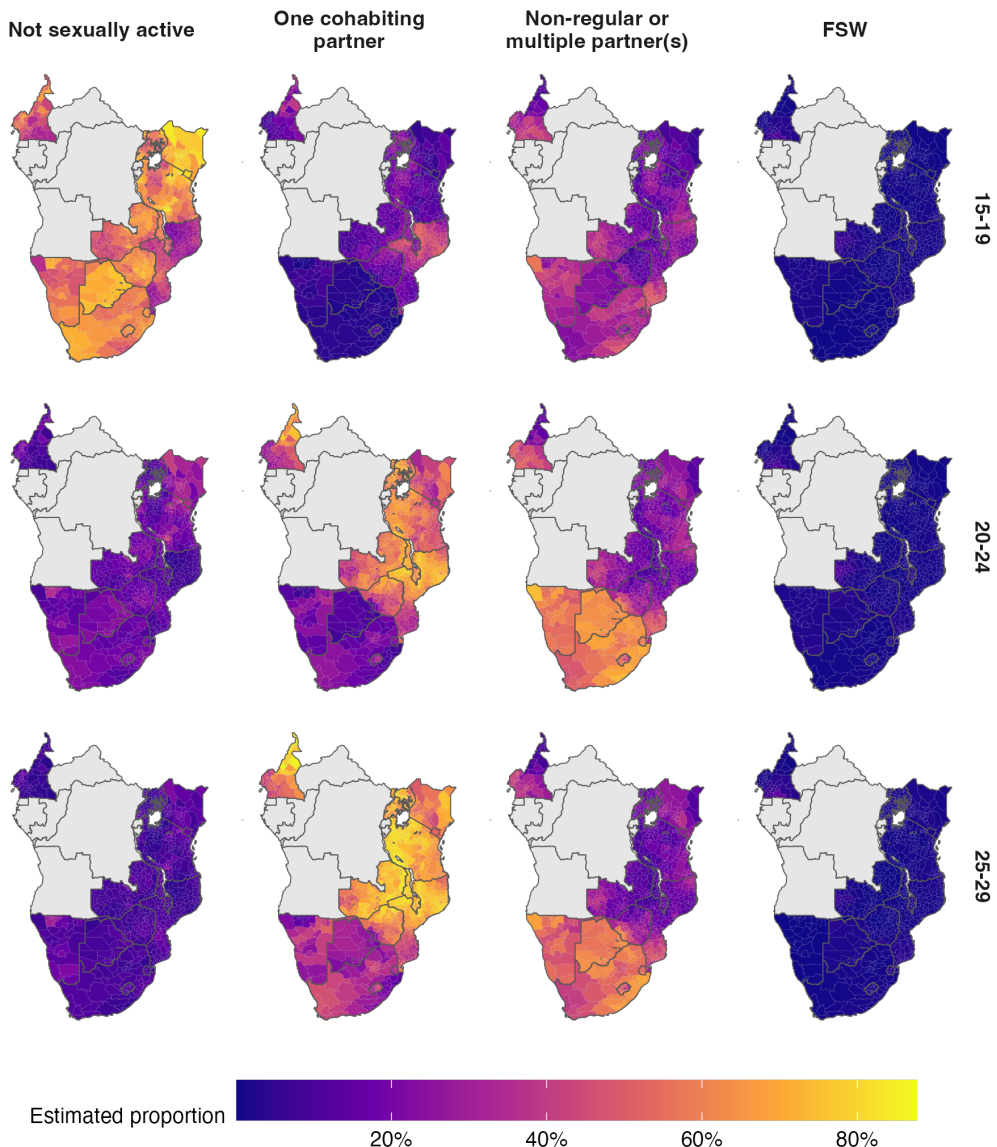


Figure 5.8: The spatial distribution (posterior mean) of the AGYW risk group proportions in 2018. Estimates are stratified by risk group (columns) and five-year age group (rows). Countries in grey were not included in the analysis. A limitation of this figure is that using a common colour scale, desirable for other reasons, makes it challenging to see spatial variation in the FSW risk group.

A model for risk group proportions

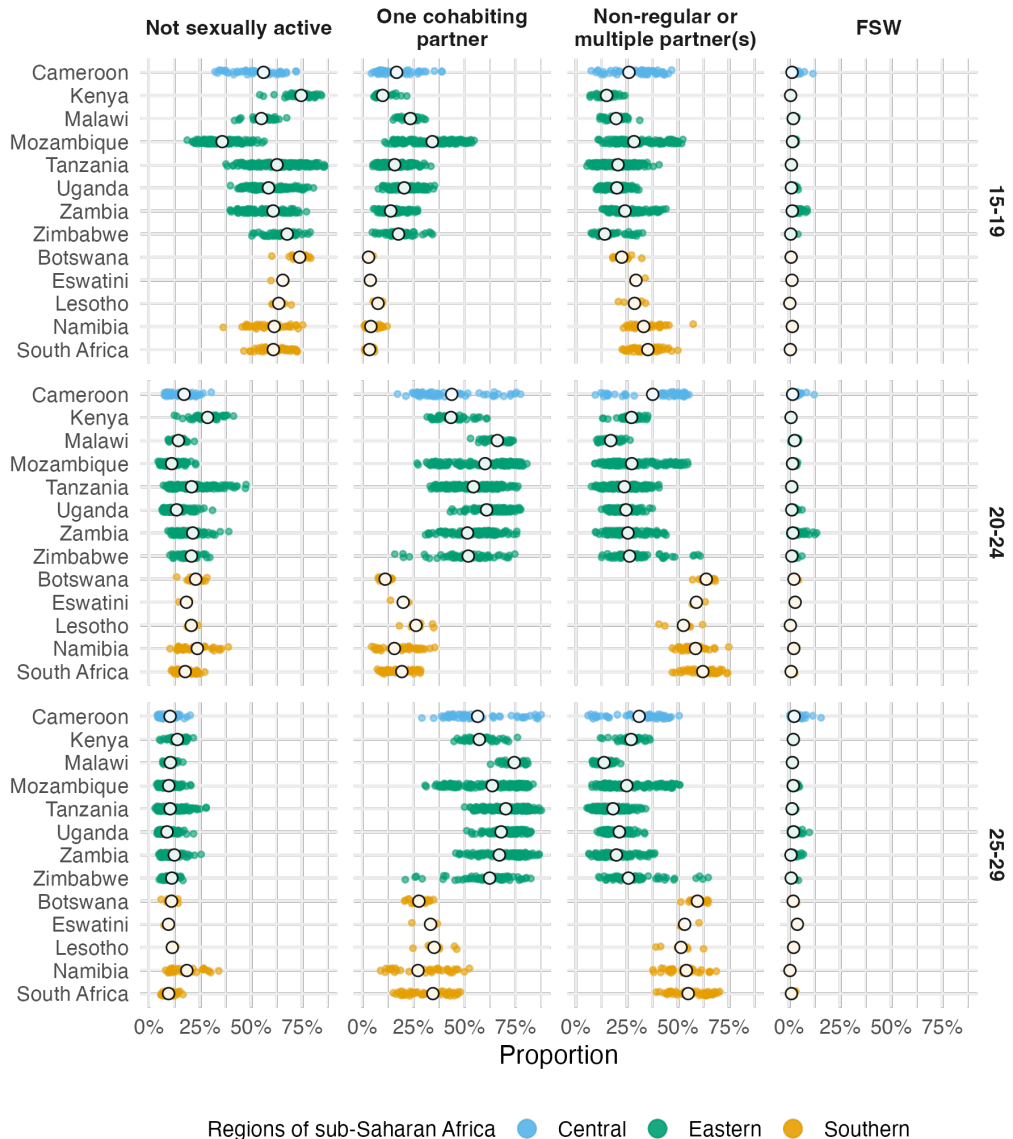


Figure 5.9: National (in white) and subnational (in color) posterior means of the risk group proportions. Estimates are stratified by risk group (columns) and five-year age group (rows). Though the information presented is similar to that of Figure 5.8, this figure presents a clear view of within- and between-country variation in risk group proportions.

A model for risk group proportions

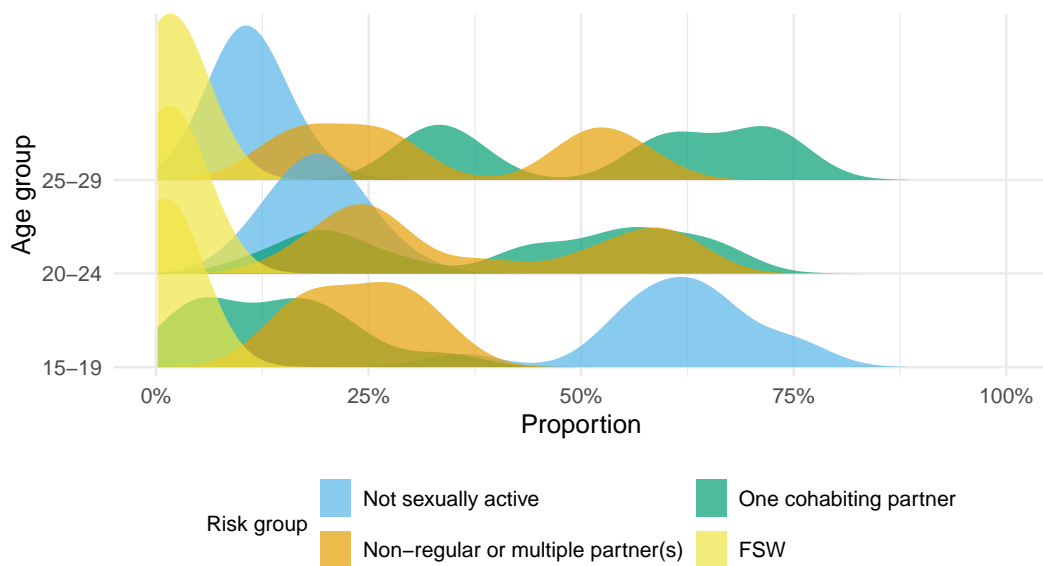


Figure 5.10: Figure caption.

central Africa (Cameroon, Kenya, Malawi, Mozambique, Tanzania, Uganda, Zambia and Zimbabwe) had a higher proportion of women in these age groups cohabiting (63.1% [95% CI 35–78.7%] compared with 21.3% [95% CI 10.1–48.8%] with non-regular partner[s]). In contrast, countries in southern Africa (Botswana, Eswatini, Lesotho, Namibia and South Africa) had a higher proportion with non-regular or multiple partner(s) (58.9% [95% CI 43.2–70.5%], compared with 23.4% [95% CI 9.7–39.1%] cohabiting). This finding is the most notable feature of between-country variation shown in Figure 5.9. Figure 5.8 shows the geographic delineation to pass along the border of Mozambique, through the interior of Zimbabwe and along the border of Zambia.

In most districts (57.9%; 95% credible interval [CI] 27.7–79.7) adolescent girls aged 15-19 were not sexually active. The exception was Mozambique, where the majority (64.23%) were sexually active in the past year and close to a third (34.17%) were cohabiting with a partner.

Variance decomposition

Age group was the most important factor explaining variation in risk group proportions, accounting for 65.9% (95% CI 54.1–74.9%) of total variation. The

A model for risk group proportions

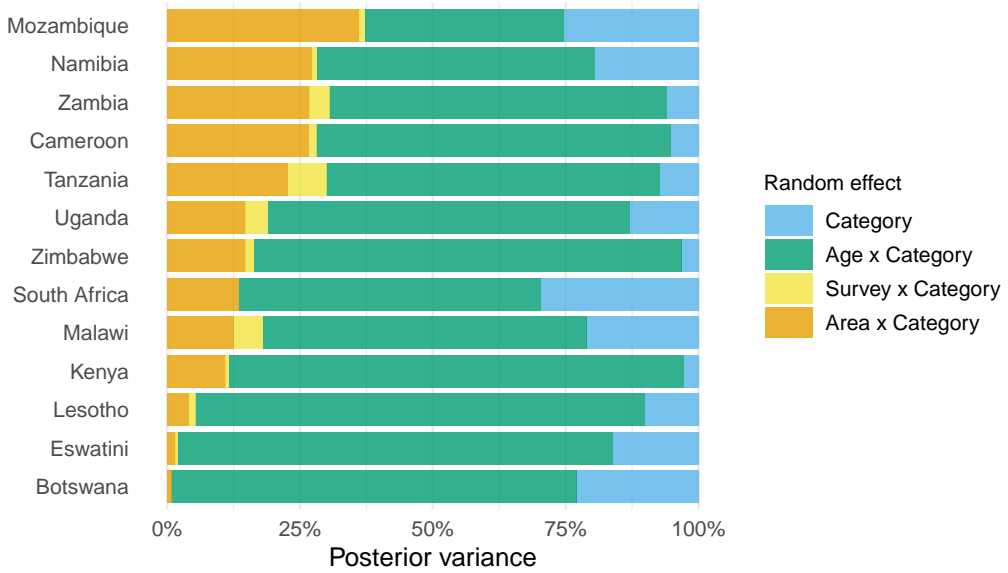


Figure 5.11: Figure caption.

primary change in risk group proportions by age group occurs between the 15-19 age group and 20-29 age group (Figure 5.8). The next most important factor was location. Country-level differences explained 20.9% (95% CI 11.9–34.5%) of variation, while district-level variation within countries explained 11.3% (95% CI 8.2–15.3%). Temporal changes only explained 0.9% (95% CI 0.6–1.4%) of variation, indicating very little change in risk group proportions over time. I found similar variance decomposition results fitting each country individually (Figure 5.11) and using other model specifications.

5.4 Prevalence and incidence by risk group

Using the most recent risk group proportion estimates, I calculated the following indicators stratified according to district, age group and risk group:

1. HIV prevalence ρ_{iak} ,
2. the number of people living with HIV (PLHIV) H_{iak} ,
3. HIV incidence λ_{iak} , and
4. the number of new HIV infections I_{iak} .

A model for risk group proportions

To do so, I disaggregated district, age group specific Naomi estimates by risk group.

5.4.1 Disaggregation of Naomi prevalence estimates

To disaggregate HIV prevalence, I began by estimating HIV prevalence log odds ratios $\log(\text{OR}_k)$ relative to the general population. To do so, I fit a logistic regression model using age, country and risk group specific HIV prevalence bio-marker survey data. I also included general population HIV prevalence data. The logistic regression model included an indicator function for each risk group, and an indicator for being in the general population, such that the regression coefficients in this model correspond to log odds. The log odds ratios may then be easily obtained by taking the difference in odds ratios.

To allow the log odds ratio for the highest risk group to vary based on general population prevalence I fit a linear regression of the FSW log odds against the general population log odds. I ensured that log odds ratios for the FSW risk group were at least as large as those for the multiple or non-regular partner(s) risk group.

Given the fitted log odds ratios, I disaggregated Naomi estimates of PLHIV H_{ia} on the logit scale using numerical optimisation. I did this by finding the values of θ_{ia} which minimise the equation

$$f(\theta_{ia}) = \sum_{k=1}^4 (\text{logistic}(\theta_{ia} + \log(\text{OR}_k)) \cdot N_{iak}) - H_{ia}, \quad (5.22)$$

where

$$\text{logistic}(x) = \exp(x)/(1 + \exp(x)), \quad (5.23)$$

such that

$$\text{logistic}(\hat{\theta}_{ia} + \log(\text{OR}_k)) = \rho_{iak}. \quad (5.24)$$

These values are given by

$$\hat{\theta}_{ia} = \arg \min_{\theta_{ia} \in [-10, 10]} f(\theta_{ia})^2. \quad (5.25)$$

The number of PLHIV were obtained by $H_{iak} = \rho_{iak}N_{iak}$, where N_{iak} is the risk group population size.

5.4.2 Disaggregation of Naomi incidence estimates

I calculated the number of new HIV infections by risk group using linear disaggregation

$$I_{ia} = \sum_k I_{iak} = \sum_k \lambda_{iak}(1 - \rho_{iak})N_{iak} \quad (5.26)$$

$$= 0 + \lambda_{ia2}(1 - \rho_{ia2})N_{ia2} + \lambda_{ia3}(1 - \rho_{ia3})N_{ia3} + \lambda_{ia4}(1 - \rho_{ia4})N_{ia4} \quad (5.27)$$

$$= \lambda_{ia2}((1 - \rho_{ia2})N_{ia2} + RR_3(1 - \rho_{ia3})N_{ia3} + RR_4(\lambda_{ia})(1 - \rho_{ia4})N_{ia4}), \quad (5.28)$$

where RR_2 , RR_3 and $RR_4(\cdot)$ are the HIV risk ratios given in Table 5.1, and $(1 - \rho_{iak})N_{iak}$ are the susceptible population sizes in each risk group. The risk ratio for FSW was defined as a function of district-level incidence in the general population λ_{ia} .

Risk group specific HIV incidence estimates were then given by

$$\lambda_{ia1} = 0, \quad (5.29)$$

$$\lambda_{ia2} = I_{ia}/((1 - \rho_{ia2})N_{ia2} + RR_3(1 - \rho_{ia3})N_{ia3} + RR_4(\lambda_{ia})(1 - \rho_{ia4})N_{ia4}), \quad (5.30)$$

$$\lambda_{ia3} = RR_3\lambda_{ia2}, \quad (5.31)$$

$$\lambda_{ia4} = RR_4(\lambda_{ia})\lambda_{ia2}. \quad (5.32)$$

I evaluated these equations using Naomi model estimates of the number of new HIV infections $I_{ia} = \lambda_{ia}N_{ia}$. The number of new HIV infections were $I_{iak} = \lambda_{iak}N_{iak}$.

5.4.3 Expected new infections reached

I calculated the number of new infections that would be reached prioritising according to each possible stratification of the population. That is, for all $2^3 = 8$ possible combinations of stratification by location, age, and risk group.

To illustrate this approach, consider stratification by age. I first aggregated the number of new HIV infections and HIV incidence such that

$$I_a = \sum_{ik} I_{iak}, \quad (5.33)$$

$$\lambda_a = I_a / \sum_{ik} (1 - \rho_{iak})N_{iak}. \quad (5.34)$$

A model for risk group proportions

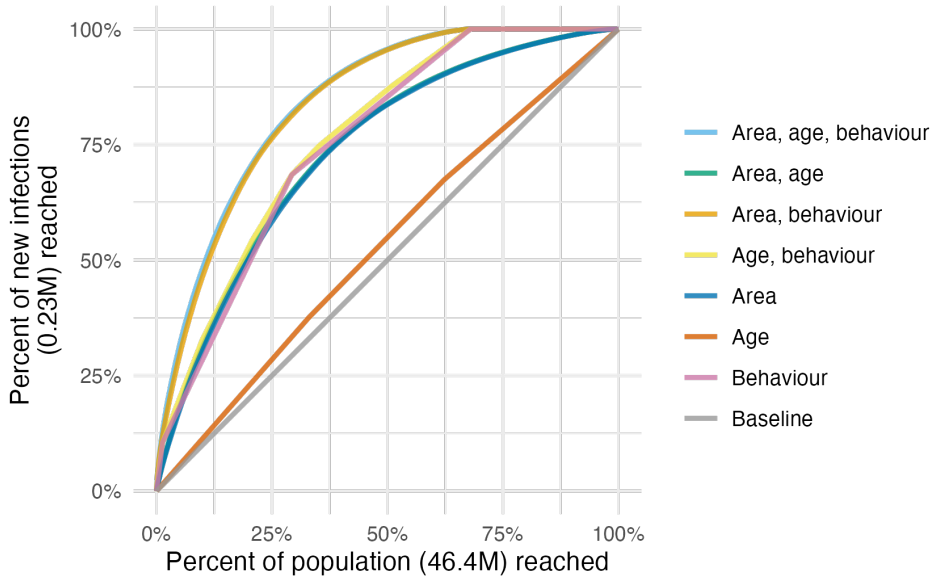


Figure 5.12: Percentage of new infections reached across all 13 countries, taking a variety of risk stratification approaches, against the percentage of at risk population required to be reached.

I then considered prioritisation individuals by age group a according to the highest HIV incidence λ_a . By cumulatively summing the expected infections, for each fraction of the total population reached I calculated the fraction of total expected new infections that would be reached. As there are three age groups, the resulting function was piecewise linear with three segments.

5.4.4 Results

For any given fraction of AGYW prioritised, substantially more new infections were reached by strategies that included behavioural risk stratification. Reaching half of all expected new infections required reaching 19.4% of the population when stratifying by subnational area and age, but only 10.6% when behavioural stratification was included (Figure 5.12). The majority of this benefit came from reaching FSW, who were 1.3% of the population but 10.6% of all new infections.

Considering each country separately, on average, reaching half of new infections in each country required reaching 14.6% (range 8.7-21.8%) of the population when stratifying by area and age, reducing to 5.1% (range 2.1-13.2%) when behaviour

A model for risk group proportions

was included. The relative importance of stratifying by age, location and behaviour varied between countries, analogous to the varying contribution of each to the total variance (Section 5.3.5).

5.5 Discussion

In this chapter, I estimated the proportion of AGYW who fall into different risk groups at a district level in 13 sub-Saharan African countries. These estimates support consideration of differentiated prevention programming according to geographic locations and risk behaviour, as outlined in the Global AIDS Strategy. Systematic differences in risk by age groups, and variation within and between countries, explained the large majority of variation in risk group proportions. Changes over time were negligible in the overall variation in risk group proportions. The proportion of 15-19 year olds who are sexually active, and among women aged 20-29 years, norms around cohabitation especially varied across districts and countries. This variation underscores the need for these granular data to implement HIV prevention options aligned to local norms and risk behaviours.

I considered four risk groups based on sexual behaviour, the most proximal determinant of risk. Other factors, such as condom usage or type of sexual act, may account for additional heterogeneity in risk from sexual behaviour. However, I did not include these factors in view of measurement difficulties, concerns about consistency across contexts, and the operational benefits of describing risk parsimoniously.

Sexual behaviour confers risk only when AGYW reside in geographic locations where there is unsuppressed viral load among their potential partners. I did not include more distal determinants, such as school attendance, orphanhood, or gender empowerment, as I expect their effects on risk to largely be mediated by more proximal determinants. However, to effectively implement programming, it is crucial to understand these factors, as well as the broader structural barriers and limits

A model for risk group proportions

to personal agency faced by AGYW. Importantly, programs must ensure that intervention prioritisation occurs without stigmatising or blaming AGYW.

By considering a range of possible risk stratification strategies, I showed that successful implementation of a risk-stratified approach would allow substantially more of those at risk for infections to be identified before infection occurs. A considerable proportion of estimated new infections were among FSW, supporting the case for HIV programming efforts focused on key population groups (Baral et al. 2012). There is substantial variation in the importance of prioritisation by age, location and behaviour within each country. This highlights the importance of understanding and tailoring HIV prevention efforts to country-specific contexts. By standardising the analysis across all 13 countries, I showed the additional efficiency benefits of resource allocation between countries.

I found a geographic delineation in the proportion of women cohabiting between southern and eastern Africa, calling attention to a divide attributable to many cultural, social, and economic factors. The delineation does not represent a boundary between predominately Christian and Muslim populations, which is further north. I also note that the high numbers of adolescent girls aged 15-19 cohabiting in Mozambique is markedly different from the other countries (UNICEF 2019).

Brugh et al. (2021) previously geographically mapped AGYW HIV risk groups using biomarker and behavioural data from the most recent surveys in Eswatini, Haiti and Mozambique to define and subsequently map risk groups with a range of machine learning techniques. My work builds on Brugh et al. (2021) by including more countries, integrating a greater number of surveys, and connecting risk group proportions with HIV epidemic indicators to help inform programming.

My modelled estimates of risk group proportions improve upon direct survey results for three reasons. First, by taking a modular modelling approach, I integrated all relevant survey information from multiple years, allowing estimation of the FSW proportion for surveys without a specific transactional sex question. Second, whereas direct estimates exhibit large sampling variability at a district level, I alleviated this issue using spatio-temporal smoothing (Figure 5.13). Third, I provided estimates

A model for risk group proportions

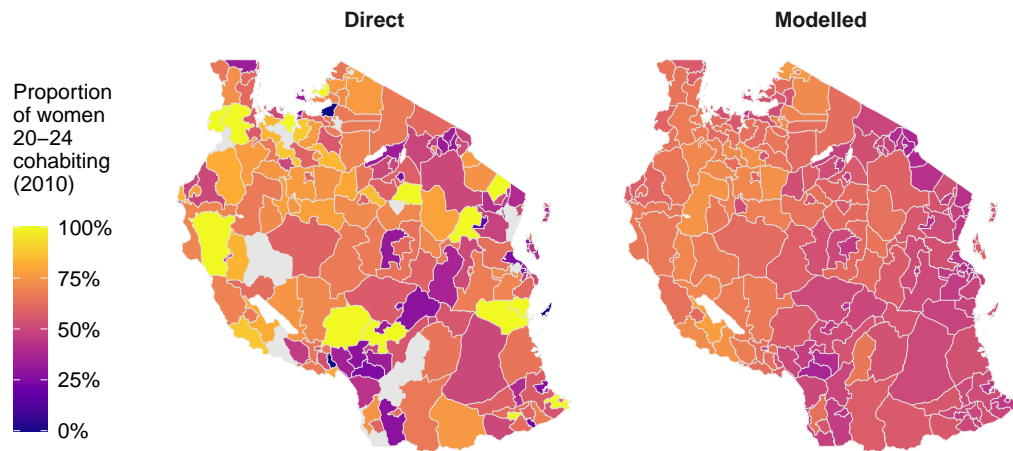


Figure 5.13: Figure caption.

in all district-years, including those not directly sampled by surveys, allowing estimates to be consistently fed into further analysis and planning pipelines such as my analysis of risk group specific prevalence and incidence (Figure 5.13).

The final surveys included in the risk model were conducted in 2018. The analysis may be updated with more surveys as they become available. I do not anticipate that the risk group proportions will change substantially, as I found that they did not change significantly over time.

My analysis focused on females aged 15-29 years, and could be extended to consider optimisation of prevention more broadly, accounting for the 0% of new infections among adults 15-49 which occur in women 30-49 and men 15-49. Estimating sexual risk behaviour in adults 15-49 would be a crucial step toward greater understanding of the dynamics of the HIV epidemic in sub-Saharan Africa, and would allow incidence models to include stratification of individuals by sexual risk.

5.5.1 Limitations

This analysis was subject to challenges shared by most approaches to monitoring sexual behaviour in the general population (Cleland et al. 2004). In particular,

A model for risk group proportions

under-reporting of higher risk sexual behaviours among AGYW could affect the validity of my risk group proportion estimates. Due to social stigma or disapproval, respondents may be reluctant to report non-marital partners (Nnko et al. 2004; Helleringer et al. 2011) or may bias their reporting of sexual debut (Zaba et al. 2004; Wringe et al. 2009; Nguyen and Eaton 2022). For guidance of resource allocation, differing rates of under-reporting by country, district, year or age group are particularly concerning to the applicability of my results; and, while it may be reasonable to assume a constant rate over space-time, the same cannot be said for age, where aspects of under-reporting have been shown to decline as respondents age (Glynn et al. 2011), suggesting that the elevated risks I found faced by younger women are likely a conservative estimate. If present, these reporting biases will also have distorted the estimates of infection risk ratios and prevalence ratios I used in my analysis, likely over-attributing risk to higher risk groups.

I have the least confidence in my estimates for the FSW risk group. As well as having the smallest sample sizes, my transactional sex estimates do not overcome the difficulties of sampling hard to reach groups. I inherent any limitations of the national FSW estimates (Stevens, Sabin, Arias Garcia, et al. 2022) which I adjust my estimates of transactional sex to match. Furthermore, I do not consider seasonal migration patterns, which may particularly affect FSW population size. More generally, I did not consider covariates potentially predictive of risk group proportions (such as sociodemographic characteristics, education, local economic activity, cultural and religious norms and attitudes), which are typically difficult to measure spatially. Identifying measurable correlates of risk, or particular settings in which time-concentrated HIV risk occurs, is an important area for further research to improve risk prioritisation and precision HIV programme delivery.

The efficiency of each stratified prevention strategy depends on the ability of programmes to identify and effectively reach those in each strata. My analysis of new infections potentially averted assumed a “best-case” scenario where AGYW of every strata can be reached perfectly, and should therefore be interpreted as illustrating the potentially obtainable benefits rather than benefits which would be

A model for risk group proportions

obtained from any specific intervention strategy. In practice, stratified prevention strategies are likely to be substantially less efficient than this best-case scenario. Factors I did not consider include the greater administrative burden of more complex strategies, variation in difficulty or feasibility of reaching individuals in each strata, variation in the range or effectiveness of interventions by strata, and changes in strata membership that may occur during the course of a year. Identifying and reaching behavioural strata may be particularly challenging. Empirical evaluations of behavioural risk screening tools have found only moderate discriminatory ability (Jia et al. 2022), and risk behaviour may change rapidly among young populations, increasing the challenge to effectively deliver appropriately timed prevention packages. This consideration may motivate selecting risk groups based on easily observable attributes, such as attendance of a particular service or facility, rather than sexual behaviour.

In conducting this work, there was insufficient engagement with country experts or civil society organisations. As a result, in early use of the risk group tool the FSW population size estimates were met with some disagreement in Malawi. In that instance, the cause of the disagreement was external model inputs used. In future, estimates should be generated and reviewed by country teams.

5.5.2 Conclusion

I estimated HIV risk group proportions, HIV prevalences and HIV incidences for AGYW aged 15-19, 20-24 and 25-29 years at a district-level in 13 priority countries. Using these estimates, I analysed the number of infections that could be reached by prioritisation based upon location, age and behaviour. Though subject to limitations, these estimates provide data that national HIV programmes can use to set targets and implement differentiated HIV prevention strategies as outlined in the Global AIDS Strategy. Successfully implementing this approach would result in more efficiently reaching a greater number of those at risk of infection.

Among AGYW, there was systematic variation in sexual behaviour by age and location, but not over time. Age group variation was primarily attributable to age

A model for risk group proportions

of sexual debut (ages 15-24). Spatial variation was particularly present between those who reported one cohabiting partner versus non-regular or multiple partners. Risk group proportions did not change substantially over time, indicating that norms relating to sexual behaviour are relatively static. These findings underscore the importance of providing effective HIV prevention options tailored to the needs of particular age groups, as well as local norms around sexual partnerships.

6

Fast approximate Bayesian inference

This chapter describes a novel Bayesian inference method. Development of the method was motivated by the Naomi small-area estimation model (Eaton et al. 2021). Over 35 countries (UNAIDS 2023b) have used the Naomi model software (<https://naomi.unaids.org>) to produce subnational estimates of HIV indicators by synthesising evidence from multiple data sources. The complexity and size of the model makes obtaining fast and accurate Bayesian inferences challenging. As such, inferences have previously been obtained using an empirical Bayes approximation to full Bayesian inference, where hyperparameters are obtained by optimisation of the marginal posterior (Casella 1985). This approximation is undesirable as it can result in underestimation of uncertainty, ultimately leading to worse policy decisions stemming from overconfidence. Instead, I propose integrating over the hyperparameters using a modification of adaptive Gauss-Hermite quadrature (Naylor and Smith 1982) for moderate dimensions.

The methods developed in this chapter combine Laplace approximations with adaptive quadrature, and are descended from the integrated nested Laplace approximation (INLA) method pioneered by Rue, Martino, and Chopin (2009). The INLA method has enabled fast and accurate Bayesian inferences for a vast array of models, across a large number of scientific fields (Rue, Riebler, et al. 2017). The success of

INLA is in large part due to its accessible implementation in the **R-INLA** software. Most applications and methodological developments of the INLA method have used **R-INLA**. Exceptions include the simplified INLA approach of Wood (2020), implemented in the **mgcv** R package, and Stringer et al. (2022). In pursuit of a suitable inference approach for the Naomi model, I implemented an INLA-like method outside **R-INLA**, building upon Stringer et al. (2022). My implementation is compatible with a wider range of models than **R-INLA**, and uses automatic differentiation to obtain the derivatives required for the Laplace approximation.

Though I began working on this project close to the start of my PhD, I only began making meaningful progress after reading Stringer et al. (2022). I am grateful to later have had the opportunity to collaborate with Alex Stringer, and work closely together during my visit to the University of Waterloo in the fall term of 2022. The results of our work are presented in Howes, Stringer, et al. (2023+). Code for the analysis in this chapter is available from <https://github.com/athowes/naomi-aghq>.

6.1 Inference methods and software

In a Bayesian analysis, the primary goal is to perform inference. That is, to obtain the posterior distribution

$$p(\boldsymbol{\phi} \mid \mathbf{y}) = \frac{p(\boldsymbol{\phi}, \mathbf{y})}{p(\mathbf{y})}, \quad (6.1)$$

or some way to compute relevant functions of it. The posterior distribution encapsulates beliefs about the parameters $\boldsymbol{\phi} = (\phi_1, \dots, \phi_d)$ having observed data $\mathbf{y} = (y_1, \dots, y_n)$, which I assume to be vectors.

Inference is a sensible goal because the posterior distribution is sufficient for use in decision making. Given a loss function $l(a, \boldsymbol{\phi})$ the expected posterior loss of a decision a depends on the data only via the posterior distribution

$$\mathbb{E}(l(a, \boldsymbol{\phi}) \mid \mathbf{y}) = \int_{\mathbb{R}^d} l(a, \boldsymbol{\phi}) p(\boldsymbol{\phi} \mid \mathbf{y}) d\boldsymbol{\phi}. \quad (6.2)$$

For example, given the posterior distribution of the current demand for HIV treatment at a particular facility, historic data about treatment demand are not required for planning of service provision.

It is usually intractable to straightforwardly obtain the posterior distribution. This is because the denominator contains a potentially high-dimensional integral, depending on the value of $d \in \mathbb{Z}^+$, over the parameters

$$p(\mathbf{y}) = \int_{\mathbb{R}^d} p(\mathbf{y}, \boldsymbol{\phi}) d\boldsymbol{\phi}, \quad (6.3)$$

sometimes called the evidence or posterior normalising constant. For this reason, approximations to the posterior distribution $\tilde{p}(\boldsymbol{\phi} | \mathbf{y})$ are typically used in place of the exact posterior distribution.

Some approximate Bayesian inference methods, like Markov chain Monte Carlo (MCMC), avoid directly calculating the posterior normalising constant, instead working with the unnormalised posterior distribution

$$p(\boldsymbol{\phi} | \mathbf{y}) \propto p(\boldsymbol{\phi}, \mathbf{y}), \quad (6.4)$$

where $p(\mathbf{y})$ is not a function of $\boldsymbol{\phi}$ and so can be removed as a constant. Other approximate Bayesian inference methods can more directly be thought of as ways to estimate the posterior normalising constant. The methods in this chapter fall into this latter category, sometimes described as deterministic Bayesian inference methods. This section provides background on these methods and the software used to implement them.

6.1.1 The Laplace approximation

Laplace's method (Laplace 1774) is a technique used to approximate integrals of the form

$$\int \exp(C h(\mathbf{z})) d\mathbf{z}, \quad (6.5)$$

where $C > 0$ is a constant, h is a function which is twice-differentiable, and \mathbf{z} are generic variables. The Laplace approximation (Tierney and Kadane 1986) is

obtained by application of Laplace's method to calculate the posterior normalising constant (Equation (6.3)). Let $h(\boldsymbol{\phi}) = \log p(\boldsymbol{\phi}, \mathbf{y})$ such that

$$p(\mathbf{y}) = \int_{\mathbb{R}^d} p(\mathbf{y}, \boldsymbol{\phi}) d\boldsymbol{\phi} = \int_{\mathbb{R}^d} \exp(h(\boldsymbol{\phi})) d\boldsymbol{\phi}. \quad (6.6)$$

Laplace's method involves approximating the function h by its second order Taylor expansion. This expansion is then evaluated at a maxima of h to eliminate the first order term. Let

$$\hat{\boldsymbol{\phi}} = \arg \max_{\boldsymbol{\phi}} h(\boldsymbol{\phi}) \quad (6.7)$$

be the posterior mode, and

$$\hat{\mathbf{H}} = -\frac{\partial^2}{\partial \boldsymbol{\phi} \partial \boldsymbol{\phi}^\top} h(\boldsymbol{\phi})|_{\boldsymbol{\phi}=\hat{\boldsymbol{\phi}}} \quad (6.8)$$

be the Hessian matrix evaluated at the posterior mode. The Laplace approximation is then

$$\tilde{p}_{\text{LA}}(\mathbf{y}) = \int_{\mathbb{R}^d} \exp \left(h(\hat{\boldsymbol{\phi}}) - \frac{1}{2} (\boldsymbol{\phi} - \hat{\boldsymbol{\phi}})^\top \hat{\mathbf{H}} (\boldsymbol{\phi} - \hat{\boldsymbol{\phi}}) \right) d\boldsymbol{\phi} \quad (6.9)$$

$$= p(\hat{\boldsymbol{\phi}}, \mathbf{y}) \cdot \frac{(2\pi)^{d/2}}{|\hat{\mathbf{H}}|^{1/2}}. \quad (6.10)$$

The result above is calculated using the known normalising constant of the Gaussian distribution

$$p_{\text{G}}(\boldsymbol{\phi} | \mathbf{y}) = \mathcal{N}(\boldsymbol{\phi} | \hat{\boldsymbol{\phi}}, \hat{\mathbf{H}}^{-1}) = \frac{|\hat{\mathbf{H}}|^{1/2}}{(2\pi)^{d/2}} \exp \left(-\frac{1}{2} (\boldsymbol{\phi} - \hat{\boldsymbol{\phi}})^\top \hat{\mathbf{H}} (\boldsymbol{\phi} - \hat{\boldsymbol{\phi}}) \right). \quad (6.11)$$

The Laplace approximation may be thought of as approximating the posterior distribution by a Gaussian distribution $p(\boldsymbol{\phi} | \mathbf{y}) \approx p_{\text{G}}(\boldsymbol{\phi} | \mathbf{y})$ such that

$$\tilde{p}_{\text{LA}}(\mathbf{y}) = \frac{p(\boldsymbol{\phi}, \mathbf{y})}{p_{\text{G}}(\boldsymbol{\phi} | \mathbf{y})} \Big|_{\boldsymbol{\phi}=\hat{\boldsymbol{\phi}}}. \quad (6.12)$$

Calculation of the Laplace approximation requires obtaining the second derivative of h with respect to $\boldsymbol{\phi}$ (Equation (6.8)). Derivatives may also be used to improve the performance of the optimisation algorithm used to obtain the maxima of h (Equation (6.7)) by providing access to the gradient of h with respect to $\boldsymbol{\phi}$.

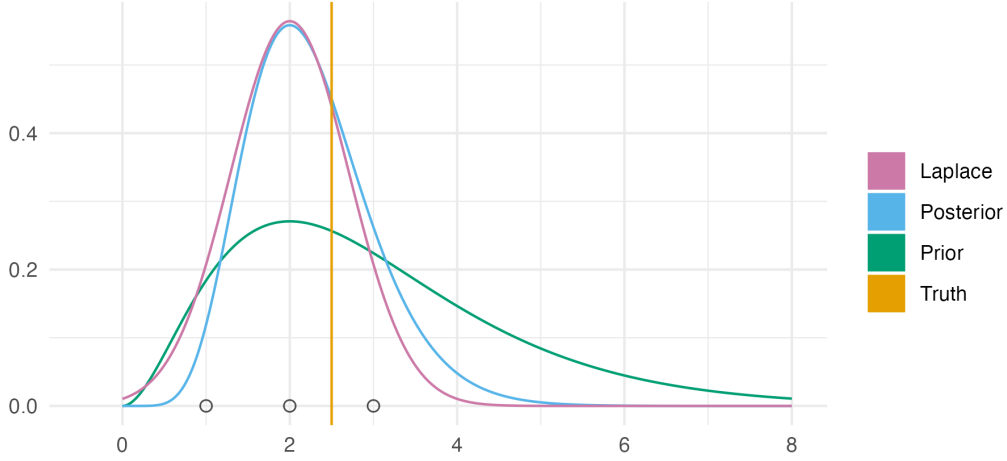


Figure 6.1: Demonstration of the Laplace approximation for the simple Bayesian inference example of Figure 3.1. The unnormalised posterior is $p(\phi, \mathbf{y}) = \phi^8 \exp(-4\phi)$, and can be recognised as the unnormalised gamma distribution $\text{Gamma}(9, 4)$. The true log normalising constant is $\log p(\mathbf{y}) = \log \Gamma(9) - 9 \log(4) = -1.872046$, whereas the Laplace approximate log normalising constant is $\log \tilde{p}_{\text{LA}}(\mathbf{y}) = -1.882458$, resulting from the Gaussian approximation $p_{\mathcal{G}}(\phi | \mathbf{y}) = \mathcal{N}(\phi | \mu = 2, \tau = 2)$.

The marginal Laplace approximation

Approximating the full joint posterior distribution using a Gaussian distribution may be inaccurate. An alternative approach is to approximate the marginal posterior distribution of some subset of the parameters. The remaining non-Gaussian parameters may then be handled using another, more appropriate, method.

Let $\boldsymbol{\phi} = (\mathbf{x}, \boldsymbol{\theta})$ and consider a three-stage hierarchical model

$$p(\mathbf{y}, \mathbf{x}, \boldsymbol{\theta}) = p(\mathbf{y} | \mathbf{x}, \boldsymbol{\theta})p(\mathbf{x} | \boldsymbol{\theta})p(\boldsymbol{\theta}), \quad (6.13)$$

where $\mathbf{x} = (x_1, \dots, x_N)$ is the latent field, and $\boldsymbol{\theta} = (\theta_1, \dots, \theta_m)$ are the hyperparameters. Applying a Gaussian approximation to the latent field, we have $h(\mathbf{x}, \boldsymbol{\theta}) = \log p(\mathbf{y}, \mathbf{x}, \boldsymbol{\theta})$ with N -dimensional posterior mode

$$\hat{\mathbf{x}}(\boldsymbol{\theta}) = \arg \max_{\mathbf{x}} h(\mathbf{x}, \boldsymbol{\theta}) \quad (6.14)$$

and $N \times N$ -dimensional Hessian matrix evaluated at the posterior mode

$$\hat{\mathbf{H}}(\boldsymbol{\theta}) = -\frac{\partial^2}{\partial \mathbf{x} \partial \mathbf{x}^\top} h(\mathbf{x}, \boldsymbol{\theta})|_{\mathbf{x}=\hat{\mathbf{x}}(\boldsymbol{\theta})}. \quad (6.15)$$

Dependence on the hyperparameters $\boldsymbol{\theta}$ is made explicit in both Equation (6.14) and (6.15). In other words, there is a Gaussian approximation to the marginal posterior of the latent field $\tilde{p}_{\mathbf{G}}(\mathbf{x} | \boldsymbol{\theta}, \mathbf{y}) = \mathcal{N}(\mathbf{x} | \hat{\mathbf{x}}(\boldsymbol{\theta}), \hat{\mathbf{H}}(\boldsymbol{\theta})^{-1})$ at each value $\boldsymbol{\theta}$ in the space \mathbb{R}^m . The resulting marginal Laplace approximation, for a particular value of the hyperparameters, is then

$$\tilde{p}_{\text{LA}}(\boldsymbol{\theta}, \mathbf{y}) = \int_{\mathbb{R}^N} \exp \left(h(\hat{\mathbf{x}}(\boldsymbol{\theta}), \boldsymbol{\theta}) - \frac{1}{2} (\mathbf{x} - \hat{\mathbf{x}}(\boldsymbol{\theta}))^\top \hat{\mathbf{H}}(\boldsymbol{\theta}) (\mathbf{x} - \hat{\mathbf{x}}(\boldsymbol{\theta})) \right) d\mathbf{x} \quad (6.16)$$

$$= \exp(h(\hat{\mathbf{x}}(\boldsymbol{\theta}), \mathbf{y})) \cdot \frac{(2\pi)^{d/2}}{|\hat{\mathbf{H}}(\boldsymbol{\theta})|^{1/2}} \quad (6.17)$$

$$= \frac{p(\mathbf{y}, \mathbf{x}, \boldsymbol{\theta})}{\tilde{p}_{\mathbf{G}}(\mathbf{x} | \boldsymbol{\theta}, \mathbf{y})} \Big|_{\mathbf{x}=\hat{\mathbf{x}}(\boldsymbol{\theta})}. \quad (6.18)$$

The marginal Laplace approximation is most accurate when the marginal posterior $p(\mathbf{x} | \boldsymbol{\theta}, \mathbf{y})$ is accurately approximated by a Gaussian distribution. For the class of latent Gaussian models (Rue, Martino, and Chopin 2009) the prior distribution on the latent field is Gaussian $\mathbf{x} \sim \mathcal{N}(\mathbf{x} | \boldsymbol{\theta})$. Although the marginal posterior distribution

$$p(\mathbf{x} | \boldsymbol{\theta}, \mathbf{y}) \propto \mathcal{N}(\mathbf{x} | \boldsymbol{\theta}) p(\mathbf{y} | \mathbf{x}, \boldsymbol{\theta}) \quad (6.19)$$

is not Gaussian, its deviation from Gaussianity can be expected to be small if $\log p(\mathbf{y} | \mathbf{x}, \boldsymbol{\theta})$ satisfies some condition which remains to be detailed.

6.1.2 Quadrature

Quadrature is a method used to approximate integrals using a weighted sum of function evaluations. As with the Laplace approximation, it is deterministic in that the computational procedure is not intrinsically random. Let \mathcal{Q} be a set of quadrature nodes $\mathbf{z} \in \mathcal{Q}$ and $\omega : \mathbb{R}^d \rightarrow \mathbb{R}$ be a weighting function. Then, quadrature can be used to estimate the posterior normalising constant (Equation (6.3)) by

$$\tilde{p}_{\mathcal{Q}}(\mathbf{y}) = \sum_{\mathbf{z} \in \mathcal{Q}} p(\mathbf{y}, \mathbf{z}) \omega(\mathbf{z}). \quad (6.20)$$

To illustrate quadrature for a simple example, consider integrating the univariate function $f(z) = z \sin(z)$ between $z = 0$ and $z = \pi$. This integral is known

analytically to be π . A quadrature approximation of this integral is

$$\pi = \int_0^\pi z \sin(z) dz \approx \sum_{z \in \mathcal{Q}} z \sin(z) \omega(z), \quad (6.21)$$

where $\mathcal{Q} = \{z_1, \dots, z_k\}$ are a set of k quadrature nodes and $\omega : \mathbb{R} \rightarrow \mathbb{R}$.

The trapezoid rule is an example of a quadrature rule, in which quadrature nodes are spaced throughout the domain according to $\epsilon_i = z_i - z_{i-1} > 0$ for $1 < i < k$. The weighting function is $\omega(z_i) = \epsilon_i$ for $1 < i < k$ and $\omega(z_1) = \epsilon_1/2$ for $i \in \{1, k\}$. Figure 6.2 shows application of the trapezoid rule to Equation (6.21). The more quadrature nodes are used, the more accurate the estimate of the integrand is. Under some regularity conditions on f , as $\epsilon \rightarrow 0$ the quadrature estimate obtained using the trapezoid rule converges to the true value of the integral. Indeed, this approach was used by Riemann to provide the first rigorous definition of the integral.

Quadrature methods are most effective when integrating over small dimensions. This is because the number of quadrature nodes required to be evaluated in the computation grows exponentially with the dimension. For even moderate dimension, this quickly becomes intractable. For example, using 5, 25, or 125 quadrature nodes per dimension, as in Figure 6.2, in three-dimensions (rather than one) would require 125, 15625 or 1953125 quadrature nodes respectively. Though quadrature is embarrassingly parallel, solutions requiring the evaluation of upwards of millions of quadrature nodes are unlikely to be tractable.

Gauss-Hermite quadrature

Gauss-Hermite quadrature [GHQ; Davis and Rabinowitz (1975)] is a quadrature rule designed to integrate functions of the form $f(\mathbf{z}) = \varphi(\mathbf{z})P_\alpha(\mathbf{z})$ exactly such that

$$\int \varphi(\mathbf{z})P_\alpha(\mathbf{z}) d\mathbf{z} = \sum_{\mathbf{z} \in \mathcal{Q}} \varphi(\mathbf{z})P_\alpha(\mathbf{z})\omega(\mathbf{z}). \quad (6.22)$$

The term $\varphi(\cdot)$ is a standard multivariate normal density $\mathcal{N}(\cdot | \mathbf{0}, \mathbf{I})$, where $\mathbf{0}$ is the zero-vector and \mathbf{I} is the identity matrix of relevant dimension, and the term $P_\alpha(\cdot)$ is a polynomial with highest degree monomial $\alpha \leq 2k - 1$, where k is the number of quadrature nodes per dimension. GHQ is attractive for Bayesian inference problems

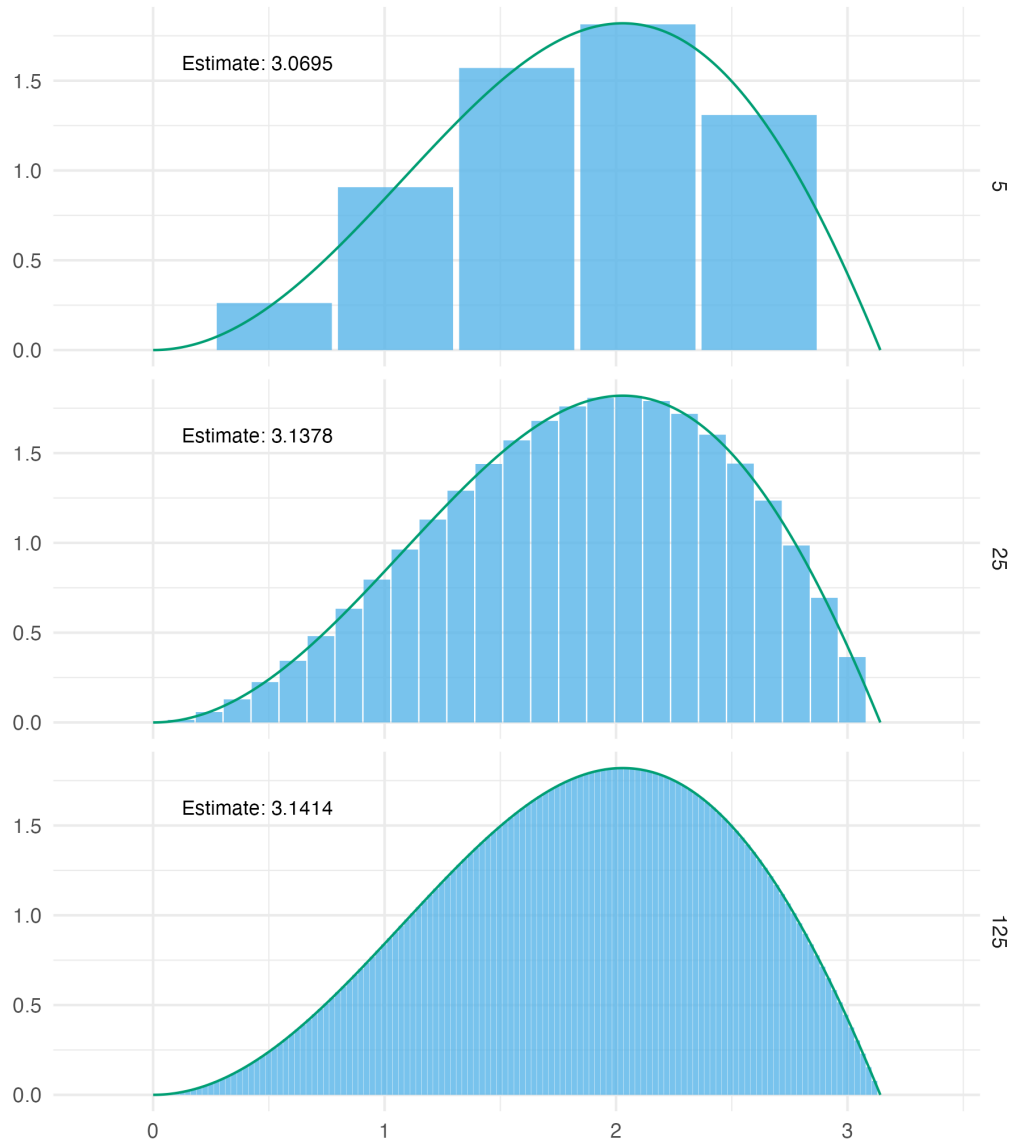


Figure 6.2: The trapezoid rule with $k = 5, 25, 125$ equally-spaced ($\epsilon_i = \epsilon > 0$) quadrature nodes can be used to integrate the function $f(z) = z \sin(z)$ in the domain $[0, \pi]$. Here, the exact solution is $\pi \approx 3.1416$. As k increases and more nodes are used in the computation, the quadrature estimate becomes closer to the exact solution.

because posterior distributions are typically well approximated by functions of this form. This statement requires support using the Bernstein–von Mises theorem in combination with other arguments.

I follow the notation for GHQ established by Bilodeau et al. (2022). First, to construct the univariate GHQ rule for $z \in \mathbb{R}$, let $H_k(z)$ be the k th (probabilist's) Hermite polynomial

$$H_k(z) = (-1)^k \exp(z^2/2) \frac{d}{dz^k} \exp(-z^2/2) = (-1)^k \exp(z^2/2) \frac{d}{dz^k} \exp(-z^2/2) \quad (6.23)$$

The Hermite polynomials are defined to be orthogonal with respect to the standard Gaussian probability density function

$$\int H_k(z) H_l(z) \varphi(z) dz = \delta_{kl}, \quad (6.24)$$

where $\delta_{kl} = 1$ if $k = l$ and $\delta_{kl} = 0$ otherwise. The relevance of the above equation is that... The GHQ nodes $z \in \mathcal{Q}(1, k)$ are given by the k zeroes of the k th Hermite polynomial. For $k = 1, 2, 3$ these zeros, up to three decimal places, are

$$H_1(z) = z = 0 \implies \mathcal{Q}(1, 1) = \{0\}, \quad (6.25)$$

$$H_2(z) = z^2 - 1 = 0 \implies \mathcal{Q}(1, 2) = \{-0.707, 0.707\}, \quad (6.26)$$

$$H_3(z) = z^3 - 3z = 0 \implies \mathcal{Q}(1, 3) = \{-1.225, 0, 1.225\}. \quad (6.27)$$

The corresponding weighting function $\omega : \mathcal{Q}(1, k) \rightarrow \mathbb{R}$ chosen to satisfy Equation (6.22) is given by

$$\omega(z) = \frac{k!}{\varphi(z) \cdot [H_{k+1}(z)]^2}. \quad (6.28)$$

Multivariate GHQ rules are usually constructed using the product rule with identical univariate GHQ rules in each dimension. In d dimensions, the multivariate GHQ nodes $\mathbf{z} \in \mathcal{Q}(d, k)$ are defined by

$$\mathcal{Q}(d, k) = \mathcal{Q}(1, k)^d = \mathcal{Q}(1, k) \times \cdots \times \mathcal{Q}(1, k). \quad (6.29)$$

The corresponding weighting function $\omega : \mathcal{Q}(d, k) \rightarrow \mathbb{R}$ is given by $\omega(\mathbf{z}) = \prod_{j=1}^d \omega(z_j)$.

Adaptive quadrature

In adaptive quadrature, the quadrature nodes and weights depend on the specific integrand being considered. Using an adaptive quadrature rules is particularly important for Bayesian inference problems because the posterior normalising constant $p(\mathbf{y})$ is a function of the data. No fixed quadrature rule can be expected to effectively integrate all possible posterior distributions produced by observation of certain data \mathbf{y} . For example, effective use of the trapezoid rule requires good choices for the start and end point, and spacing between quadrature nodes.

In adaptive GHQ [AGHQ; Naylor and Smith (1982)] the quadrature nodes are shifted by the mode of the integrand, and rotated based on a matrix decomposition of the inverse curvature at the mode. Consider application of AGHQ to calculation of the posterior normalising constant. The transformation of the GHQ nodes $\mathcal{Q}(d, k)$ is then

$$\boldsymbol{\phi}(\mathbf{z}) = \hat{\mathbf{P}}\mathbf{z} + \hat{\boldsymbol{\phi}}, \quad (6.30)$$

where $\hat{\mathbf{P}}$ is a matrix decomposition of $\hat{\mathbf{H}}^{-1} = \hat{\mathbf{P}}\hat{\mathbf{P}}^\top$. The resulting adaptive quadrature estimate of the posterior normalising constant is

$$\tilde{p}_{\text{AQ}}(\mathbf{y}) = |\hat{\mathbf{P}}| \sum_{\mathbf{z} \in \mathcal{Q}} p(\mathbf{y}, \boldsymbol{\phi}(\mathbf{z})) \omega(\mathbf{z}) = |\hat{\mathbf{P}}| \sum_{\mathbf{z} \in \mathcal{Q}} p(\mathbf{y}, \hat{\mathbf{P}}\mathbf{z} + \hat{\boldsymbol{\phi}}) \omega(\mathbf{z}). \quad (6.31)$$

The quantities $\hat{\boldsymbol{\phi}}$ and $\hat{\mathbf{H}}$ are exactly those given in Equations (6.7) and (6.8) and used in the Laplace approximation. Indeed, when $k = 1$ then AGHQ corresponds exactly to the Laplace approximation. To see this, we have $H_1(z)$ with zero $z = 0$ such that the adapted node is given by the mode $\boldsymbol{\phi}(\mathbf{z} = \mathbf{0}) = \hat{\boldsymbol{\phi}}$. The weighting function is given by

$$\omega(0)^d = \left(\frac{1!}{\varphi(0) \cdot H_2(0)^2} \right)^d = \left(\frac{1}{\varphi(0)} \right)^d = (2\pi)^{d/2}. \quad (6.32)$$

The AGHQ estimate of the normalising constant for $k = 1$ is given by

$$\tilde{p}_{\text{AQ}}(\mathbf{y}) = p(\mathbf{y}, \hat{\boldsymbol{\phi}}) \cdot |\hat{\mathbf{P}}| \cdot (2\pi)^{d/2} = p(\mathbf{y}, \hat{\boldsymbol{\phi}}) \cdot \frac{(2\pi)^{d/2}}{|\hat{\mathbf{H}}|^{1/2}}, \quad (6.33)$$

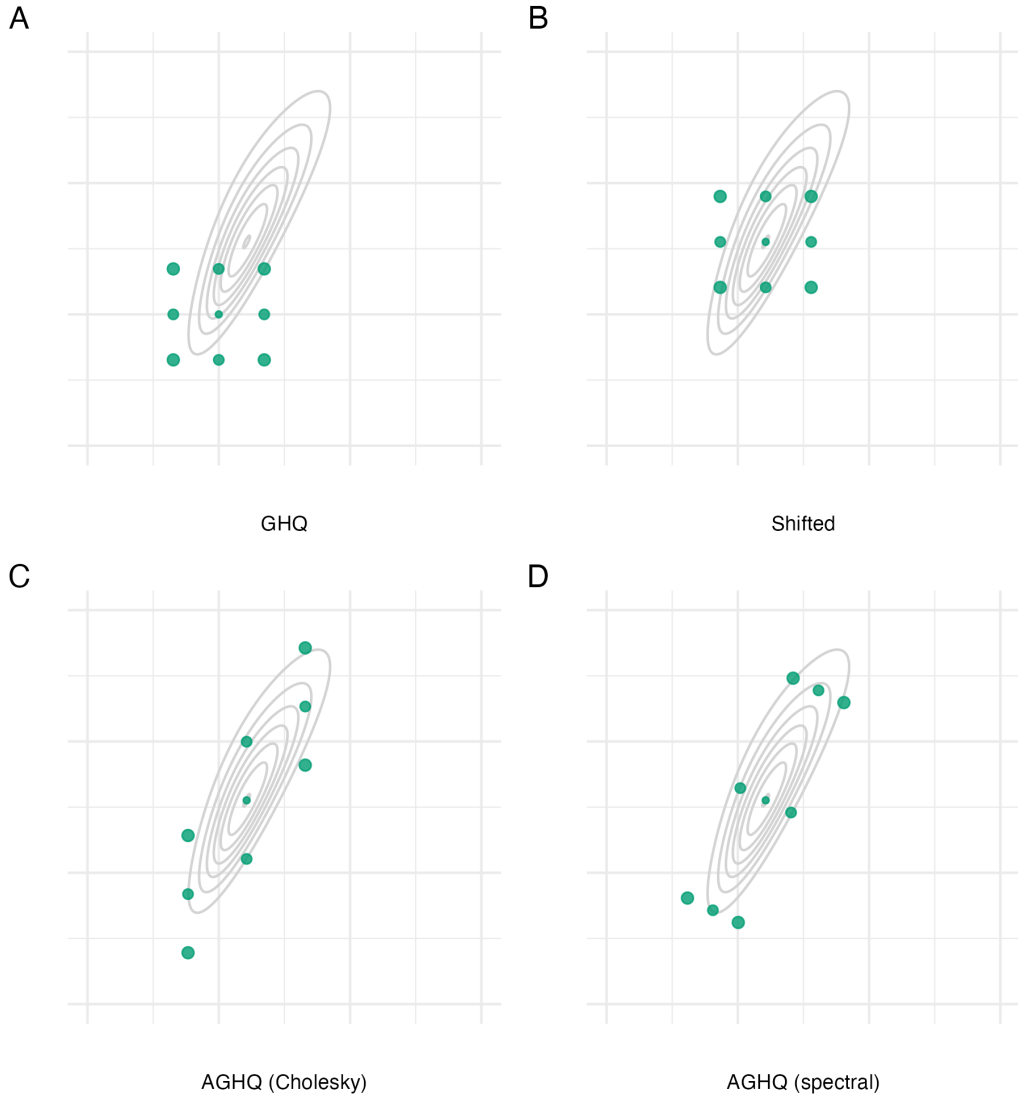


Figure 6.3: The Gauss-Hermite quadrature nodes $\mathbf{z} \in \mathcal{Q}(2, 3)$ for a two-dimensional integral with three nodes per dimension (A). Adaption occurs based on the mode (B) and covariance of the integrand via either the Cholesky (C) or spectral (D) decomposition of the inverse curvature at the mode. Here, the integrand is $f(z_1, z_2) = \text{sn}(0.5z_1, \alpha = 2) \cdot \text{sn}(0.8z_1 - 0.5z_2, \alpha = -2)$, where $\text{sn}(\cdot)$ is the standard skewnormal probability density function with shape parameter $\alpha \in \mathbb{R}$. For each quadrature rule, the estimate of the integral is given by...

and corresponds exactly to the Laplace approximation $\tilde{p}_{\text{LA}}(\mathbf{y})$ given in Equation (6.10).

Two alternatives for the matrix decomposition $\hat{\mathbf{H}}^{-1} = \hat{\mathbf{P}}\hat{\mathbf{P}}^\top$ are the Cholesky and spectral decomposition (Jäckel 2005). For the Cholesky decomposition $\hat{\mathbf{P}} = \hat{\mathbf{L}}$, where $\hat{\mathbf{L}}$ is lower triangular. For the spectral decomposition $\hat{\mathbf{P}} = \hat{\mathbf{E}}\hat{\Lambda}^{1/2}$, where $\hat{\mathbf{E}} = (\hat{\mathbf{e}}_1, \dots, \hat{\mathbf{e}}_m)$ contains the eigenvectors of $\hat{\mathbf{H}}^{-1}$ and $\hat{\Lambda}$ is a diagonal matrix containing its eigenvalues $(\hat{\lambda}_1, \dots, \hat{\lambda}_m)$. Figure 6.3 demonstrates GHQ and AGHQ for a two-dimensional example, using both decomposition approaches. Using the Cholesky decomposition results in adapted quadrature nodes which collapse along one of the dimensions, as a result of the matrix $\hat{\mathbf{L}}$ being lower triangular. On the other hand, using the spectral decompositions results in adapted quadrature nodes which lie along the orthogonal eigenvectors of $\hat{\mathbf{H}}^{-1}$.

6.1.3 Integrated nested Laplace approximation

The integrated nested Laplace approximation (INLA) method (Rue, Martino, and Chopin 2009) combines marginal Laplace approximations with quadrature to enable approximation of posterior marginal distributions. Consider the marginal Laplace approximation of Section 6.1.1 for a three-stage hierarchical model given by

$$\tilde{p}_{\text{LA}}(\boldsymbol{\theta}, \mathbf{y}) = \frac{p(\mathbf{y}, \mathbf{x}, \boldsymbol{\theta})}{\tilde{p}_{\text{G}}(\mathbf{x} | \boldsymbol{\theta}, \mathbf{y})} \Big|_{\mathbf{x}=\hat{\mathbf{x}}(\boldsymbol{\theta})}. \quad (6.34)$$

To complete approximation of the posterior normalising constant, the marginal Laplace approximation can be integrated over the hyperparameters using a quadrature rule. Following Stringer et al. (2022) I consider use of AGHQ as the particular quadrature rule. Let $\mathbf{z} \in \mathcal{Q}(m, k)$ be the m -dimensional GHQ nodes constructed using the product rule with k nodes per dimension, and $\omega : \mathbb{R}^m \rightarrow \mathbb{R}$ the corresponding weighting function. These nodes are adapted by $\boldsymbol{\theta}(\mathbf{z}) = \hat{\mathbf{P}}_{\text{LA}}\mathbf{z} + \hat{\boldsymbol{\theta}}_{\text{LA}}$ where

$$\hat{\boldsymbol{\theta}}_{\text{LA}} = \arg \max_{\boldsymbol{\theta}} \log \tilde{p}_{\text{LA}}(\boldsymbol{\theta}, \mathbf{y}), \quad (6.35)$$

$$\hat{\mathbf{H}}_{\text{LA}} = -\frac{\partial^2}{\partial \boldsymbol{\theta} \partial \boldsymbol{\theta}^\top} \log \tilde{p}_{\text{LA}}(\boldsymbol{\theta}, \mathbf{y}) \Big|_{\boldsymbol{\theta}=\hat{\boldsymbol{\theta}}_{\text{LA}}}, \quad (6.36)$$

$$\hat{\mathbf{H}}_{\text{LA}}^{-1} = \hat{\mathbf{P}}_{\text{LA}} \hat{\mathbf{P}}_{\text{LA}}^\top. \quad (6.37)$$

The nested AGHQ estimate of the posterior normalising constant is then

$$\tilde{p}_{\text{AQ}}(\mathbf{y}) = |\hat{\mathbf{P}}_{\text{LA}}| \sum_{\mathbf{z} \in \mathcal{Q}(m,k)} \tilde{p}_{\text{LA}}(\boldsymbol{\theta}(\mathbf{z}), \mathbf{y}) \omega(\mathbf{z}). \quad (6.38)$$

The normalised marginal Laplace approximation is

$$\tilde{p}_{\text{LA}}(\boldsymbol{\theta} | \mathbf{y}) = \frac{\tilde{p}_{\text{LA}}(\boldsymbol{\theta}, \mathbf{y})}{\tilde{p}_{\text{AQ}}(\mathbf{y})}. \quad (6.39)$$

The posterior marginals $\tilde{p}(\theta_j | \mathbf{y})$ may be obtained by...

The following sections discuss methods for obtaining $\tilde{p}(\mathbf{x} | \mathbf{y})$.

Gaussian marginals

Inferences for the latent field can be obtained by approximation of $p(\mathbf{x} | \mathbf{y})$ using nested application of the quadrature rule (Rue and Martino 2007)

$$p(\mathbf{x} | \mathbf{y}) = \int p(\mathbf{x}, \boldsymbol{\theta} | \mathbf{y}) d\boldsymbol{\theta} = \int p(\mathbf{x} | \boldsymbol{\theta}, \mathbf{y}) p(\boldsymbol{\theta} | \mathbf{y}) d\boldsymbol{\theta} \quad (6.40)$$

$$\approx |\hat{\mathbf{P}}_{\text{LA}}| \sum_{\mathbf{z} \in \mathcal{Q}(m,k)} \tilde{p}_{\text{G}}(\mathbf{x} | \boldsymbol{\theta}(\mathbf{z}), \mathbf{y}) \tilde{p}_{\text{LA}}(\boldsymbol{\theta}(\mathbf{z}) | \mathbf{y}) \omega(\mathbf{z}). \quad (6.41)$$

The quadrature rule $\mathbf{z} \in \mathcal{Q}(m, k)$ is used both internally to normalise the marginal Laplace approximation, and externally to perform integration with respect to the hyperparameters. Equation (6.41) is a mixture of Gaussian distributions $p_{\text{G}}(\mathbf{x} | \boldsymbol{\theta}(\mathbf{z}), \mathbf{y})$ with multinomial probabilities

$$\lambda(\mathbf{z}) = |\hat{\mathbf{P}}_{\text{LA}}| p_{\text{LA}}(\boldsymbol{\theta}(\mathbf{z}) | \mathbf{y}) \omega(\mathbf{z}), \quad (6.42)$$

where $\sum \lambda(\mathbf{z}) = 1$ and $\lambda(\mathbf{z}) > 0$. Samples may therefore be easily obtained for the complete vector \mathbf{x} jointly by first drawing a node $\mathbf{z} \in \mathcal{Q}(m, k)$ with multinomial probabilities $\lambda(\mathbf{z})$ then drawing a sample from the corresponding Gaussian distribution. Algorithms for fast and exact simulation from a Gaussian distribution have been developed by Rue (2001). The posterior marginals for any subset of the complete vector, including $p(x_i | \mathbf{y})$, can be simply obtained by keeping the relevant entries of \mathbf{x} .

Laplace marginals

An alternative more accurate, but more computationally intensive, approach is to calculate a Laplace approximation to the marginal posterior

$$\tilde{p}_{\text{LA}}(x_i, \boldsymbol{\theta}, \mathbf{y}) = \frac{p(x_i, \mathbf{x}_{-i}, \boldsymbol{\theta}, \mathbf{y})}{\tilde{p}_{\text{G}}(\mathbf{x}_{-i} | x_i, \boldsymbol{\theta}, \mathbf{y})} \Big|_{\mathbf{x}_{-i}=\hat{\mathbf{x}}_{-i}(x_i, \boldsymbol{\theta})}. \quad (6.43)$$

The variable x_i is excluded from the Gaussian approximation

$$p_{\text{G}}(\mathbf{x}_{-i} | x_i, \boldsymbol{\theta}, \mathbf{y}) = \mathcal{N}(\mathbf{x}_{-i} | \hat{\mathbf{x}}_{-i}(x_i, \boldsymbol{\theta}), \hat{\mathbf{H}}_{-i,-i}(x_i, \boldsymbol{\theta})) \quad (6.44)$$

with $(N-1)$ -dimensional posterior mode and $(N-1) \times (N-1)$ -dimensional Hessian matrix evaluated at the posterior mode

$$\hat{\mathbf{x}}_{-i}(x_i, \boldsymbol{\theta}) = \arg \max_{\mathbf{x}_{-i}} \log p(\mathbf{y}, x_i, \mathbf{x}_{-i}, \boldsymbol{\theta}), \quad (6.45)$$

$$\hat{\mathbf{H}}_{-i,-i}(x_i, \boldsymbol{\theta}) = -\frac{\partial^2}{\partial \mathbf{x}_{-i} \partial \mathbf{x}_{-i}^\top} \log p(\mathbf{y}, x_i, \mathbf{x}_{-i}, \boldsymbol{\theta})|_{\mathbf{x}_{-i}=\hat{\mathbf{x}}_{-i}(x_i, \boldsymbol{\theta})}. \quad (6.46)$$

The approximate posterior marginal $\tilde{p}(x_i | \mathbf{y})$ can be obtained by normalisation of the marginal Laplace approximation, and integration with respect to the hyperparameters, similarly to Equation (6.41)

$$p(x_i | \mathbf{y}) = \int p(x_i, \boldsymbol{\theta} | \mathbf{y}) d\boldsymbol{\theta} = \int p(x_i | \boldsymbol{\theta}, \mathbf{y}) p(\boldsymbol{\theta} | \mathbf{y}) d\boldsymbol{\theta} \quad (6.47)$$

$$\approx |\hat{\mathbf{P}}_{\text{LA}}| \sum_{\mathbf{z} \in \mathcal{Q}(m, k)} \tilde{p}_{\text{LA}}(x_i | \boldsymbol{\theta}(\mathbf{z}), \mathbf{y}) \tilde{p}_{\text{LA}}(\boldsymbol{\theta}(\mathbf{z}) | \mathbf{y}) \omega(\mathbf{z}). \quad (6.48)$$

The term $\tilde{p}_{\text{LA}}(x_i, \boldsymbol{\theta} | \mathbf{y})$ is obtained by normalising Equation (6.43) using an estimate of the evidence $\tilde{p}(\mathbf{y})$. It's possible to reuse the previously obtained posterior normalising constant estimate from Equation (6.38). Alternatively...

Simplified Laplace marginals

Rue, Martino, and Chopin (2009) use the properties of Gauss-Markov random fields (GMRFs) to efficiently approximate the Laplace marginals.

Simplified INLA

Wood (2020) approximates the Laplace marginals without relying so heavily on sparsity via GMRFs and still achieves good performance. For splines, as with extended latent Gaussian models [ELGMs; Stringer et al. (2022)], the precision matrix is not as sparse.

6.1.4 Software

R-INLA

The R-INLA software (Martins et al. 2013) implements the INLA method, as well as the stochastic partial differential equation (SPDE) approach of Lindgren et al. (2011). R-INLA is the R interface to the core `inla` program, which is written in C (Martino and Rue 2009) and uses algorithms from the `GMRFLib` C library (Rue and Follstad 2001). A formula interface of the form $y \sim \dots$ to specify the connection between the latent field \mathbf{x} and the structured additive predictor $\boldsymbol{\eta}$. For example, a model with one fixed effect \mathbf{a} and one IID random effect \mathbf{b} is written as `y ~ a + f(b, model = "iid")`. This interface is easy to engage with for new users, but be limiting for more advanced users. For more information, including recent developments, see the R-INLA website <https://r-inla.org>. The `inlabru` R package (Bachl et al. 2019) is one notable example. Gaedke-Merzhäuser et al. (2023) review recent computational improvements to R-INLA, including parallelism via OpenMP (Diaz et al. 2018) and use of the PARDISO sparse linear equation solver (Bollhöfer et al. 2020).

The approach used to compute the marginals $\tilde{p}(x_i | \mathbf{y})$ can chosen by setting `method` to "gaussian" (Section 6.1.3), "laplace" (Section 6.1.3) or "simplified.laplace" (Section 6.1.3). The quadrature grid used can be chosen by setting `int.strategy` to "eb" (empirical Bayes), "grid", or "ccd" [Box-Wilson central composite design; Box and Wilson (1992)]. Figure demonstrates these three integration strategies.

TMB

Template Model Builder [TMB, or when referring to the software TMB; Kristensen et al. (2016)] is an R package which implements the Laplace approximation. In TMB derivatives are obtained using automatic differentiation [AD; Baydin et al. (2017)], a rule-based method based on decomposition of calculations into elementary operations, which can be combined by repeated use of the chain rule. Give an example of TMB use.

TMB C++ templates are compatible with other software. `tmbstan` (Monnahan and Kristensen 2018) allows running HMC via Stan. `aghq` (Stringer 2021b) allows use of AGHQ via `mvQuad` (Weiser 2016).

`mrgcv`

Talk a little about `mrgcv::ginla` and what it is capable of.

6.2 A universal INLA implementation based on AD

In this section, I implement the INLA method, with Laplace marginals, using the TMB package. This implementation is universal in that it is compatible with any model with a TMB C++ template. This leads the way for application of INLA to models which are not compatible with R-INLA. Indeed, Martino and Riebler (2019) note that “implementing INLA from scratch is a complex task” and as a result “applications of INLA are limited to the (large class of) models implemented [in R-INLA]”. The potential benefits of a more flexible INLA implementation based on AD were noted by Skaug (2009) (a coauthor of TMB) in discussion of Rue, Martino, and Chopin (2009), noting that such a system would be “fast, flexible, and easy-to-use”. This suggestion was made close to 15 years ago, so it is surprising that its potential remains unrealised.

6.2.1 Epilepsy example

Consider the epilepsy generalised linear mixed model example of Spiegelhalter, Thomas, et al. (1996). This model is based on that of Breslow and Clayton (1993), a modification of Thall and Vail (1990), and the data are from an epilepsy drug double-blind clinical trial (Leppik et al. 1985). Rue, Martino, and Chopin (2009) (Section 5.2) demonstrate the INLA method using this example, and find a significant difference in approximation error depending on use of Gaussian or Laplace marginals. As such, it is a good choice of example to use as demonstration.

In the trial, patients $i = 1, \dots, 59$ were each assigned either the new drug $\text{Trt}_i = 1$ or placebo $\text{Trt}_i = 0$. Each patient made four visits the clinic $j = 1, \dots, 4$, and the observations y_{ij} are the number of seizures of the i th person in the two weeks preceding their j th visit. The covariates used in the model were age Age_i , baseline seizure counts Base_i and an indicator for the final clinic visit V_4 , which were all centred. The observations were modelled using a Poisson distribution $y_{ij} \sim \text{Poisson}(e^{\eta_{ij}})$ with linear predictor

$$\begin{aligned}\eta_{ij} = & \beta_0 + \beta_{\text{Base}} \log(\text{Baseline}_j/4) + \beta_{\text{Trt}} \text{Trt}_i + \beta_{\text{Trt} \times \text{Base}} \text{Trt}_i \times \log(\text{Baseline}_j/4) \\ & + \beta_{\text{Age}} \log(\text{Age}_i) + \beta_{V_4} V_{4j} + \epsilon_i + \nu_{ij}, \quad i \in [59], \quad j \in [4],\end{aligned}$$

where the prior distribution on each of the regression parameters, including the intercept, was $\mathcal{N}(0, 100^2)$. The patient $\epsilon_i \sim \mathcal{N}(0, 1/\tau_\epsilon)$ and patient-visit $\nu_{ij} \sim \mathcal{N}(0, 1/\tau_\nu)$ random effects were IID with precision prior distributions $\tau_\epsilon, \tau_\nu \sim \Gamma(0.001, 0.001)$.

The linear predictor for this model can be specified in R-INLA by:

```
formula <- y ~ 1 + CTrt + ClBase4 + CV4 + ClAge + CBT +
f(rand, model = "iid", hyper = tau_prior) + #' Nu random effect
f(Ind, model = "iid", hyper = tau_prior)      #' Epsilon random effect
```

The TMB C++ template for the model is in Appendix C.1.1.

6.2.2 Another example

Choose an example of a model that R-INLA can't fit but INLA with TMB can. Demonstrate Laplace marginals making a difference to accuracy as compared with Gaussian marginals.

6.3 The Naomi model

The Naomi small-area estimation model (Eaton et al. 2021) synthesises data from multiple sources to estimate HIV indicators at a district-level, by age and sex.

6.3.1 Model structure

I consider a simplified version of Naomi defined only at the time of the most recent household survey with HIV testing. This version omits nowcasting and temporal projection. These time points involve limited inferences.

Household survey component {household}

Consider a country in sub-Saharan Africa where a household survey with complex survey design has taken place. Let $x \in \mathcal{X}$ index district, $a \in \mathcal{A}$ index five-year age group, and $s \in \mathcal{S}$ index sex. For ease of notation, let i index the finest district-age-sex division included in the model. Let $I \subseteq \mathcal{X} \times \mathcal{A} \times \mathcal{S}$ be a set of indices i for which an aggregate observation is reported, and \mathcal{I} be the set of all I such that $I \in \mathcal{I}$.

Let $N_i \in \mathbb{N}$ be the known, fixed population size. HIV prevalence $\rho_i \in [0, 1]$, antiretroviral therapy (ART) coverage $\alpha_i \in [0, 1]$, and annual HIV incidence rate $\lambda_i > 0$ are modelled using linked regression equations.

Independent logistic regression models are specified for HIV prevalence and ART coverage in the general population such that $\text{logit}(\rho_i) = \eta_i^\rho$ and $\text{logit}(\alpha_i) = \eta_i^\alpha$. HIV incidence rate is modelled on the log scale as $\log(\lambda_i) = \eta_i^\lambda$, and depends on adult HIV prevalence and adult ART coverage. Let κ_i be the proportion recently infected among HIV positive persons. This proportion is linked to HIV incidence via

$$\kappa_i = 1 - \exp\left(-\lambda_i \cdot \frac{1 - \rho_i}{\rho_i} \cdot (\Omega_T - \beta_T) - \beta_T\right), \quad (6.49)$$

where the mean duration of recent infection Ω_T and the proportion of long-term HIV infections misclassified as recent β_T are strongly informed by prior distributions for the particular survey.

These processes are each informed by household survey data. Weighted aggregate survey observations are calculated as

$$\hat{\theta}_I = \frac{\sum_j w_j \cdot \theta_j}{\sum_j w_j},$$

with individual responses $\theta_j \in \{0, 1\}$ and design weights w_j for each of $\theta \in \{\rho, \alpha, \kappa\}$. The design weights are provided by the survey and aim to reduce bias by decreasing

possible correlation between response and recording mechanism (Meng 2018). The index j runs across all individuals in strata $i \in I$ within the relevant denominator i.e. for ART coverage, only those individuals who are HIV positive. The weighted observed number of outcomes is $y_I^\theta = m_I^\theta \cdot \hat{\theta}_I$ where

$$m_I^\theta = \frac{(\sum_j w_j)^2}{\sum_j w_j^2},$$

is the Kish effective sample size (ESS) (Kish 1965). As the Kish ESS is maximised by constant design weights, in exchange for reducing bias the ESS is reduced and hence variance increased. The weighted observed number of outcomes are modelled using a binomial working likelihood (Chen et al. 2014) defined to operate on the reals

$$y_I^\theta \sim \text{xBin}(m_I^\theta, \theta_I),$$

where θ_I are the following weighted aggregates

$$\rho_I = \frac{\sum_{i \in I} N_i \rho_i}{\sum_{i \in I} N_i}, \quad \alpha_I = \frac{\sum_{i \in I} N_i \rho_i \alpha_i}{\sum_{i \in I} N_i \rho_i}, \quad \kappa_I = \frac{\sum_{i \in I} N_i \rho_i \kappa_i}{\sum_{i \in I} N_i \rho_i}.$$

6.3.2 Connection to ELGMs

Naomi is a spatio-temporal model with a large Gaussian latent field, governed by a smaller number of hyperparameters. However, it is an ELGM rather than an LGM, for the reasons below. Note that when dependence on a specific number of structured additive predictors is given, it is for that factor in isolation.

6.4 AGHQ in moderate dimensions

The Naomi model has $m = 24$ hyperparameters. AGHQ with the product rule grid requires evaluation of $|\mathcal{Q}(m, k)| = k^m$ quadrature points. This is intractable for $m = 24$. This section focuses on the development of AGHQ rules for moderate dimensions, for use within the nested Laplace approximation algorithm.

6.4.1 AGHQ with variable levels

Let $\mathbf{k} = (k_1, \dots, k_m)$ be a vector of levels for each dimension of $\boldsymbol{\theta}$. We may then define $\mathcal{Q}(m, \mathbf{k}) = \mathcal{Q}(1, k_1) \times \dots \times \mathcal{Q}(1, k_m)$ to be a GHQ grid with possible variable levels of size $|\mathcal{Q}(m, \mathbf{k})| = \prod_{j=1}^m k_j$. Let $\mathcal{Q}(m, s, k)$ correspond to $\mathcal{Q}(m, \mathbf{k})$ with choice of levels $k_j = k, j \leq s$ and $k_j = 1, j > s$ for some $s \leq m$. For example, for $m = 2$ and $s = 1$ then $\mathbf{k} = (k, 1)$. In combination with use of the spectral decomposition, this choice of levels is analogous to a principal components analysis (PCA) approach to AGHQ. We refer to this approach as PCA-AGHQ, with corresponding estimate of the normalising constant given by

$$\tilde{p}_{\text{PCA}}(\mathbf{y}) = |\hat{\mathbf{E}}_{\text{LA}} \hat{\Lambda}_{\text{LA}}^{1/2}| \sum_{\mathbf{z} \in \mathcal{Q}(m, s, k)} \tilde{p}_{\text{LA}}(\hat{\mathbf{E}}_{\text{LA},s} \hat{\Lambda}_{\text{LA},s}^{1/2} \mathbf{z} + \hat{\boldsymbol{\theta}}_{\text{LA}}, \mathbf{y}) \omega(\mathbf{z}), \quad (6.50)$$

where $\hat{\mathbf{E}}_{\text{LA},s}$ is an $m \times s$ matrix containing the first s eigenvectors, $\hat{\Lambda}_{\text{LA},s}$ is the $s \times s$ diagonal matrix containing the first s eigenvalues, and $\omega(\mathbf{z}) = \prod_{j=1}^s \omega_s(z_j) \times \prod_{j=s+1}^d \omega_1(z_j)$. Panel C of Figure ?? illustrates PCA-AGHQ for a case when $m = 2$ and $s = 1$. As AGHQ with $k = 1$ corresponds to the Laplace approximation, PCA-AGHQ can be interpreted as performing AGHQ on the first s principal components of the inverse curvature, and a Laplace approximation on the remaining $m - s$ principal components. Inference for the latent field follows analogously to Equation ??.

6.4.2 Principal components analysis

6.5 Malawi case-study

The Naomi model, as described in Section 6.3, was fit to data from Malawi using three inferential approaches.

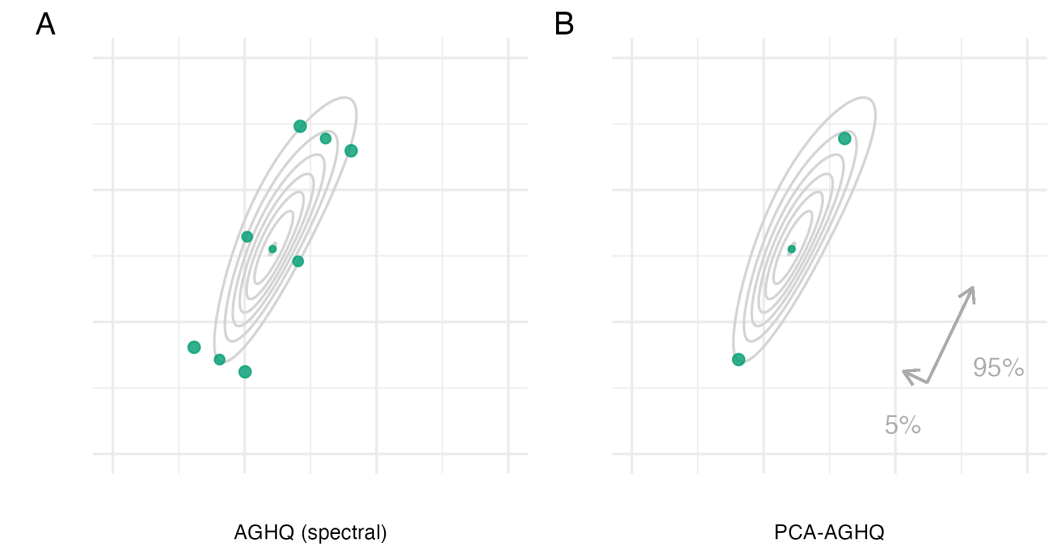


Figure 6.4: See Figure 6.3.

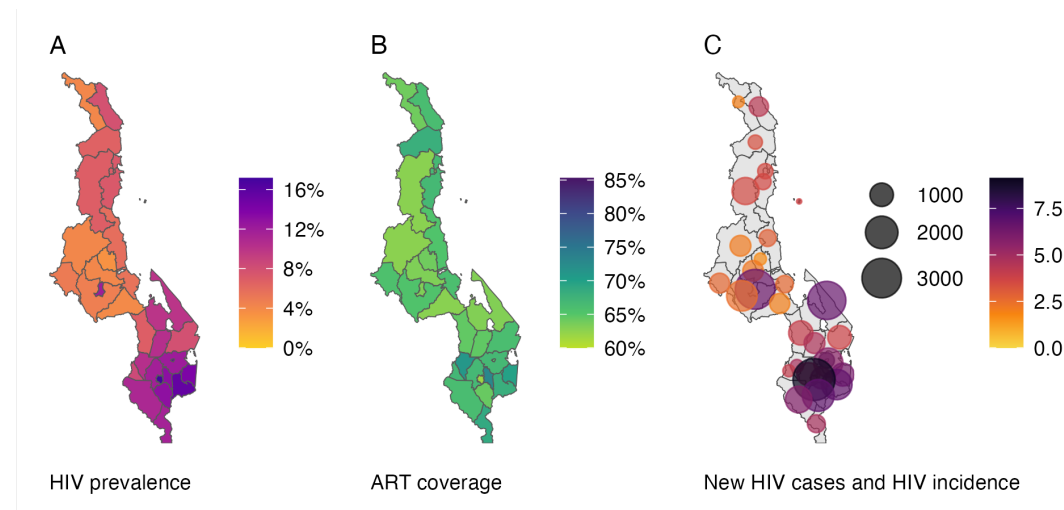


Figure 6.5: Figure caption.

6.5.1 NUTS convergence

6.5.2 Use of PCA-AGHQ

6.5.3 Model assessment

6.5.4 Inference comparison

6.5.5 Exceedance probabilities

6.6 Discussion

We developed an approximate Bayesian inference algorithm, combining AGHQ with PCA, motivated by a challenging problem in small-area estimation of HIV indicators. For the simplified Naomi model in Malawi (Section ??) we demonstrated the method to be more accurate at inferring posterior distributions of model parameters, across a broad range of metrics, than TMB, and substantially faster than NUTS. However, improvements in accuracy for model parameters did not translate into model outputs. Indeed, we found posterior exceedance probabilities (Section ??) from both TMB and PCA-AGHQ to have systematically inaccuracies, with the potential to meaningfully mislead policy. If possible, though not a desirable situation, it could be advisable to provide gold-standard NUTS results after the workshop has concluded. However, running NUTS for Naomi took days, in countries with 100s of districts it may simply not be feasible.

PCA-AGHQ could be added to the Naomi web interface as an alternative to TMB. Analysts may then quickly iterate over model options using a fast inference approach, before switching to a more accurate approach once they are happy with the results. By selecting s and k , PCA-AGHQ can be adjusted to suit the computational budget available. We selected s based on the Scree plot, and for the most part fixed $k = 3$. Whether it is preferable, for a given computational budget, to increase s or increase k is an open question. Further strategies, such as gradually lowering k over the principal components, could also be considered.

We hope that our work further encourages use of deterministic inference algorithms for ELGMs in applied settings, as well as methodological exploration

of their accuracy and limitations. Among the ELGM-type structures of particular interest in spatial epidemiology are aggregated Gaussian process models (Nandi et al. 2020) and evidence synthesis models (Amoah et al. 2020).

6.6.1 Suggestions for future work

Improved quadrature grids for moderate dimensions

We aimed to develop a quadrature grid which allocates more effort to more important dimensions. While PCA is a sensible approach, there are avenues where it does not behave as one might hope, or otherwise overlooks potential benefits. The first challenge we identified was using PCA when the dimensions have different scales. Specifically, we found logit-scale hyperparameters to be systematically favoured over those on the log-scale. Second, the amount of variation explained for the Hessian matrix is not of direct interest, rather the effect of the different dimensions on the relevant outputs. Using measures of importance from sensitivity analysis, such as Shapley values (Shapley et al. 1953) may be preferable. Third, it is more important to allocate quadrature nodes to those marginals which are non-Gaussian. This is because the Laplace approximation is exact when the integrand is Gaussian, so a single quadrature node is sufficiently. The difficulty is, of course, knowing in advance which marginals will be non-Gaussian. This could be done if there were a cheap way to obtain posterior means, which could then be compared to posterior modes obtained using optimisation. Another approach would be to measure the fit of marginal samples from a cheap approximation, like TMB. The main challenge is that the measurements have to be for marginals, ruling out approaches like PSIS which operate on joint distributions (Yao et al. 2018).

Computational speed-ups

Integration over a moderate number of hyperparameters posed a challenge, and led us to use a quadrature grids with a large number of nodes. However, computation at each node is independent, such that the run-time of the algorithm could potentially

be significantly improved by parallel computing. Further computational speed-ups might be obtained using graphics processing units (GPUs) specialised for the relevant matrix operations.

Comparison to other MCMC algorithms

Blocked Gibbs sampling (Geman and Geman 1984) or slice sampling (Neal 2003), may be better suited than NUTS to sampling from Naomi. These algorithms are available, and customisable, including e.g. choice of block structure within the **NIMBLE** probabilistic programming language (de Valpine et al. 2017).

Implementation into probabilistic programming languages

Though gaining in popularity, the user-base of **TMB** remains relatively small. Furthermore, for users unfamiliar with C++, it can be challenging to use. As such, it could be beneficial to implement AGHQ within other probabilistic programming languages. Implementation in **NIMBLE** could be relatively straightforward, as it (for version $>1.0.0$) includes functionality for automatic differentiation and Laplace approximation, built using **CppAD** like **TMB**. Similarly, implementation in Stan could be possible by use of the **bridgestan** package (Ward 2023) together with the adjoint-differentiated Laplace approximation of Margossian et al. (2020).

Statistical theory

Stringer et al. (2022) (Theorem 1) bound the total variation error of AGHQ, establishing convergence in probability of coverage probabilities under the approximate posterior distribution to those under the true posterior distribution. Similar theory might be established for PCA-AGHQ, or more generally AGHQ with varying numbers of nodes per dimension. The challenge of connecting this theory to use of the quadrature rule within nested computations remains an open question.

7

Future work and conclusions

7.1 Strengths

7.1.1 Chapter 4

- I designed experiments to thoroughly compare models for spatial structure using tools for model assessment such as proper scoring rules and posterior predictive checks.

7.1.2 Chapter 5

- I estimated HIV risk group proportions for AGYW, enabling countries to prioritise their delivery of HIV prevention services.
- I analysed the number of new infections that might be reached under a variety of risk stratification strategies.
- I used R-INLA to specify multinomial spatio-temporal models via the Poisson-multinomial transformation. This includes complex two- and three-way Kronecker product interactions defined using the `group` and `replicate` options.

Conclusions

7.1.3 Chapter 6

- I developed a novel Bayesian inference method, motivated by a challenging and practically important problem in HIV inference.
- The method enables integrated nested Laplace approximations to be fit to and studied on a wider class of models than was previously possible.
- My implementation of the method was straightforward, building on the **TMB** and **aghq** packages, and described completely and accessibly in Howes, Stringer, et al. (2023+).

7.2 Future work

Avenues for future work include:

1. Extending the risk group model described in Chapter 5 to include all adults 15–49. This may involve modelling of age-stratified sexual partnerships (Wolock et al. 2021). Such a model would likely fall out of the scope of **R-INLA**, but would be possible to write with **TMB** and therefore amenable to the methods discussed in Chapter 6.
2. Speeding up the implementation of Laplace marginals using the matrix algebra approximations described in Wood (2020).
3. Evaluating the accuracy of deterministic Bayesian inference methods for a broader variety of extended latent Gaussian models.

7.3 Conclusions

- Modelling complex data, more often than not, pushes the boundaries of the statistical toolkit available.
- A challenge I encountered was the difficulty of implementing identical models across multiple frameworks with the aim of studying the inference method. Or, of a similarly fraught nature, comparing different models implemented in different frameworks with the aim of studying model differences. The

Conclusions

frequently asked questions section of the R-INLA website (Rue 2023) notes that “the devil is in the details”. I have resolved this challenge by using a given TMB model template to fit models using multiple inference methodologies. The benefits of such a ecosystem of packages are noted by Stringer (2021a). I particularly highlight the benefit of enabling analysts to easily vary their choice of inference method based on the stage of model development that they are in.

- To the best of my abilities, I have written this thesis, and the work described within it, in keeping with the principles of open science. I hope that doing so allows my work to be scrutinised, and optimistically built upon. This would not have been possible without a range of tools from the R ecosystem such as `rmarkdown` and `rticles`, as well as those developed within the MRC Centre for Global Infectious Disease Analysis such as `orderly` and `didehpc`.

Appendices

A

Models for spatial structure

B

A model for risk group proportions

B.1 The Global AIDS Strategy

Prioritisation strata	Criterion
Low	0.3-1.0% incidence and low-risk behaviour, or <0.3% incidence and high-risk behaviour
Moderate	1.0-3.0% incidence and low-risk behaviour, or 0.3-1.0% incidence and high-risk behaviour
High	1.0-3.0% incidence and high-risk behaviour
Very high	>3.0% incidence

Table B.1: Prioritisation strata according to HIV incidence in the general population and behavioural risk.

Intervention	Low	Moderate	High	Very High
Condoms and lube for those with non-regular partners(s) with unknown STI status and not on PrEP	50%	70%	95%	95%
STI screening and treatment	10%	10%	80%	80%
Access to PEP	-	-	50%	90%
PrEP use	-	5%	50%	50%
Economic empowerment	-	-	20%	20%

Table B.2: Commitments to be met for each intervention in terms of proportion of the prioritisation strata reached. The symbol "-" represents no commitment.

B. A model for risk group proportions

B.2 Household survey data

Type	Year	Transactional sex question	Sample size				
			15-19	20-24	25-29	Total	
Botswana							
	BAIS	2013	✓	557	588	649	1794
	Total			557	588	649	1794
Cameroon							
	DHS	2004	✗	2675	2207	1732	6614
	DHS	2011	✗	3588	3115	2655	9358
	PHIA	2017	✗	2620	2339	2259	7218
	DHS	2018	✓	3349	2463	2345	8157
	Total			12232	10124	8991	31347
Kenya							
	DHS	2003	✗	1819	1709	1391	4919
	DHS	2008	✗	1767	1743	1419	4929
	DHS	2014	✗	2861	2534	2858	8253
	Total			6447	5986	5668	18101
Lesotho							
	DHS	2004	✗	1761	1455	1026	4242
	DHS	2009	✗	1833	1543	1194	4570
	DHS	2014	✗	1537	1292	1067	3896
	PHIA	2017	✓	1156	1202	1054	3412
	Total			6287	5492	4341	16120
Mozambique							
	AIS	2009	✗	1031	1106	987	3124
	DHS	2011	✗	2932	2299	2206	7437
	AIS	2015	✗	1552	1389	1080	4021
	Total			5515	4794	4273	14582
Malawi							
	DHS	2000	✗	2914	2998	2358	8270
	DHS	2004	✗	2407	2823	2135	7365
	DHS	2010	✗	5031	4387	4309	13727
	DHS	2015	✓	5273	5094	3976	14343
	PHIA	2016	✓	1646	1934	1511	5091
	Total			17271	17236	14289	48796
Namibia							
	DHS	2000	✗	1427	1313	1098	3838

B. A model for risk group proportions

	DHS	2006	x	2203	1869	1544	5616
	DHS	2013	x	1852	1709	1481	5042
	PHIA	2017	✓	1491	1525	1370	4386
Total				6973	6416	5493	18882
Eswatini							
	DHS	2006	x	1265	1027	731	3023
	PHIA	2017	x	1031	895	811	2737
Total				2296	1922	1542	5760
Tanzania							
	AIS	2003	x	1466	1377	1270	4113
	AIS	2007	x	2137	1676	1509	5322
	DHS	2010	x	2221	1860	1613	5694
	AIS	2012	x	2474	1923	1815	6212
	PHIA	2016	✓	2999	2845	2521	8365
Total				11297	9681	8728	29706
Uganda							
	DHS	2000	x	1687	1541	1326	4554
	DHS	2006	x	1948	1660	1404	5012
	AIS	2011	x	2451	2164	1921	6536
	DHS	2011	x	2025	1664	1614	5303
	DHS	2016	✓	4276	3782	3014	11072
	PHIA	2016	x	3289	3059	2574	8922
Total				15676	13870	11853	41399
South Africa							
	DHS	2016	✓	1505	1408	1397	4310
Total				1505	1408	1397	4310
Zambia							
	DHS	2007	x	1598	1405	1373	4376
	DHS	2013	x	3685	3036	2789	9510
	PHIA	2016	✓	2120	2045	1619	5784
	DHS	2018	✓	3112	2687	2166	7965
Total				10515	9173	7947	27635
Zimbabwe							
	DHS	1999	x	1467	1230	1011	3708
	DHS	2005	x	2128	1943	1438	5509
	DHS	2010	x	1963	1796	1679	5438
	DHS	2015	✓	2154	1777	1646	5577
	PHIA	2016	✓	2114	1817	1573	5504
Total				9826	8563	7347	25736

B. A model for risk group proportions

Total	106397	95253	82518	284168
-------	--------	-------	-------	--------

Table B.3: All of the surveys that used in the analysis and their sample sizes, disaggregated by respondent age.

Survey	Exclusion reason
MOZ2003DHS	No GPS coordinates available to place survey clusters within districts.
TZA2015DHS	Insufficient sexual behaviour questions.
UGA2004AIS	Unable to download region boundaries.
ZMB2002DHS	No GPS coordinates available to place survey clusters within districts.

Table B.4: All of that surveys that were excluded from the analysis.

B.3 Spatial analysis levels

Country	Number of areas	Analysis level
Botswana	27	3
Cameroon	58	2
Kenya	47	2
Lesotho	10	1
Mozambique	161	3
Malawi	33	5
Namibia	38	2
Eswatini	4	1
Tanzania	195	4
Uganda	136	3
South Africa	52	2
Zambia	116	2
Zimbabwe	63	2

Table B.5: The numer of areas and analysis levels for each country that were used in the analysis.

B.4 Survey questions and risk group allocation

B. A model for risk group proportions

Variable(s)	Description
v501	Current marital status of the respondent.
v529	Computed time since last sexual intercourse.
v531	Age at first sexual intercourse—imputed.
v766b	Number of sexual partners during the last 12 months (including husband).
v767[a, b, c]	Relationship with last three sexual partners. Options are: spouse, boyfriend not living with respondent, other friend, casual acquaintance, relative, commercial sex worker, live-in partner, other.
v791a	Had sex in return for gifts, cash or anything else in the past 12 months. Asked only to women 15–24 who are not in a union.

Table B.6: The survey questions included in AIDS Indicator Survey (AIS) and Demographic and Health Surveys (DHS).

Variable(s)	Description
part12monum	Number of sexual partners during the last 12 months (including husband).
part12modkr	Reason for leaving part12monum blank.
partlivew[1, 2, 3]	Does the person you had sex with live in this household?
partrelation[1, 2, 3]	Relationship with last three sexual partners. Options are: husband, live-in partner, partner (not living with), ex-spouse/partner, friend/acquaintance, sex worker, sex worker client, stranger, other, don't know, refused.
sellssx12mo	Had sex for money and/or gifts in the last 12 months.
buyssx12mo	Paid money or given gifts for sex in the last 12 months.

Table B.7: The survey questions included in Population-Based HIV Impact Assessment (PHIA) surveys.

C

Fast approximate Bayesian inference

C.1 Epilepsy example

C.1.1 TMB C++ template

```
// epi.l.cpp

#include <TMB.hpp>

template <class Type>
Type objective_function<Type>::operator()()
{
    DATA_INTEGER(N);
    DATA_INTEGER(J);
    DATA_INTEGER(K);
    DATA_MATRIX(X);
    DATA_VECTOR(y);
    DATA_MATRIX(E); // Epsilon matrix

    PARAMETER_VECTOR(beta);
```

C. Fast approximate Bayesian inference

```

PARAMETER_VECTOR(epsilon);
PARAMETER_VECTOR(nu);
PARAMETER(l_tau_epsilon);
PARAMETER(l_tau_nu);

Type tau_epsilon = exp(l_tau_epsilon);
Type tau_nu = exp(l_tau_nu);
Type sigma_epsilon = sqrt(1 / tau_epsilon);
Type sigma_nu = sqrt(1 / tau_nu);
vector<Type> eta(X * beta + nu + E * epsilon); // Linear predictor
vector<Type> lambda(exp(eta));

Type nll;
nll = Type(0.0);

// Note: dgamma() is parameterised as (shape, scale)
// R-INLA is parameterised as (shape, rate)
nll -= dlgamma(l_tau_epsilon, Type(0.001), Type(1.0 / 0.001), true);
nll -= dlgamma(l_tau_nu, Type(0.001), Type(1.0 / 0.001), true);
nll -= dnorm(epsilon, Type(0), sigma_epsilon, true).sum();
nll -= dnorm(nu, Type(0), sigma_nu, true).sum();
nll -= dnorm(beta, Type(0), Type(100), true).sum();

nll -= dpois(y, lambda, true).sum();

ADREPORT(tau_epsilon);
ADREPORT(tau_nu);

return(nll);
}

```

C. Fast approximate Bayesian inference

C.2 Simplified Naomi model description

This section describes the simplified version of the Naomi model (Eaton et al. 2021) in complete detail.

C.2.1 Process specification

Table C.1

	Model component	Latent field	Hyperparameter
C.2.1	HIV prevalence	$22 + 5n$	9
C.2.1	ART coverage	$25 + 5n$	9
C.2.1	HIV incidence rate	$2 + n$	3
C.2.1	ANC testing	$2 + 2n$	2
C.2.1	ART attendance	n	1
	Total	$51 + 14n$	24

HIV prevalence

HIV prevalence $\rho_{x,s,a} \in [0, 1]$ was modelled on the logit scale using the linear predictor

$$\text{logit}(\rho_{x,s,a}) = \beta_0^\rho + \beta_S^{\rho,s=M} + \mathbf{u}_a^\rho + \mathbf{u}_a^{\rho,s=M} + \mathbf{u}_x^\rho + \mathbf{u}_x^{\rho,s=M} + \mathbf{u}_x^{\rho,a<15} + \boldsymbol{\eta}_{R_{x,s,a}}^\rho. \quad (\text{C.1})$$

Table C.2 provides a description of the terms included in Equation (C.1). Independent half-normal prior distributions were chosen for the five standard deviation terms

$$\{\sigma_A^\rho, \sigma_{AS}^\rho, \sigma_X^\rho, \sigma_{XS}^\rho, \sigma_{XA}^\rho\} \sim \mathcal{N}^+(0, 2.5), \quad (\text{C.2})$$

independent uniform prior distributions for the two AR1 correlation parameters

$$\{\phi_A^\rho, \phi_{AS}^\rho\} \sim \mathcal{U}(-1, 1), \quad (\text{C.3})$$

and independent beta prior distributions for the two BYM2 proportion parameters

$$\{\phi_X^\rho, \phi_{XS}^\rho\} \sim \text{Beta}(0.5, 0.5). \quad (\text{C.4})$$

C. Fast approximate Bayesian inference

Table C.2

Term	Distribution	Description
β_0^ρ	$\mathcal{N}(0, 5)$	Intercept
$\beta_s^{\rho, s=M}$	$\mathcal{N}(0, 5)$	The difference in logit prevalence for men compared to women
\mathbf{u}_a^ρ	AR1($\sigma_A^\rho, \phi_A^\rho$)	Age random effects for women
$\mathbf{u}_a^{\rho, s=M}$	AR1($\sigma_{AS}^\rho, \phi_{AS}^\rho$)	Age random effects for the difference in logit prevalence for men compared to women age a
\mathbf{u}_x^ρ	BYM2($\sigma_X^\rho, \phi_X^\rho$)	Spatial random effects for women
$\mathbf{u}_x^{\rho, s=M}$	BYM2($\sigma_{XS}^\rho, \phi_{XS}^\rho$)	Spatial random effects for the difference in logit prevalence for men compared to women in district x
$\mathbf{u}_x^{\rho, a < 15}$	ICAR(σ_{XA}^ρ)	Spatial random effects for the ratio of paediatric prevalence to adult women prevalence
$\boldsymbol{\eta}_{R_x, s, a}^\rho$	—	Fixed offsets specifying assumed odds ratios for prevalence outside the age ranges for which data were available

ART coverage

ART coverage $\alpha_{x,s,a} \in [0, 1]$ was modelled on the logit scale using the linear predictor

$$\text{logit}(\alpha_{x,s,a}) = \beta_0^\alpha + \beta_S^{\alpha, s=M} + \mathbf{u}_a^\alpha + \mathbf{u}_a^{\alpha, s=M} + \mathbf{u}_x^\alpha + \mathbf{u}_x^{\alpha, s=M} + \mathbf{u}_x^{\alpha, a < 15} + \boldsymbol{\eta}_{R_x, s, a}^\alpha \quad (\text{C.5})$$

with terms and priors analogous to the HIV prevalence process model in Section C.2.1 above.

HIV incidence rate

HIV incidence rate $\lambda_{x,s,a} > 0$ was modelled on the log scale using the linear predictor

$$\log(\lambda_{x,s,a}) = \beta_0^\lambda + \beta_S^{\lambda, s=M} + \log(\rho_x^{15-49}) + \log(1 - \omega \cdot \alpha_x^{15-49}) + \mathbf{u}_x^\lambda + \boldsymbol{\eta}_{R_x, s, a}^\lambda. \quad (\text{C.6})$$

Table ?? provides a description of the terms included in Equation C.6.

C. Fast approximate Bayesian inference

Term	Distribution	Description
β_0^λ	$\mathcal{N}(0, 5)$	Intercept term proportional to the average HIV transmission rate for untreated HIV positive adults
$\beta_S^{\lambda, s=M}$	$\mathcal{N}(0, 5)$	The log incidence rate ratio for men compared to women
ρ_x^{15-49}	—	The HIV prevalence among adults 15-49 calculated by aggregating age-specific HIV prevalences
α_x^{15-49}	—	The ART coverage among adults 15-49 calculated by aggregating age-specific ART coverages
$\omega = 0.7$	—	Average reduction in HIV transmission rate per increase in population ART coverage fixed based on inputs to the Estimation and Projection Package (EPP) model
\mathbf{u}_x^λ	$\mathcal{N}(0, \sigma^\lambda)$	IID spatial random effects with $\sigma^\lambda \sim \mathcal{N}^+(0, 1)$
$\boldsymbol{\eta}_{R_x, s, a}^\lambda$	—	Fixed log incidence rate ratios by sex and age group calculated from Spectrum model output

The proportion recently infected among HIV positive persons $\kappa_{x,s,a} \in [0, 1]$ were modelled as

$$\kappa_{x,s,a} = 1 - \exp\left(-\lambda_{x,s,a} \cdot \frac{1 - \rho_{x,s,a}}{\rho_{x,s,a}} \cdot (\Omega_T - \beta_T) - \beta_T\right), \quad (\text{C.7})$$

where $\Omega_T \sim \mathcal{N}(\Omega_{T_0}, \sigma^{\Omega_T})$ is the mean duration of recent infection, and $\beta_T \sim \mathcal{N}^+(\beta_{T_0}, \sigma^{\beta_T})$ is the false recent ratio. The prior distribution for Ω_T was informed by the characteristics of the recent infection testing algorithm. For PHIA surveys this was $\Omega_{T_0} = 130$ days and $\sigma^{\Omega_T} = 6.12$ days, and further there was assumed to be no false recency, such that $\beta_{T_0} = 0.0$ and $\sigma^{\beta_T} = 0.0$.

ANC testing

HIV prevalence $\rho_{x,a}^{\text{ANC}}$ and ART coverage $\alpha_{x,a}^{\text{ANC}}$ among pregnant women were modelled as being offset on the logit scale from the corresponding district-age indicators $\rho_{x,F,a}$ and $\alpha_{x,F,a}$ according to

$$\text{logit}(\rho_{x,a}^{\text{ANC}}) = \text{logit}(\rho_{x,F,a}) + \beta^{\rho^{\text{ANC}}} + \mathbf{u}_x^{\rho^{\text{ANC}}} + \boldsymbol{\eta}_{R_x, a}^{\rho^{\text{ANC}}}, \quad (\text{C.8})$$

$$\text{logit}(\alpha_{x,a}^{\text{ANC}}) = \text{logit}(\alpha_{x,F,a}) + \beta^{\alpha^{\text{ANC}}} + \mathbf{u}_x^{\alpha^{\text{ANC}}} + \boldsymbol{\eta}_{R_x, a}^{\alpha^{\text{ANC}}}. \quad (\text{C.9})$$

Table ?? provides a description of the terms included in Equation C.8 and Equation C.9.

C. Fast approximate Bayesian inference

Term	Distribution	Description
$\beta^{\theta^{\text{ANC}}}$	$\mathcal{N}(0, 5)$	Intercept giving the average difference between population and ANC outcomes
$\mathbf{u}_x^{\theta^{\text{ANC}}}$	$\mathcal{N}(0, \sigma_X^{\theta^{\text{ANC}}})$	IID district random effects with $\sigma_X^{\theta^{\text{ANC}}} \sim \mathcal{N}^+(0, 1)$
$\boldsymbol{\eta}_{R_x,a}^{\theta^{\text{ANC}}}$	—	Offsets for the log fertility rate ratios for HIV positive women compared to HIV negative women and for women on ART to HIV positive women not on ART, calculated from Spectrum model outputs for region R_x

In the full Naomi model, for adult women 15-49 the number of ANC clients $\Psi_{x,a} > 0$ were modelled as

$$\log(\Psi_{x,a}) = \log(N_{x,F,a}) + \psi_{R_x,a} + \beta^\psi + \mathbf{u}_x^\psi,$$

where $N_{x,F,a}$ are the female population sizes, $\psi_{R_x,a}$ are fixed age-sex fertility ratios in Spectrum region R_x , β^ψ are log rate ratios for the number of ANC clients relative to the predicted fertility, and $\mathbf{u}_x^\psi \sim \mathcal{N}(0, \sigma^\psi)$ are district random effects. Here we fix $\beta^\psi = 0$ and $\mathbf{u}_x^\psi = \mathbf{0}$ such that $\Psi_{x,a}$ are simply constants.

ART attendance

Let $\gamma_{x,x'} \in [0, 1]$ be the probability that a person on ART residing in district x receives ART in district x' . We assume that $\gamma_{x,x'} = 0$ for $x \notin \{x, \text{ne}(x)\}$ such that individuals seek treatment only in their residing district or its neighbours $\text{ne}(x) = \{x' : x' \sim x\}$, where \sim is an adjacency relation, and $\sum_{x' \in \{x, \text{ne}(x)\}} \gamma_{x,x'} = 1$. To model $\gamma_{x,x'}$ for $x \sim x'$ we use a multinomial logistic regression model, based on the log-odds ratios

$$\tilde{\gamma}_{x,x'} = \log \left(\frac{\gamma_{x,x'}}{1 - \gamma_{x,x'}} \right) = \tilde{\gamma}_0 + \mathbf{u}_x^{\tilde{\gamma}}, \quad (\text{C.10})$$

where $\tilde{\gamma}_0 = -4$ is a fixed intercept, and $\mathbf{u}_x^{\tilde{\gamma}} \sim \mathcal{N}(0, \sigma_X^{\tilde{\gamma}})$ were district random effects with $\sigma_X^{\tilde{\gamma}} \sim \mathcal{N}^+(0, 2.5)$. Note that Equation C.10 does not depend on x' , such that $\gamma_{x,x'}$ is only a function of x . Choice of $\tilde{\gamma}_0 = -4$ implies a prior mean on $\gamma_{x,x'}$ of 1.8%, such that $(100 - 1.8 \times \text{ne}(x))\%$ of ART clients in district x

C. Fast approximate Bayesian inference

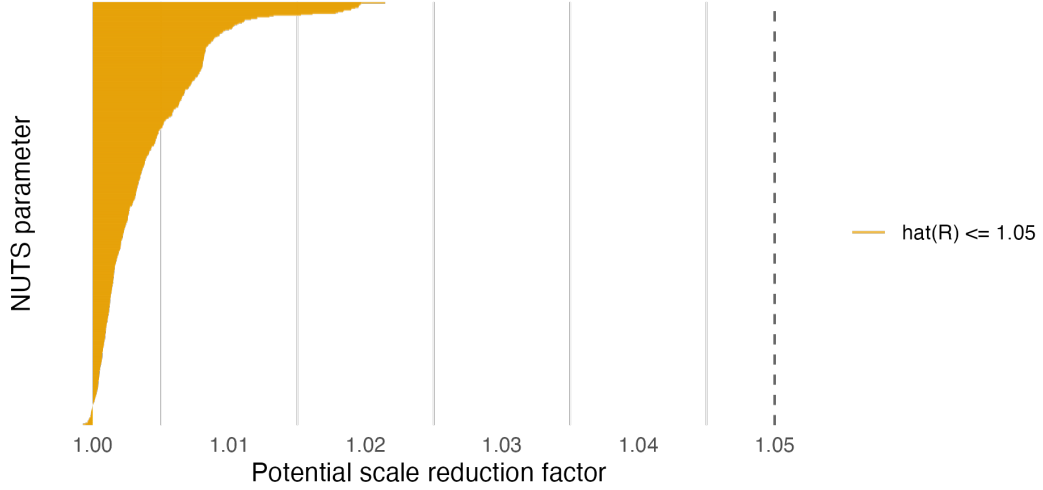


Figure C.1: The potential scale reduction factor compares between- and within- estimates of univariate parameters. It is recommended only to use NUTS results if the value is less than 1.05, which it is for all parameters.

obtain treatment in their home district, a-priori. We fix $\tilde{\gamma}_{x,x} = 0$ and recover the multinomial probabilities using the softmax

$$\gamma_{x,x'} = \frac{\exp(\tilde{\gamma}_{x,x'})}{\sum_{x^* \in \{x, \text{ne}(x)\}} \exp(\tilde{\gamma}_{x,x^*})}. \quad (\text{C.11})$$

Given the total number of PLHIV on ART $A_{x,s,a} = N_{x,s,a} \cdot \rho_{x,s,a} \cdot \alpha_{x,s,a}$, the number of ART clients who reside in district x and obtain ART in district x' are $A_{x,x',s,a} = A_{x,s,a} \cdot \gamma_{x,x'}$, and the total attending ART facilities in district x' are

$$\tilde{A}_{x',s,a} = \sum_{x \in \{x', \text{ne}(x')\}} A_{x,x',s,a}. \quad (\text{C.12})$$

C.3 Model assessment

C.4 AGHQ and PCA-AGHQ details

C.5 Normalising constant estimation

C.6 Inference comparison

C.7 MCMC convergence and suitability

Works Cited

- Amoah, Benjamin, Peter J Diggle, and Emanuele Giorgi (2020). “A geostatistical framework for combining spatially referenced disease prevalence data from multiple diagnostics”. In: *Biometrics* 76.1, pp. 158–170.
- Auvert, Bertran et al. (2005). “Randomized, controlled intervention trial of male circumcision for reduction of HIV infection risk: the ANRS 1265 Trial”. In: *PLoS medicine* 2.11, e298.
- Bachl, Fabian E et al. (2019). “inlabru: an R package for Bayesian spatial modelling from ecological survey data”. In: *Methods in Ecology and Evolution* 10.6, pp. 760–766.
- Bailey, Robert C et al. (2007). “Male circumcision for HIV prevention in young men in Kisumu, Kenya: a randomised controlled trial”. In: *The Lancet* 369.9562, pp. 643–656.
- Baker, Stuart G (1994). “The multinomial-Poisson transformation”. In: *Journal of the Royal Statistical Society: Series D (The Statistician)* 43.4, pp. 495–504.
- Baral, Stefan et al. (2012). “Burden of HIV among female sex workers in low-income and middle-income countries: a systematic review and meta-analysis”. In: *The Lancet Infectious Diseases* 12.7, pp. 538–549.
- Barré-Sinoussi, Françoise et al. (1983). “Isolation of a T-lymphotropic retrovirus from a patient at risk for acquired immune deficiency syndrome (AIDS)”. In: *Science* 220.4599, pp. 868–871.
- Baydin, Atilim Güneş et al. (2017). “Automatic differentiation in machine learning: a survey”. In: *The Journal of Machine Learning Research* 18.1, pp. 5595–5637.
- Berger, James (2006). “The case for objective Bayesian analysis”. In.
- Bernardo, José M and Adrian FM Smith (2001). *Bayesian theory*. John Wiley & Sons.
- Besag, Julian, Jeremy York, and Annie Mollié (1991). “Bayesian image restoration, with two applications in spatial statistics”. In: *Annals of the Institute of Statistical Mathematics* 43.1, pp. 1–20.
- Bilodeau, Blair, Alex Stringer, and Yanbo Tang (2022). “Stochastic convergence rates and applications of adaptive quadrature in Bayesian inference”. In: *Journal of the American Statistical Association*, pp. 1–11.
- Bivand, Roger S et al. (2008). *Applied spatial data analysis with R*. Vol. 747248717. Springer.
- Blei, David M, Alp Kucukelbir, and Jon D McAuliffe (2017). “Variational inference: A review for statisticians”. In: *Journal of the American statistical Association* 112.518, pp. 859–877.
- Bollhöfer, Matthias et al. (2020). “State-of-the-art sparse direct solvers”. In: *Parallel algorithms in computational science and engineering*, pp. 3–33.
- Bosse, Nikos I. et al. (2022). *Evaluating Forecasts with scoringutils in R*. DOI: 10.48550/ARXIV.2205.07090. URL: <https://arxiv.org/abs/2205.07090>.
- Box, George EP and Kenneth B Wilson (1992). “On the experimental attainment of optimum conditions”. In: *Breakthroughs in statistics: methodology and distribution*. Springer, pp. 270–310.

Works Cited

- Breslow, Norman E and David G Clayton (1993). “Approximate inference in generalized linear mixed models”. In: *Journal of the American statistical Association* 88.421, pp. 9–25.
- Broyles, Laura N et al. (2023). “The risk of sexual transmission of HIV in individuals with low-level HIV viraemia: a systematic review”. In: *The Lancet*.
- Brugh, Kristen N et al. (2021). “Characterizing and mapping the spatial variability of HIV risk among adolescent girls and young women: A cross-county analysis of population-based surveys in Eswatini, Haiti, and Mozambique”. In: *PLoS One* 16.12, e0261520.
- Carpenter, Bob et al. (2017). “Stan: A probabilistic programming language”. In: *Journal of Statistical Software* 76.1.
- Casella, George (1985). “An introduction to empirical Bayes data analysis”. In: *The American Statistician* 39.2, pp. 83–87.
- Chen, Cici, Jon Wakefield, and Thomas Lumely (2014). “The use of sampling weights in Bayesian hierarchical models for small area estimation”. In: *Spatial and spatio-temporal epidemiology* 11, pp. 33–43.
- Chopin, Nicolas, Omiros Papaspiliopoulos, et al. (2020). *An introduction to sequential Monte Carlo*. Vol. 4. Springer.
- Cleland, John et al. (2004). “Monitoring sexual behaviour in general populations: a synthesis of lessons of the past decade”. In: *Sexually Transmitted Infections* 80.suppl 2, pp. ii1–ii7.
- Cohen, Myron S et al. (2011). “Prevention of HIV-1 infection with early antiretroviral therapy”. In: *New England journal of medicine* 365.6, pp. 493–505.
- Cressie, Noel and Christopher K Wikle (2015). *Statistics for spatio-temporal data*. John Wiley & Sons.
- Davis, Philip J and Philip Rabinowitz (1975). *Methods of numerical integration*. Academic Press.
- Dawid, A Philip (1984). “Present position and potential developments: Some personal views statistical theory the prequential approach”. In: *Journal of the Royal Statistical Society: Series A (General)* 147.2, pp. 278–290.
- Dean, CB, MD Ugarte, and AF Militino (2001). “Detecting interaction between random region and fixed age effects in disease mapping”. In: *Biometrics* 57.1, pp. 197–202.
- De Valpine, Perry et al. (2017). “Programming with models: writing statistical algorithms for general model structures with NIMBLE”. In: *Journal of Computational and Graphical Statistics* 26.2, pp. 403–413.
- DHS (2012). *Sampling and Household Listing Manual: Demographic and Health Surveys Methodology*.
- Diaz, Jose Monsalve et al. (2018). “Openmp 4.5 validation and verification suite for device offload”. In: *Evolving OpenMP for Evolving Architectures: 14th International Workshop on OpenMP, IWOMP 2018, Barcelona, Spain, September 26–28, 2018, Proceedings* 14. Springer, pp. 82–95.
- Duane, Simon et al. (1987). “Hybrid Monte Carlo”. In: *Physics letters B* 195.2, pp. 216–222.
- Eaton, Jeffrey W et al. (2021). “Naomi: A New Modelling Tool for Estimating HIV Epidemic Indicators at the District Level in Sub-Saharan Africa”. In.
- Economist Impact (2023). “A triple dividend: the health, social and economic gains from financing the HIV response in Africa”. In.

Works Cited

- Fisher, Ronald Aylmer (1936). “Design of experiments”. In: *British Medical Journal* 1.3923, p. 554.
- Follestad, Turid and Håvard Rue (2003). *Modelling spatial variation in disease risk using Gaussian Markov random field proxies for Gaussian random fields*. Tech. rep. SIS-2003-305.
- Freni-Storti, Anna, Massimo Ventrucci, and Håvard Rue (2018). “A note on intrinsic conditional autoregressive models for disconnected graphs”. In: *Spatial and spatio-temporal epidemiology* 26, pp. 25–34.
- Gaedke-Merzhäuser, Lisa et al. (2023). “Parallelized integrated nested Laplace approximations for fast Bayesian inference”. In: *Statistics and Computing* 33.1, p. 25.
- Gelfand, Alan E, Li Zhu, and Bradley P Carlin (2001). “On the change of support problem for spatio-temporal data”. In: *Biostatistics* 2.1, pp. 31–45.
- Gelman, Andrew (2005). “Analysis of variance—why it is more important than ever”. In. — (2007). “Struggles with survey weighting and regression modeling”. In.
- Gelman, Andrew, John B Carlin, et al. (2013). *Bayesian data analysis*. CRC press.
- Gelman, Andrew, Aki Vehtari, et al. (2020). “Bayesian workflow”. In: *arXiv preprint arXiv:2011.01808*.
- Geman, Stuart and Donald Geman (1984). “Stochastic relaxation, Gibbs distributions, and the Bayesian restoration of images”. In: *IEEE Transactions on pattern analysis and machine intelligence* 6, pp. 721–741.
- Giordano, Ryan, Tamara Broderick, and Michael I. Jordan (2018). “Covariances, Robustness, and Variational Bayes”. In: *Journal of Machine Learning Research* 19.51, pp. 1–49. URL: <http://jmlr.org/papers/v19/17-670.html>.
- Global Burden of Disease Collaborative Network (2019). *Global Burden of Disease Study 2019 (GBD 2019) Results*. URL: <https://vizhub.healthdata.org/gbd-results/>.
- Glynn, Judith R et al. (2011). “Assessing the validity of sexual behaviour reports in a whole population survey in rural Malawi”. In: *PLoS One* 6.7, e22840.
- Gómez-Rubio, Virgilio (2020). *Bayesian inference with INLA*. CRC Press.
- Gottlieb, Michael S et al. (1981). “Pneumocystis pneumonia—Los Angeles”. In: *Mmwr* 30.21, pp. 1–3.
- Gray, Ronald H et al. (2007). “Male circumcision for HIV prevention in men in Rakai, Uganda: a randomised trial”. In: *The Lancet* 369.9562, pp. 657–666.
- Hájek, Jaroslav (1971). “Discussion of ‘An essay on the logical foundations of survey sampling, part I’”. In: *Foundations of Statistical Inference (Proc. Sympos., Univ. Waterloo, Ontario, 1970)*, p. 236.
- Hastie, Trevor and Robert Tibshirani (1987). “Generalized additive models: some applications”. In: *Journal of the American Statistical Association* 82.398, pp. 371–386.
- Hastings, W Keith (1970). “Monte Carlo sampling methods using Markov chains and their applications”. In.
- Helleringer, Stéphane et al. (2011). “The reliability of sexual partnership histories: implications for the measurement of partnership concurrency during surveys”. In: *AIDS (London, England)* 25.4, p. 503.
- Hodgins, Caroline et al. (2022). “Population sizes, HIV prevalence, and HIV prevention among men who paid for sex in sub-Saharan Africa (2000–2020): A meta-analysis of 87 population-based surveys”. In: *PLoS Medicine* 19.1, e1003861.
- Hoffman, Matthew D, Andrew Gelman, et al. (2014). “The No-U-Turn sampler: adaptively setting path lengths in Hamiltonian Monte Carlo.” In: *J. Mach. Learn. Res.* 15.1, pp. 1593–1623.

Works Cited

- Howes, Adam, Jeffrey W. Eaton, and Seth R. Flaxman (2023+). “Beyond borders: evaluating the suitability of spatial adjacency for small-area estimation”. In.
- Howes, Adam, Kathryn A. Risher, et al. (Apr. 2023). “Spatio-temporal estimates of HIV risk group proportions for adolescent girls and young women across 13 priority countries in sub-Saharan Africa”. In: *PLOS Global Public Health* 3.4, pp. 1–14. DOI: 10.1371/journal.pgph.0001731. URL: <https://doi.org/10.1371/journal.pgph.0001731>.
- Howes, Adam, Alex Stringer, et al. (2023+). “Fast approximate Bayesian inference of HIV indicators using PCA adaptive Gauss-Hermite quadrature”. In.
- Jäckel, Peter (2005). “A note on multivariate Gauss-Hermite quadrature”. In: *London: ABN-Amro. Re.*
- Jia, Katherine M et al. (2022). “Risk scores for predicting HIV incidence among adult heterosexual populations in sub-Saharan Africa: a systematic review and meta-analysis”. In: *Journal of the International AIDS Society* 25.1, e25861.
- Johnson, L and RE Dorrington (2020). “Thembisa version 4.3: A model for evaluating the impact of HIV/AIDS in South Africa”. In: *View Article*.
- Khoury, Muin J, Michael F Iademarco, and William T Riley (2016). “Precision public health for the era of precision medicine”. In: *American journal of preventive medicine* 50.3, pp. 398–401.
- Kish, Leslie (1965). *Survey sampling*. 04; HN29, K5.
- Knorr-Held, Leonhard (2000). “Bayesian modelling of inseparable space-time variation in disease risk”. In: *Statistics in medicine* 19.17-18, pp. 2555–2567.
- Kristensen, Kasper et al. (2016). “TMB: Automatic Differentiation and Laplace Approximation”. In: *Journal of Statistical Software* 70.i05.
- Laplace, P. S. (1774). “Memoire sur la probabilite de causes par les evenements”. In: *Memoire de l'Academie Royale des Sciences*.
- Leppik, IE et al. (1985). “A double-blind crossover evaluation of progabide in partial seizures”. In: *Neurology* 35.4, p. 285.
- Leroux, Brian G, Xingye Lei, and Norman Breslow (2000). “Estimation of disease rates in small areas: a new mixed model for spatial dependence”. In: *Statistical Models in Epidemiology, the Environment, and Clinical Trials*. Springer, pp. 179–191.
- Lindgren, Finn, Håvard Rue, and Johan Lindström (2011). “An explicit link between Gaussian fields and Gaussian Markov random fields: the stochastic partial differential equation approach”. In: *Journal of the Royal Statistical Society Series B: Statistical Methodology* 73.4, pp. 423–498.
- Margossian, Charles et al. (2020). “Hamiltonian Monte Carlo using an adjoint-differentiated Laplace approximation: Bayesian inference for latent Gaussian models and beyond”. In: *Advances in Neural Information Processing Systems* 33, pp. 9086–9097.
- Martin, Gael M, David T Frazier, and Christian P Robert (2023). “Computing Bayes: From then ‘til now”. In: *Statistical Science* 1.1, pp. 1–17.
- Martino, Sara and Andrea Riebler (2019). “Integrated nested Laplace approximations (INLA)”. In: *arXiv preprint arXiv:1907.01248*.
- Martino, Sara and Håvard Rue (2009). “Implementing approximate Bayesian inference using Integrated Nested Laplace Approximation: A manual for the inla program”. In: *Department of Mathematical Sciences, NTNU, Norway*.
- Martins, Thiago G et al. (2013). “Bayesian computing with INLA: new features”. In: *Computational Statistics & Data Analysis* 67, pp. 68–83.

Works Cited

- “Maximum likelihood from incomplete data via the EM algorithm” (1977). In: *Journal of the royal statistical society: series B (methodological)* 39.1, pp. 1–22.
- McCullagh, Peter and John A Nelder (1989). *Generalized linear models*. Routledge.
- McElreath, Richard (2020). *Statistical rethinking: A Bayesian course with examples in R and Stan*. CRC press.
- Meng, Xiao-Li (2018). “Statistical paradises and paradoxes in big data (i) law of large populations, big data paradox, and the 2016 us presidential election”. In: *The Annals of Applied Statistics* 12.2, pp. 685–726.
- Metropolis, Nicholas et al. (1953). “Equation of state calculations by fast computing machines”. In: *The journal of chemical physics* 21.6, pp. 1087–1092.
- Minka, Thomas P (2001). “Expectation Propagation for approximate Bayesian inference”. In: *Proceedings of the 17th Conference in Uncertainty in Artificial Intelligence*, pp. 362–369.
- Monnahan, Cole C and Kasper Kristensen (2018). “No-U-turn sampling for fast Bayesian inference in ADMB and TMB: Introducing the adnuts and tmbstan R packages”. In: *PloS one* 13.5, e0197954.
- Monod, Mélodie et al. (2023). “Growing gender disparity in HIV infection in Africa: sources and policy implications”. In: *medRxiv*, pp. 2023–03.
- Nandi, Anita K et al. (2020). “Disaggregation: an R package for Bayesian spatial disaggregation modelling”. In: *arXiv preprint arXiv:2001.04847*.
- Naylor, John C and Adrian FM Smith (1982). “Applications of a method for the efficient computation of posterior distributions”. In: *Journal of the Royal Statistical Society Series C: Applied Statistics* 31.3, pp. 214–225.
- Neal, Radford M (2003). “Slice sampling”. In: *The Annals of Statistics* 31.3, pp. 705–767.
- Neal, Radford M et al. (2011). “MCMC using Hamiltonian dynamics”. In: *Handbook of Markov chain Monte Carlo* 2.11, p. 2.
- Nguyen, Van Kính and Jeffrey W. Eaton (2022). “Trends and country-level variation in age at first sex in sub-Saharan Africa among birth cohorts entering adulthood between 1985 and 2020”. In: *BMC Public Health* 22.1, p. 1120. DOI: 10.1186/s12889-022-13451-y. URL: <https://doi.org/10.1186/s12889-022-13451-y>.
- Nnko, Soori et al. (2004). “Secretive females or swaggering males?: An assessment of the quality of sexual partnership reporting in rural Tanzania”. In: *Social Science & Medicine* 59.2, pp. 299–310.
- Openshaw, S and P.J. Taylor (1979). “A million or so correlation coefficients, three experiments on the modifiable areal unit problem”. In: *Statistical Applications in the Spatial Science*, pp. 127–144.
- Ord, Toby (2013). “The moral imperative toward cost-effectiveness in global health”. In: *Center for Global Development* 12.
- Paciorek, Christopher J et al. (2013). “Spatial models for point and areal data using Markov random fields on a fine grid”. In: *Electronic Journal of Statistics* 7, pp. 946–972.
- Pettit, LI (1990). “The conditional predictive ordinate for the normal distribution”. In: *Journal of the Royal Statistical Society: Series B (Methodological)* 52.1, pp. 175–184.
- Pfeffermann, Danny et al. (2013). “New Important Developments in Small Area Estimation”. In: *Statistical Science* 28.1, pp. 40–68.

Works Cited

- Porcu, Emilio, Reinhard Furrer, and Douglas Nychka (2021). "30 Years of space–time covariance functions". In: *Wiley Interdisciplinary Reviews: Computational Statistics* 13.2, e1512.
- R Core Team (2022). *R: A Language and Environment for Statistical Computing*. R Foundation for Statistical Computing. Vienna, Austria. URL: <https://www.R-project.org>.
- Risher, Kathryn A et al. (2021). "Age patterns of HIV incidence in eastern and southern Africa: a modelling analysis of observational population-based cohort studies". In: *The Lancet HIV* 8.7, e429–e439.
- Robert, Christian P and George Casella (2005). *Monte Carlo Statistical Methods (Springer Texts in Statistics)*.
- Roberts, Gareth O and Jeffrey S Rosenthal (2004). "General state space Markov chains and MCMC algorithms". In.
- Rue, Håvard (2001). "Fast sampling of Gaussian Markov random fields". In: *Journal of the Royal Statistical Society: Series B (Statistical Methodology)* 63.2, pp. 325–338.
- (2020). "Comment on R-INLA Discussion Group thread". In.
- Rue, Havard (2023). "‘R-INLA’ Project - FAQ". Accessed 23/01/2023. URL: <https://www.r-inla.org/faq>.
- Rue, Havard and Leonhard Held (2005). *Gaussian Markov random fields: theory and applications*. CRC press.
- Rue, Håvard and Turid Follestad (2001). *GMRFLib: a C-library for fast and exact simulation of Gaussian Markov random fields*. Tech. rep. SIS-2002-236.
- Rue, Håvard and Sara Martino (2007). "Approximate Bayesian inference for hierarchical Gaussian Markov random field models". In: *Journal of Statistical Planning and Inference* 137.10, pp. 3177–3192.
- Rue, Håvard, Sara Martino, and Nicolas Chopin (2009). "Approximate Bayesian inference for latent Gaussian models by using integrated nested Laplace approximations". In: *Journal of the Royal Statistical Society: Series B (Statistical Methodology)* 71.2, pp. 319–392.
- Rue, Håvard, Andrea Riebler, et al. (2017). "Bayesian computing with INLA: a review". In: *Annual Review of Statistics and Its Application* 4, pp. 395–421.
- Säilynoja, Teemu, Paul-Christian Bürkner, and Aki Vehtari (2021). "Graphical Test for Discrete Uniformity and its Applications in Goodness of Fit Evaluation and Multiple Sample Comparison". In: *arXiv preprint arXiv:2103.10522*.
- Saul, Janet et al. (2018). "The DREAMS core package of interventions: a comprehensive approach to preventing HIV among adolescent girls and young women". In: *PLoS One* 13.12, e0208167.
- Shapley, Lloyd S et al. (1953). "A value for n-person games". In.
- Shumway, Robert H and David S Stoffer (2017). "Time Series Analysis and Its Applications With R Examples". In.
- Siegfried, Nandi et al. (2011). "Antiretrovirals for reducing the risk of mother-to-child transmission of HIV infection". In: *Cochrane database of systematic reviews* 7.
- Simpson, Daniel et al. (2017). "Penalising model component complexity: A principled, practical approach to constructing priors". In: *Statistical Science* 32.1, pp. 1–28.
- Skaug, Hans J. (2009). "Discussion of "Approximate Bayesian inference for latent Gaussian models by using integrated nested Laplace approximations"". In: vol. 71. 2. Wiley Online Library, pp. 319–392.

Works Cited

- Slaymaker, Emma et al. (2020). "Risk factors for new HIV infections in the general population in sub-Saharan Africa". In:
- Sørbye, Sigrunn Holbek and Håvard Rue (2014). "Scaling intrinsic Gaussian Markov random field priors in spatial modelling". In: *Spatial Statistics* 8, pp. 39–51.
- (2017). "Penalised complexity priors for stationary autoregressive processes". In: *Journal of Time Series Analysis* 38.6, pp. 923–935.
- Spiegelhalter, David, Andrew Thomas, et al. (1996). "BUGS 0.5 Examples". In: *MRC Biostatistics Unit, Institute of Public health, Cambridge, UK* 256.
- Spiegelhalter, David J, Nicola G Best, et al. (2002). "Bayesian measures of model complexity and fit". In: *Journal of the Royal Statistical Society: Series B (statistical Methodology)* 64.4, pp. 583–639.
- Stevens, Oliver, Keith Sabin, Sonia Arias Garcia, et al. (2022). "Estimating key population size, HIV prevalence, and ART coverage for sub-Saharan Africa at the national level". In:
- Stevens, Oliver, Keith Sabin, Sonia Arias Garcia, et al. (2022). "Key population size, HIV prevalence, and ART coverage in sub-Saharan Africa: systematic collation and synthesis of survey data". In: *medRxiv*, pp. 2022–07.
- Stover, John and Yu Teng (2021). "The impact of condom use on the HIV epidemic". In: *Gates Open Research* 5.
- Stringer, Alex (2021a). "Implementing Approximate Bayesian Inference Using Adaptive Quadrature". Statistics Graduate Student Research Day 2021, The Fields Institute for Research in Mathematical Sciences. URL:
<http://www.fields.utoronto.ca/talks/Implementing-Approximate-Bayesian-Inference-Using-Adaptive-Quadrature>.
- (2021b). "Implementing Approximate Bayesian Inference using Adaptive Quadrature: the aghq Package". In: *arXiv preprint arXiv:2101.04468*.
- Stringer, Alex, Patrick Brown, and Jamie Stafford (2022). "Fast, scalable approximations to posterior distributions in extended latent Gaussian models". In: *Journal of Computational and Graphical Statistics*, pp. 1–15.
- Tanser, Frank et al. (2014). "Concentrated HIV sub-epidemics in generalized epidemic settings". In: *Current Opinion in HIV and AIDS* 9.2, p. 115.
- Tatem, Andrew J (2017). "WorldPop, open data for spatial demography". In: *Scientific data* 4.1, pp. 1–4.
- Thall, Peter F and Stephen C Vail (1990). "Some covariance models for longitudinal count data with overdispersion". In: *Biometrics*, pp. 657–671.
- The Global Fund (2018). *The Global Fund Measurement Framework for Adolescent Girls and Young Women Programs*. Accessed 30/08/2021. URL:
https://www.theglobalfund.org/media/8076/me_adolescentsgirlsandyoungwomenprograms_frameworkmeasurement_en.pdf.
- Tierney, Luke and Joseph B Kadane (1986). "Accurate approximations for posterior moments and marginal densities". In: *Journal of the American Statistical Association* 81.393, pp. 82–86.
- Tobler, Waldo R (1970). "A computer movie simulating urban growth in the Detroit region". In: *Economic geography* 46.sup1, pp. 234–240.
- U.S. Department of State (2022). *Latest Global Program Results*.
https://www.state.gov/wp-content/uploads/2022/11/PEPFAR-Latest-Global-Results_December-2022.pdf. Accessed: 10/08/2023.

Works Cited

- UNAIDS (2021a). *2021 UNAIDS Global AIDS Update - Confronting Inequalities - Lessons for pandemic responses from 40 Years of AIDS*. Accessed: June 2023.
- (2021b). “Global AIDS strategy 2021–2026. End inequalities. End AIDS”. In: Accessed: June 2023.
- (2022). *In Danger: UNAIDS Global AIDS Update 2022*.
<https://www.unaids.org/en/resources/documents/2022/in-danger-global-aids-update>. Accessed: June 2023.
- (2023a). *AIDSinfo: Global data on HIV epidemiology and response*.
<https://aidsinfo.unaids.org/>. Accessed: August 2023.
- (2023b). *The path that ends AIDS: UNAIDS Global AIDS Update 2023*. <https://www.unaids.org/en/resources/documents/2023/global-aids-update-2023>. Accessed: August 2023.
- UNICEF (2019). *Adolescent & social norms situation in Mozambique*. Accessed 25/03/2022. URL:
<https://www.unicef.org/mozambique/en/adolescent-social-norms>.
- Wakefield, Jonathan and Hilary Lyons (Mar. 2010). “Spatial Aggregation and the Ecological Fallacy”. In: vol. 2010, pp. 541–558. DOI: 10.1201/9781420072884-c30.
- Ward, Brian (2023). *bridgestan: BridgeStan, Accessing Stan Model Functions in R*. R package version 1.0.1.
- Watanabe, Sumio (2013). “A widely applicable Bayesian information criterion”. In: *Journal of Machine Learning Research* 14.Mar, pp. 867–897.
- Weiser, Constantin (2016). *mvQuad: Methods for Multivariate Quadrature*. (R package version 1.0-6). URL: <http://CRAN.R-project.org/package=mvQuad>.
- Wolock, Timothy M et al. (June 2021). “Evaluating distributional regression strategies for modelling self-reported sexual age-mixing”. In: *eLife* 10. Ed. by Eduardo Franco, Talía Malagón, and Adam Akullian, e68318. DOI: 10.7554/eLife.68318. URL:
<https://doi.org/10.7554/eLife.68318>.
- Wood, Simon N (2017). *Generalized additive models: an introduction with R*. CRC press.
- (2020). “Simplified integrated nested Laplace approximation”. In: *Biometrika* 107.1, pp. 223–230.
- World Health Organization (2005). “Guidelines for measuring national HIV prevalence in population-based surveys”. In.
- (2017). “Consolidated guidelines on person-centred HIV patient monitoring and case surveillance”. In.
- Wringe, A et al. (2009). “Comparative assessment of the quality of age-at-event reporting in three HIV cohort studies in sub-Saharan Africa”. In: *Sexually transmitted infections* 85.Suppl 1, pp. i56–i63.
- Yao, Yuling et al. (2018). “Yes, but did it work?: Evaluating variational inference”. In: *International Conference on Machine Learning*. PMLR, pp. 5581–5590.
- Zaba, Basia et al. (2004). “Age at first sex: understanding recent trends in African demographic surveys”. In: *Sexually transmitted infections* 80.suppl 2, pp. ii28–ii35.